

**UNDERSTANDING AND MITIGATING
EFFECTS OF CHLORIDE DEICER
EXPOSURE ON CONCRETE**

Final Report

SPR 742



Oregon Department of Transportation

UNDERSTANDING AND MITIGATING EFFECTS OF CHLORIDE DEICER EXPOSURE ON CONCRETE

Final Report

SPR 742

by

Xianming Shi, Ph.D., P.E.

Ning Xie, Ph.D.

Yudong Dang, Ph.D.

Anburaj Muthumani, M.Sc.

Jiang Huang, M.Sc.

Adam Hagel, Shane Forsythe, Elizabeth Selig, Dustin Falk

Eli McVey, Amanda Kessel, Callie Martins, Yan Zhang, Yida Fang

for

Oregon Department of Transportation

Research Section

555 13th Street NE, Suite 1

Salem OR 97301

and

Federal Highway Administration

400 Seventh Street, SW

Washington, DC 20590-0003

September 2014

1. Report No. FHWA-OR-RD-15-08		2. Government Accession No.		3. Recipient's Catalog No.	
4. Title and Subtitle UNDERSTANDING AND MITIGATING EFFECTS OF CHLORIDE DEICER EXPOSURE ON CONCRETE				5. Report Date -September 2014-	
				6. Performing Organization Code	
7. Author(s) Xianming Shi*, Ning Xie, Yudong Dang, Anburaj Muthumani, Jiang Huang, Adam Hagel, Shane Forsythe, Elizabeth Selig, Dustin Falk, Eli McVey, Amanda Kessel, Callie Martins, Yan Zhang, Yida Fang				8. Performing Organization Report No.	
9. Performing Organization Name and Address Western Transportation Institute P. O. Box 174250, Montana State University Bozeman, MT 59717-4250				10. Work Unit No. (TRAIS)	
				11. Contract or Grant No. SPR 742	
12. Sponsoring Agency Name and Address Oregon Dept. of Transportation Research Section and Federal Highway Admin. 555 13 th Street NE, Suite 1 400 Seventh Street, SW Salem, OR 97301 Washington, DC 20590-0003				13. Type of Report and Period Covered Final Report	
				14. Sponsoring Agency Code	
15. Supplementary Notes Principal Investigator now with the Washington State University					
16. Abstract: Field and laboratory investigations were conducted to examine the effects of chloride deicers on concrete bridge decks and to identify and evaluate best practices and products to mitigate such effects. The concrete bridge decks exposed to KAc or MgCl ₂ deicer showed significant reductions in their compressive strength, splitting tensile strength and microhardness, whereas those exposed to NaCl deicer and without signs of surface distress did not. Visual inspection would be misleading for assessing the condition of concrete bridge decks exposed to MgCl ₂ deicer, as the chemical attack by MgCl ₂ generally does not exhibit apparent signs of distress. Chloride penetration as low as 0.1 in (2.5 mm) based on AgNO ₃ spray method does not guarantee the integrity of the concrete exposed to MgCl ₂ deicer. At least half of cored ODOT bridge decks exhibited air void spacing factor higher than 200 microns (0.008 inches) per the ASTM C457 test method, indicating that they no longer have a proper air-void system for freeze-thaw resistance. The role of MgCl ₂ in the carbonation and ASR of field concrete, if any, is not significant, but KAc may play a significant role in contributing to ASR in concrete containing reactive aggregate. The microscopic evidence further suggests that the concrete in the field environment had been affected by both physical and chemical degradation by the joint action of freeze-thaw cycles and MgCl ₂ . A set of mortar samples can be deployed to assess the cumulative MgCl ₂ exposure at a given site. A simplistic empirical-mechanistic model was developed to evaluate the conditions of the current bridge decks. Surface treatments, especially penetrating sealers and water repellents should be used to protect new concrete and existing concrete without too much chloride contamination. For any surface treatment to be used, it is important to select products with high resistance to both gas and water penetration to maximize the concrete's resistance to "salt scaling". When the concrete surface has deteriorated to a more severe degree, overlays should be used. For concrete decks exposed to freeze-thaw and wet-dry cycles and both NaCl and MgCl ₂ deicers, silica fume modified cementitious overlays and micro-fiber modified cementitious overlays should be used. For decks mainly exposed to MgCl ₂ deicer, Castek T48 polymer overlay is a good candidate. For areas that are also subjected to studded tires and high risk of abrasion, Castek T48 and KwikBond PPC-1121 polymer overlays should be used instead of cementitious overlays.					
17. Key Words: deicers, magnesium chloride, sodium chloride, bridge decks, cores, scaling, alkali silica reactions, sealers, water repellants, overlays, electron microscopes, chemical analysis, microhardness, permeability, splitting tensile strength, freeze thaw, abrasion, condition surveys			18. Distribution Statement Copies available from NTIS, and online at http://www.oregon.gov/ODOT/TD/TP_RES/		
19. Security Classification (of this report) Unclassified		20. Security Classification (of this page) Unclassified		21. No. of Pages 166	22. Price

SI* (MODERN METRIC) CONVERSION FACTORS

APPROXIMATE CONVERSIONS TO SI UNITS					APPROXIMATE CONVERSIONS FROM SI UNITS				
Symbol	When You Know	Multiply By	To Find	Symbol	Symbol	When You Know	Multiply By	To Find	Symbol
<u>LENGTH</u>					<u>LENGTH</u>				
in	inches	25.4	millimeters	mm	mm	millimeters	0.039	inches	in
ft	feet	0.305	meters	m	m	meters	3.28	feet	ft
yd	yards	0.914	meters	m	m	meters	1.09	yards	yd
mi	miles	1.61	kilometers	km	km	kilometers	0.621	miles	mi
<u>AREA</u>					<u>AREA</u>				
in ²	square inches	645.2	millimeters squared	mm ²	mm ²	millimeters squared	0.0016	square inches	in ²
ft ²	square feet	0.093	meters squared	m ²	m ²	meters squared	10.764	square feet	ft ²
yd ²	square yards	0.836	meters squared	m ²	m ²	meters squared	1.196	square yards	yd ²
ac	acres	0.405	hectares	ha	ha	hectares	2.47	acres	ac
mi ²	square miles	2.59	kilometers squared	km ²	km ²	kilometers squared	0.386	square miles	mi ²
<u>VOLUME</u>					<u>VOLUME</u>				
fl oz	fluid ounces	29.57	milliliters	ml	ml	milliliters	0.034	fluid ounces	fl oz
gal	gallons	3.785	liters	L	L	liters	0.264	gallons	gal
ft ³	cubic feet	0.028	meters cubed	m ³	m ³	meters cubed	35.315	cubic feet	ft ³
yd ³	cubic yards	0.765	meters cubed	m ³	m ³	meters cubed	1.308	cubic yards	yd ³
NOTE: Volumes greater than 1000 L shall be shown in m ³ .									
<u>MASS</u>					<u>MASS</u>				
oz	ounces	28.35	grams	g	g	grams	0.035	ounces	oz
lb	pounds	0.454	kilograms	kg	kg	kilograms	2.205	pounds	lb
T	short tons (2000 lb)	0.907	megagrams	Mg	Mg	megagrams	1.102	short tons (2000 lb)	T
<u>TEMPERATURE (exact)</u>					<u>TEMPERATURE (exact)</u>				
°F	Fahrenheit	(F-32)/1.8	Celsius	°C	°C	Celsius	1.8C+32	Fahrenheit	°F

*SI is the symbol for the International System of Measurement

ACKNOWLEDGEMENTS

The authors acknowledge the financial support for this project provided by the Oregon Department of Transportation (ODOT) as well as the USDOT Research & Innovative Technology Administration (RITA) through Alaska University Transportation Center and Western Transportation Institute. The authors are indebted to the ODOT Research Coordinator Steven Soltesz and the AUTC project manager Billy Connor. The authors thank members of the technical panel (Michael Coffey at Alaska DOT&PF; Tim Rogers at FHWA; and Rick Poecker, Ray Bottenberg, and James Garrard at ODOT) for their guidance and other ODOT engineers (Bert Hartman, Theresa Yih, Erick Cain, Adam Bradford, Susan Mead, Gretchen Harvey, Chad Crockett) for their support. The gratitude is due to the Utah DOT (esp. David Stevens, Lonnie Marchant, and Joshua Sletten) and Nebraska DOT (esp. Lieska Halsey) for providing cores from their concrete decks and associated information. The gratitude is also due to the professionals who responded to the practitioner surveys. Part of the task of developing deicer exposure maps was undertaken by the ITSNode LLC through a subcontract with Montana State University. The authors thank Transpo Industries, Inc., Castek Inc., Kwik Bond Polymers, and Advanced Chemical Technologies, Inc. for supplying the sealer and overlay products for this study. The authors also extend their sincere gratitude to many students at the WTI Corrosion & Sustainable Infrastructure Lab (Stephen Mery, Amanda Olsen, Andrew Benson, and Peng Lei) and colleagues at WTI (Michelle Akin, Zach Zupan, and Jaydeep Chaudhari) for their assistance in some tasks. The authors would also like to thank Prof. Jueshi Qian, Mr. Maowei Niu and Mr. Zhou Wu in Chongqing University for their assistance in the microhardness testing.

DISCLAIMER

This document is disseminated under the sponsorship of the Oregon Department of Transportation and the United States Department of Transportation in the interest of information exchange. The State of Oregon and the United States Government assume no liability of its contents or use thereof.

The contents of this report reflect the view of the authors who are solely responsible for the facts and accuracy of the material presented. The contents do not necessarily reflect the official views of the Oregon Department of Transportation or the United States Department of Transportation.

The State of Oregon and the United States Government do not endorse products of manufacturers. Trademarks or manufacturers' names appear herein only because they are considered essential to the object of this document.

This report does not constitute a standard, specification, or regulation.

TABLE OF CONTENTS

1.0	INTRODUCTION.....	1
1.1	PROBLEM STATEMENT	1
1.2	RESEARCH OBJECTIVES	2
1.3	ANTICIPATED BENEFITS.....	2
1.4	SCOPE OF WORK AND REPORT ORGANIZATION	2
2.0	POTENTIAL DEICER EFFECTS ON CONCRETE BRIDGE DECKS: DEVELOPING EXPOSURE MAPS.....	5
2.1	INTRODUCTION	5
2.2	METHODOLOGY	6
2.2.1	<i>Bridge Deck Selection Process</i>	7
2.2.2	<i>Data Collection for the Exposure Map Development</i>	8
2.3	RESULTS AND DISCUSSION	9
2.3.1	<i>Stakeholder Perspective: Winter Maintenance Mangers</i>	9
2.3.2	<i>Stakeholder Perspective Regional Bridge Managers</i>	11
2.3.3	<i>A Method of Developing Exposure Maps: ODOT Case Study</i>	11
2.4	CONCLUDING REMARKS	17
3.0	EFFECTS OF DEICER EXPOSURE ON CONCRETE BRIDGE DECKS: A COMPARATIVE STUDY OF FIELD CORES EXPOSED TO POTASSIUM ACETATE, SODIUM CHLORIDE, OR MAGNESIUM CHLORIDE.....	19
3.1	METHODOLOGY	19
3.1.1	<i>Field Sampling</i>	19
3.1.2	<i>Laboratory Testing</i>	20
3.2	RESULTS AND DISCUSSION: A COMPARATIVE STUDY OF UTAH AND NEBRASKA DECKS ...	26
3.2.1	<i>Historical Information of the Bridges</i>	26
3.2.2	<i>Mechanical Properties</i>	27
3.2.3	<i>Transport Properties of Cored Concrete Decks</i>	30
3.2.4	<i>ASR</i>	34
3.3	RESULTS AND DISCUSSION: A CASE STUDY OF ODOT DECKS.....	35
3.3.1	<i>Statistical Correlations</i>	35
3.3.2	<i>Mechanical Properties</i>	38
3.3.3	<i>Transport Properties</i>	50
3.3.4	<i>ASR</i>	56
3.4	MICROSCOPIC ANALYSIS OF SELECT ODOT CORE SAMPLES	58
3.4.1	<i>SEM Analysis</i>	58
3.4.2	<i>SEM/EDS Analysis</i>	63
3.5	CONCLUSIONS	68
4.0	DEVELOPING DEICER EXPOSURE MEASUREMENT METHOD	70
4.1	MOTAR SPECIMENS.....	70
4.1.1	<i>Materials and Methods</i>	70
4.1.2	<i>Results and Discussion</i>	73
4.2	METALLIC SPECIMENS	85

4.2.1	<i>Materials and Methods</i>	85
4.2.2	<i>Results and Discussion</i>	86
4.3	POLYMERIC SPECIMENS	90
4.4	CONCLUDING REMARKS	90
5.0	DAMAGE ANALYSIS TOOL	92
5.1	INTRODUCTION.....	92
5.2	PREDICTION OF THE SERVICE CONDITION OF THE CURRENT BRIDGES	93
5.2.1	<i>Gas Permeability</i>	93
5.2.2	<i>Mechanical Properties</i>	93
5.2.3	<i>Coupling the Influential Factors</i>	94
5.3	CONCLUDING REMARKS	97
6.0	ACCELERATED LABORATORY EVALUATION OF SURFACE TREATMENTS FOR PROTECTING CONCRETE BRIDGE DECKS FROM “SALT SCALING”	99
6.1	INTRODUCTION.....	99
6.2	EXPERIMENTAL PROCEDURE.....	101
6.2.1	<i>Concrete Constituents, Mixing, and Curing</i>	101
6.2.2	<i>Surface Treatments</i>	102
6.2.3	<i>Abrasion Resistance Test</i>	104
6.2.4	<i>Salt Scaling Test</i>	104
6.2.5	<i>Water Absorption Test</i>	104
6.2.6	<i>Gas Permeability Test</i>	104
6.2.7	<i>Water Contact Angle Measurements</i>	106
6.3	RESULTS AND DISCUSSION	106
6.3.1	<i>Abrasion Resistance of concrete with Various Surface Treatments</i>	106
6.3.2	<i>Scaling Resistance of concrete with Various Surface Treatments</i>	107
6.3.3	<i>Water Absorption of Concrete with Various Surface Treatments</i>	108
6.3.4	<i>Gas Permeability of Concrete with Various Surface Treatments</i>	110
6.3.5	<i>Water Contact Angle of Concrete with Various Surface Treatments</i>	111
6.3.6	<i>Splitting Tensile Strengths of the Samples Protected by Various Surface Treatments</i>	112
6.4	CONCLUSIONS AND FUTURE WORK	113
7.0	ACCELERATED LABORATORY EVALUATION OF OVERLAYS FOR PROTECTING CONCRETE BRIDGE DECKS FROM “SALT SCALING”	116
7.1	INTRODUCTION.....	116
7.2	MATERIALS AND METHODS.....	116
7.2.1	<i>Materials and Proportion of Concrete Substrate Slabs</i>	116
7.2.2	<i>Information of Overlays</i>	117
7.2.3	<i>Images of the Application of Overlays</i>	119
7.3	EXPERIMENTAL METHODS FOR EVALUATING THE OVERLAYS	120
7.3.1	<i>Procedures of Freeze/Thaw and Wet/Dry Cycles</i>	120
7.3.2	<i>Splitting Tensile Strength</i>	120
7.3.3	<i>Bond Strength</i>	121
7.3.4	<i>Gas Permeability</i>	121
7.3.5	<i>Abrasion Resistance</i>	123
7.4	RESULTS AND DISCUSSION.....	124
7.4.1	<i>Bond Strength</i>	124
7.4.2	<i>Splitting Tensile Strength</i>	126
7.4.3	<i>Abrasion Resistance</i>	126
7.4.4	<i>Gas Permeability</i>	131
7.5	CONCLUSIONS	132

8.0	CONCLUSIONS AND RECOMMENDATIONS.....	134
8.1	CONCLUSIONS	134
8.2	IMPLEMENTATION RECOMMENDATIONS	136
9.0	REFERENCES.....	138

APPENDIX A: DEICER USAGE PER YEAR FOR EACH ODOT BRIDGE SELECTED IN THIS STUDY

LIST OF TABLES

Table 2.1:	Winter Maintenance Practices of Selected Four ODOT Districts	10
Table 2.2:	List of 12 Selected ODOT Highway Bridges	12
Table 2.3:	Estimated Freeze/Thaw Cycles for Fiscal Years 2005 – 2011, along with Other Data for the Select Bridge Decks.....	16
Table 3.1:	Historical information of the decks exposed to different deicers in UT and NE	26
Table 3.2:	The compressive and splitting tensile strengths of the cored bridge deck samples	28
Table 3.3:	Chloride penetration depth of the bridge decks in UT and NE.....	31
Table 3.4:	The air void characteristics of the bridge deck samples from UT and NE	33
Table 3.5:	Water absorption and pore parameters of the UT & NE bridge deck cores.....	34
Table 3.6:	Average data for the 12 selected ODOT bridge decks	39
Table 3.7:	Parameters of splitting tensile test	40
Table 3.8:	Parameters from the compressive strength test.....	43
Table 3.9:	Maximum chloride penetration vs. splitting tensile strength of the 12 ODOT concrete decks	51
Table 3.10:	The parameters calculated using the phenolphthalein and air-void tests	52
Table 3.11:	Parameters from the absorption test for the ODOT bridge decks.....	55
Table 3.12:	Summary of microstructure analysis of the select ODOT bridge decks, along with other key parameters and rankings	67
Table 4.1:	Factors and Levels for the Statistical DoE.....	73
Table 4.2:	Mechanical properties of mortar specimens after various deicer exposure conditions.....	74
Table 4.3:	Surface resistivity (in K Ω .cm) as a function of influential factors	79
Table 4.4:	Deploying mortar specimens for periodical surface resistivity measurements.....	84
Table 4.5:	Deploying mortar specimens for periodical sampling and mechanical testing.....	84
Table 5.1:	Summary of the 12 ODOT concrete bridge decks, with the new ratings by CSIL.....	96
Table 6.1:	Mix proportion and properties of concrete	102
Table 6.2:	Technical data about the surface treatments	103
Table 7.1:	Mix Proportion and Properties of Concrete	117
Table 7.2:	Information of cement based overlays.....	117
Table 7.3:	Information of organic overlays	118

LIST OF FIGURES

Figure 2.1:	The Bridge Selection Procedure in a Flowchart.....	8
Figure 2.2:	The Oregon DOT Districts that Responded to the Winter Maintenance Survey (Highlighted in Purple)...	9
Figure 2.3:	Example of ODOT Deck Concrete Mix Design.....	12

Figure 2.4: Annual Deicer Usage Data for the ODOT District 13, 12, 8 and 2B	14
Figure 2.5: FY2011 Exposure Map for the 12 selected ODOT Bridge Decks	17
Figure 3.1: The setup of the splitting tensile strength test.	22
Figure 3.2: Example of chloride penetration in an ODOT concrete sample	23
Figure 3.3: Cutting of Samples for Absorption Test.....	25
Figure 3.4: The microhardness distribution of the core samples from the concrete bridge decks: a) ITZ area (UT), b) ITZ area (NE), c) paste area (UT), and d) paste area (NE)	29
Figure 3.5: Typical chloride concentration in profile in (a) laboratory concretes after 26 weekly cycles of 24-h wetting in 3% NaCl solution and 6-d drying in 20°C, 50% RH (<i>Polder and Peelen 2002</i>); (b) field concretes subjected to periodical salt applications (<i>Rösli and Harnik 1980</i>).	30
Figure 3.6: Cl ⁻ penetration staining test results of cores from a) NE and b) UT.....	31
Figure 3.7: the image of a core sample processed for phenolphthalein and air-void tests.....	32
Figure 3.8: Staining image illustrating the presence of ASR in concrete samples from a) NE and b) UT	35
Figure 3.9: The gas permeability as a function of the splitting tensile strength of the decks built in different years a) 2000-2005, b) 1985-1990, and c) before 1980.	41
Figure 3.10: The splitting tensile strength as a function of annual deicer usage.	42
Figure 3.11: The microhardness of concrete specimens from two ODOT bridge decks, exposed to a) 105 and b) 3784 gln/ln-mi/FY, respectively	44
Figure 3.12: The microhardness of three concrete decks experienced MgCl ₂ deicer at over 2000 per lane mile per year: a) bridge 19681; b) bridge 8682; c) bridge 18940.....	45
Figure 3.13: Lab concrete samples exposed to 5 F/T cycles in MgCl ₂ and NaCl solutions, respectively	47
Figure 3.14: Lab concrete samples exposed to 10 F/T cycles in MgCl ₂ and NaCl solutions, respectively	49
Figure 3.15: Splitting tensile strength of lab concrete samples exposed to F/T cycles in NaCl and MgCl ₂ solution.	50
Figure 3.16: Water absorption as a function of deck number and sample depth	56
Figure 3.17: Images from ASR test of select ODOT core samples	57
Figure 3.18: SEM micrographs of ODOT bridge deck 16844: a) low magnification and b) high magnification	59
Figure 3.19: SEM micrograph of ODOT bridge deck 08682:	60
Figure 3.20: SEM micrographs of ODOT bridge deck 16440:.....	61
Figure 3.21: SEM micrographs of ODOT bridge deck 19681:.....	62
Figure 3.22: SEM micrographs of ODOT bridge deck 16534:.....	63
Figure 3.23: SEM/EDS analysis of 16844 bridge deck	64
Figure 3.24: SEM/EDS analysis of 08682 bridge deck	65
Figure 3.25: SEM/EDS analysis of 19681 bridge deck	66
Figure 4.1: Setup of four electrode measurement of concrete resistivity.....	72
Figure 4.2: Average compressive strength as a function of various factors	75
Figure 4.3: Average splitting tensile strength as a function of the influential factors	76
Figure 4.4: Average Young's modulus as a function of the influential factors	77
Figure 4.5: Mechanical properties of mortar specimens as reliable indicator of MgCl ₂ deicer exposure.....	81
Figure 4.6: Surface resistivity of mortar specimens as reliable indicator of MgCl ₂ deicer exposure	83
Figure 4.7: Rockwell hardness of carbon steel coupons as possible indicator of MgCl ₂ deicer exposure.....	86
Figure 4.8: Mass loss of metallic coupons as a function of MgCl ₂ deicer exposure.....	87
Figure 4.9: Surface resistivity of magnesium alloy coupons as a function of MgCl ₂ deicer exposure.....	88
Figure 4.10: Representative digital photos of metallic coupons as a function of metal type and MgCl ₂ deicer exposure	89
Figure 5.1: Schematic illustration of field concrete in a small area but with different external environmental conditions	93
Figure 6.1: Schematic illustration of: (a) water absorption test setup; (b) gas permeability test setup.....	105
Figure 6.2: Abrasion mass loss of concrete samples with various surface treatments. The error bars show the standard deviations.	106
Figure 6.3: Exterior images of concrete cylinders after the deicer exposure and 15 F/T and W/D cycles	108
Figure 6.4: Mass loss of concrete cylinders after the deicer exposure and a given number of F/T and W/D cycles. The error bars show the standard deviations.	108
Figure 6.5: Rates of water absorption of concrete specimens with various surface treatments. The error bars show the standard deviations.	109
Figure 6.6: Gas permeability coefficient of samples with various surface treatments. Average value and standard deviation are shown.	110

Figure 6.7: Water contact angle of samples with various surface treatments	111
Figure 6.8: Splitting tensile strength of concrete samples surface treated with different sealers after F/T and W/D cycles in 3% NaCl solution	112
Figure 6.9: Splitting tensile strength of concrete samples surface treated with different sealers after F/T and W/D cycles in 3% MgCl ₂ solution.....	113
Figure 7.1: Preparation of the cement based overlays	119
Figure 7.2: Preparation of the organic overlays.....	120
Figure 7.3: Bond strength tests	121
Figure 7.4: Schematic drawing for the gas permeability test setup	121
Figure 7.5: Samples of cement based overlays including overlay (0.5'') and concrete (0.5'') used for gas permeability test.....	122
Figure 7.6: Samples of organic overlays including overlay (1/3'') and concrete (2/3'') used for gas permeability test	123
Figure 7.7: Rotating-Cutter Drill Press.....	123
Figure 7.8: Bond strengths of various overlays	124
Figure 7.9: Digital photos of concrete samples after bond strength tests	126
Figure 7.10: Splitting tensile strengths of various overlays.....	126
Figure 7.11: Abrasion resistance of various overlays after F/T W/D cycles in 15% NaCl solutions	128
Figure 7.12: Abrasion resistance of various overlays after F/T W/D cycles in 15% MgCl ₂ solutions	129
Figure 7.13: Abrasion test surfaces of cored overlay cylinders after freeze/thaw and wet/dry cycles in 15% NaCl solutions	130
Figure 7.14: Gas permeability of various overlays after F/T and W/D cycles in 15% NaCl solutions.....	131
Figure 7.15: Gas permeability of various overlays after F/T and W/D cycles in 15% MgCl ₂ solutions	131

1.0 INTRODUCTION

1.1 PROBLEM STATEMENT

Currently, the Oregon Department of Transportation (ODOT) does not know the damaging effects that chloride deicers may impact on Oregon's concrete infrastructure over time. To maintain safe and productive roadways during the winter season, ODOT applies a magnesium chloride ($MgCl_2$) solution for snow and ice control in accordance with guidelines established by the Pacific Northwest Snowfighters Association and others. The corrosive effect of chloride on embedded steel reinforcement is well known; however, it is unclear whether deicers based on chloride salts deteriorate concrete. Laboratory studies using concentrated solutions to accelerate testing have demonstrated that magnesium chloride has the potential to damage concrete. However, field cores extracted from sites in Colorado, Idaho, Iowa, Montana, and South Dakota did not exhibit damage conclusively attributable to deicers (*Sutter et al, 2008*).

There is no known practical means to measure deicer exposure in order to focus on those bridges or components potentially at highest risk. The exposure to deicers at a specific site may depend not only on application frequency but also on other factors such as environmental and traffic conditions and bridge configuration. Deicer may be applied directly to a bridge deck or roadway, but other nearby concrete elements such as rails, barriers, and columns may be vulnerable due to splash. Consequently, not all bridges or concrete components (e.g., decks, beams/crossbeams, diaphragms, abutments, piers and piles) are expected to have the same likelihood of damage.

At the national level, the United States spends approximately \$2.3 billion annually to keep highways free of snow and ice. Associated corrosion and environmental impacts add at least \$5 billion each year (*FHWA 2005*). Every year approximately 20 million tons of road salt is applied on roadways in the United States for snow and ice control.

Without an idea of the potential damage induced by $MgCl_2$ deicer, there is no widely accepted strategy for protecting existing concrete structures and components. For managing the risk due to exposure to traditional sodium chloride ($NaCl$) deicer, there is existing research demonstrating the use of mineral admixtures (e.g., silica fume and slag) to improve the mechanical properties of concrete and effectively mitigate the distresses that pose risk to the concrete's durability. The use of proper air entrainment, high-quality cementitious materials and aggregates, and mineral admixtures is promising in minimizing the $NaCl$ impact on new concrete.

There is an urgent need for DOTs to identify and evaluate best practices and products for preserving the integrity and durability of concrete infrastructure in the presence of $MgCl_2$ or $NaCl$ deicers. As early as 1967, Yamasaki reviewed the use of surface coatings (e.g., linseed oil, epoxy paving cements, and silicones) to protect concrete from the damaging effects of deicers. Li and Su (*Li and Su 2010*) demonstrated that the use of an organosilicone coating on the concrete surface was able to "distinctly decrease the formation of cubic $NaCl$ crystals and microcracks

inside concrete,” accompanied by significantly less scaling and less loss in the dynamic modulus of elasticity after 56 freeze–thaw cycles in the presence of NaCl solution. Sutter et al. (*Sutter et al. 2008*) recommended the following strategies to mitigate the deleterious effects of deicers: 1) use less deicers; 2) use NaCl brines wherever possible; 3) use concrete sealants (e.g., siloxanes and silanes) and concrete mixtures with supplementary cementitious materials (SCMs, e.g., ground granulated blast furnace slag and coal fly ash). Van Dam et al. (2008) suggested that “better mixture design and proportioning, improved consolidation, and the timely and thorough application of an effective membrane-forming curing compound would prevent much of the distress observed” in concrete pavements at dedicated aircraft deicing facilities, where glycol-based deicers are used. Numbered lists should be consistent throughout the document on their indentation according to body text used, numbering format, and how they are used.

1.2 RESEARCH OBJECTIVES

The objectives of this project were to investigate the effects of chloride deicers on Oregon DOT concrete bridge decks and to identify and evaluate best practices and products to mitigate such effects in the State of Oregon.

1.3 ANTICIPATED BENEFITS

This research will provide useful guidance for assessing and mitigating the negative effects of chloride deicers on concrete bridge decks in Oregon and beyond, thus extending the service life of bridge decks and postponing their replacement. The recommendations from this study will provide information that the practitioners can immediately implement in their daily operations and in the overall bridge management program and/or bridge preservation program. With respect to damage from MgCl₂ deicer, the outcome from this project will allow ODOT to focus preservation dollars on those bridge components that will provide the largest benefit-to-cost value.

1.4 SCOPE OF WORK AND REPORT ORGANIZATION

To accomplish the proposed objectives, this project was designed to include multiple tasks as follows: (1) determine whether the accumulated application of MgCl₂ and sodium chloride (NaCl) deicers have caused significant damage to the concrete typically seen in the bridge decks maintained by the Oregon DOT and other DOTs; (2) quantify the chloride ingress from winter road operations and estimate the potential for damage to reinforced concrete; (3) develop a practical, on-site measurement method to assess the exposure of concrete components to chloride deicers; (4) create a tool to estimate current and future damage states due to applying MgCl₂ deicer; and (5) identify, test, and recommend methods of mitigating deicer-induced damage to existing concrete infrastructure in the State of Oregon.

The following chapter presents the ODOT case study on developing concrete bridge deck exposure maps. Chapter 3 presents the collection, examination and testing of field concrete cored from 12 selected ODOT bridge decks (dominantly exposed to MgCl₂ deicer), as well as those of field concrete cored from two Utah DOT bridge decks (dominantly exposed to NaCl deicer) and two Nebraska Department of Roads bridge decks (mainly exposed to potassium acetate deicer). Chapter 4 presents the development of a deicer exposure measurement method, and Chapter 5

presents the development of a damage analysis tool via modeling. Chapter 6 and Chapter 7 present the accelerated laboratory evaluation of surface treatments and overlays, respectively, for protecting concrete bridge decks from the combined attack by freeze/thaw cycling and chloride deicers. Finally, Chapter 8 summarizes the key findings from this work followed by recommendations for implementation by ODOT.

2.0 POTENTIAL DEICER EFFECTS ON CONCRETE BRIDGE DECKS: DEVELOPING EXPOSURE MAPS

2.1 INTRODUCTION

There are multiple dimensions to the use of chemicals for snow and ice control on roadways. These chemicals, referred to as deicers, are important tools used by roadway agencies to maintain a reasonably high level of service during wintery weather, as there are substantial implications in highway safety, reliability, and mobility (*Qiu and Nixon 2008, Usman et al., 2010, Shahdah and Fu, 2010, Shi 2010, Strong et al. 2010, Ye et al. 2013*). Yet, there have been growing concerns over the potential negative effects of such chemicals on the natural environment, transportation infrastructure and motor vehicles (*Ramakrishna and Viraraghavan 2005, Spragg et al. 2011, Fay and Shi 2011, 2012, Pan et al. 2008, Shi et al. 2009a, 2010a, 2012a, 2013, Özgan et al. 2013*). The U.S. spends approximately \$2.3 billion annually to keep highways free of snow and ice, and the associated corrosion and environmental impacts add at least \$5 billion to that cost (*FHWA 2005*). Currently, approximately 20 million tons of sodium chloride (NaCl) is applied on roadways each year in the U.S. for snow and ice control. Recent years have seen growing concerns over the corrosion and environmental effects associated with the use of such roadway deicers.

The corrosive effect of chlorides-based deicers on embedded steel reinforcement is well-known (*Jang et al 1995, Shi et al. 2010b*). The use of chemical deicers has also raised concerns over their potential negative effects on the performance and durability of concrete infrastructure (*Pigeon and Pleau 1995*). Physical mechanisms of attack by deicers can lead to damage of Portland cement concrete (PCC) in the common forms of scaling, map cracking, or paste disintegration (*Sutter, 2008*). Existing laboratory research also suggests that chloride deicers may have detrimental effects on concrete through their reactions with cement paste and/or aggregates and thus reduce concrete integrity and strength (*Neville 1995, Sutter, 2008, Shi, 2008, Shi et al. 2009b*). This, in turn, may foster the ingress of moisture, oxygen and aggressive agents (e.g., chloride anions) onto the surface of rebar or dowel bar and promote their corrosion in concrete (*Yu et al. 2010, Shi et al. 2011, 2012b, Liu and Shi 2012*).

Accumulative studies have been conducted in the laboratory setting, often in an accelerated manner, which reported the physicochemical deterioration of concrete as a function of deicer type and test protocol (*Sutter et al. 2008, Shi et al. 2010a, 2011, Fay and Shi 2011*). These results illustrate the complexity of this concrete durability issue and suggest that there is more than one mechanism at work. In a laboratory study, Shi et al. (*Shi et al. 2010a*) subjected Portland cement concrete (PCC) specimens to the joint action of freeze/thaw cycling and exposure to deicers diluted by 3:100 from their applied concentration. Each investigated deicer (chlorides, acetates, and formates) was found to not only exacerbate physical distresses in the PCC but also chemically react with some of the cement hydrates. The PCC specimens exposed to the diluted NaCl-based deicers exhibited the highest mass loss, whereas those exposed to the diluted magnesium chloride (MgCl₂)-based deicer exhibited the lowest mass loss. This implies

that the diluted NaCl solution severely aggravated the freeze/thaw damage of PCC, mainly through physical deterioration. In another laboratory study, Shi et al. (*Shi et al. 2011*) reported that nearly one year of continuous immersion to 8 wt.% commercial deicers (with NaCl, calcium chloride – CaCl₂, or MgCl₂ as the main freezing point depressant) at room temperature induced detectable changes in the chemistry and morphology of cement hydrates inside the concrete specimens. The PCC specimens exposed to the MgCl₂-based deicer exhibited the most reduction in compressive strength, whereas those exposed to the NaCl-based deicers exhibited much less reduction in compressive strength. This implies that the MgCl₂ severely degraded the integrity of PCC, mainly through chemical deterioration. In yet another study, the laboratory investigation using concentrated solutions to accelerate testing demonstrated that the MgCl₂-based deicer has great potential to chemically damage concrete, relative to the NaCl-based deicer. Nonetheless, the field cores extracted from selected concrete bridge decks (mainly two cores from each deck, one in Montana exposed to MgCl₂ deicers and another in South Dakota exposed to both NaCl and MgCl₂ deicers) exhibited some damage or distress but could not conclusively attribute those to the chemical attack by deicers (*Sutter et al. 2008*).

Thus far, there is little research on how the durability of concrete decks in the field environment might be affected by their exposure to the deicers. The exposure to deicers at a specific site may depend not only on application frequency but also on deicer type, environmental and traffic conditions. Hong and Hooton (*Hong and Hooton 1999*) revealed that “a good relationship exists between the depth of (sodium) chloride penetration and the square root of the number of (wet/dry) cycles”. It remains unclear whether the chemical or physical attack of ice control chemicals would lead to significant degradation of concrete infrastructure in the field environment, where the deicer/concrete interactions are complicated by many other factors at play (e.g., deicer dilution by precipitation, temperature cycling, wet/dry cycling, and mechanical loadings). In order to isolate the effect of a single factor (e.g., deicer exposure) on the durability of concrete, groundwork research is needed to establish a framework under which the relevant data can be identified, collected, integrated, and made ready for subsequent analyses.

In this context, this work presents a streamlined method of developing exposure maps that can be used to better understand the potential effects that deicer usage and other relevant variables may have on an agency’s concrete infrastructure. The ODOT was used as a case study to illustrate the processes, elements, and challenges in developing exposure maps.

2.2 METHODOLOGY

This work started with a survey of two relevant stakeholder groups, the ODOT winter maintenance managers and the ODOT regional bridge managers. The survey helped to achieve a high-level understanding of the current and past practices of ODOT practitioners in managing their winter roads and concrete bridge decks. Subsequently, a process was established to select decks that would represent the population of ODOT concrete bridge decks with various levels of age, winter severity (deicer usage), and traffic volume. Finally, relevant data were collected to develop the exposure maps for 12 selected representative ODOT concrete bridge decks. The data categories were the recent annual Average Daily Traffic (ADT) data and the percent of truck traffic; the number of freeze/thaw cycles estimated using the historical air temperature data from a nearby weather station; the bridge category, concrete mix design, and deck rehabilitation information from the ODOT bridge management system; the cumulative or annual deicer usage

data from past winter season(s); and the annual precipitation total. Ultimately, a graphic information system (GIS)-based map showing the estimated amount of deicers used on the selected ODOT concrete bridge decks (along with the other key parameters) was developed.

2.2.1 Bridge Deck Selection Process

To describe how specific bridge decks were selected for exposure maps, a guideline along with a flowchart (Figure 2-1: The Bridge Selection Procedure in a Flowchart) is provided in this section. In this case study, the deck selection avoided the coastal districts where chlorides from the marine environment may reach the deck and compromise the role of deicer-borne chlorides in the investigation. Decks without nearby weather station and decks that have been rehabilitated with a polymer sealer or microsilica overlay were also avoided, as the investigation focused on the effects of deicers on the PCC decks themselves.

By using the ArcGIS (or any other GIS software), a bridge geo-database was created to include the shape files of ODOT maintenance districts, highway functional classification, concrete bridges, and road weather information system (RWIS)/MesoWest weather stations, each with the required attributes available. Then, the bridge deck selection process was initiated following the steps detailed below.

Firstly, the ODOT maintenance districts were selected based on their geolocation and winter severity. Specifically, the districts along the coast were eliminated from the selection to avoid the possible effect of marine-borne chlorides. Then, the remaining districts were grouped into low or high winter severity based on their estimated deicer usage from past winter seasons. This information was obtained from the survey of winter maintenance managers. The cutoff level was set to an estimated deicer usage of 400,000 gallons per year.

Secondly, the bridge decks were further sub-grouped by the bridge age. Specifically, for the list of low-winter-severity concrete bridges, they were categorized according to their built year: 1996-2011, 1981-1995, and before 1980. This generated three table lists and their associated files. The same approach was applied to the list of high-winter-severity concrete bridges. Therefore, a total of six table lists and shape files were generated.

Thirdly, the bridge decks were further sub-grouped by the annual ADT. Specifically, the bridges within the aforementioned six lists were categorized based on its most recent annual ADT value. The cutoff level was set to 10,000. In the end, a total of 12 table lists and shape files were generated to group the ODOT concrete bridge deck population into 12 categories.

Fourthly, in each of the 12 categories mentioned above, only the bridges within 10-mile radius of a RWIS or MesoWest weather station were selected. Only one bridge was randomly selected from each of the 12 groups of remaining bridges. Colors were used to highlight the various group levels in Table 2-1 and Table 2-2. If the deck was overlaid with microsilica or rehabilitated with a polymer sealer, then it was eliminated and another random selection from the group was conducted. In the end, a total of 12 concrete bridge decks were selected, each representing one category of the ODOT concrete bridge deck population.

2.2.2 Data Collection for the Exposure Map Development

For developing the exposure maps to fully illustrate the factors that might have played a significant role in the properties and durability of ODOT concrete bridge decks, a wide array of data elements was collected for each specific bridge site, as detailed in this section. The bridge mix design, ADT, and other relevant bridge data were obtained from the ODOT bridge management system. For some agencies, the deicer usage data may be available from their maintenance management system. For this case study, the deicer usage data were not available in any digital form; instead, paper records were sorted before it was possible to estimate the amount of deicers used on the selected decks over the past winter seasons.

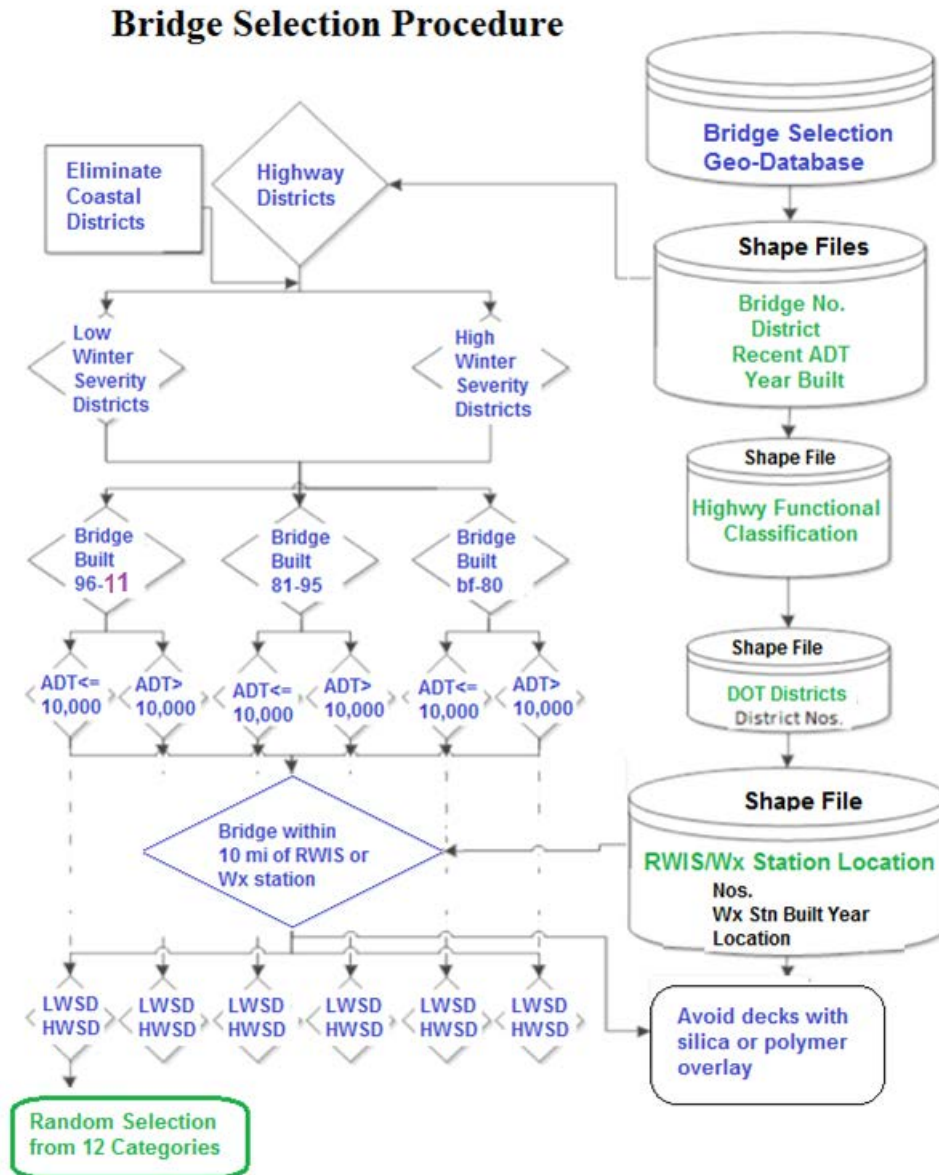


Figure 2.1: The Bridge Selection Procedure in a Flowchart

The number of annual freeze/thaw cycles for the selected bridge decks was estimated by dividing the number of times the ambient air temperature crossed the 0°C (32°F, freezing point of moisture) threshold by two. It is based on the fact that the surface temperature of bridge decks usually tracks the ambient air temperature more closely than do the adjacent roadway pavements (Roosevelt 2004). In this case study, hourly and sub-hourly historical air temperature data from a nearby weather station were utilized for estimating the number of annual freeze/thaw cycles. This approach is different from how hourly air temperature data from weather stations were utilized to determine the number of freeze/thaw cycles in the new mechanistic empirical pavement design guide (MEPDG) developed by the American Association of State Highway and Transportation Officials (AASHTO). In the latter case, a heat balance equation is used to simulate the freeze/thaw conditions in the pavement as a function of time (Zapata et al. 2007).

2.3 RESULTS AND DISCUSSION

2.3.1 Stakeholder Perspective: Winter Maintenance Managers

The 2011 winter maintenance survey was designed and distributed to understand the ODOT current and past winter maintenance practices. The questions covered the type of deicing, anti-icing or pre-wetting products used and their respective application rates, rules of practice, winter severity and road weather scenarios, annual deicer usage, and the possible negative effects of chloride deicers to winter roadways, etc. The ODOT is divided into five geographic regions with 16 maintenance districts. Each maintenance district has developed its own strategies to address the needed level of service for their winter highways. Eight out of the sixteen districts responded to this survey, which resulted in a 50% response rate. Figure 2-2 shows where the survey responses came from by district (as highlighted in purple).

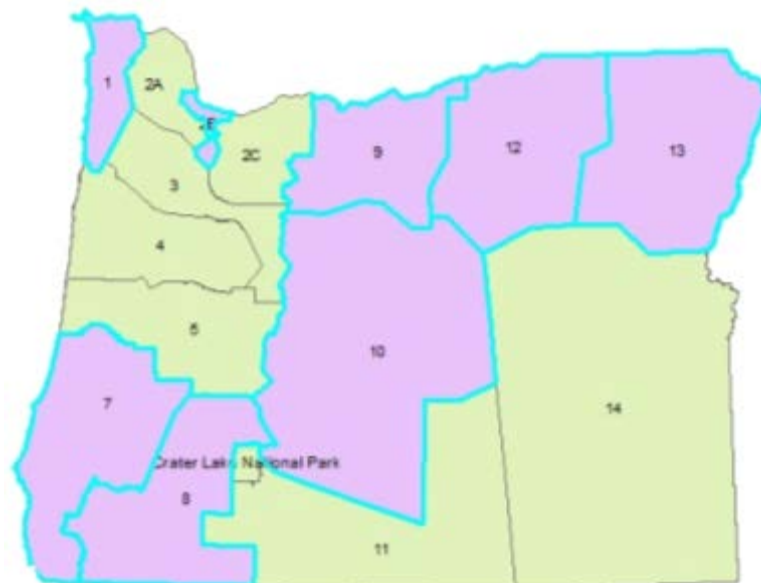


Figure 2.2: The Oregon DOT Districts that Responded to the Winter Maintenance Survey (Highlighted in Purple).

All the participating districts were using chemicals for anti-icing and deicing. With the exception of one district (D2B), seven out of the eight districts had used anti-icing as well as deicing for over ten years. Only one district (D10) used pre-wetting for less than ten years, while the other seven districts did not use pre-wetting at all. The primary chemical type used in all these eight districts was MgCl₂. Six of the eight districts reported a change in the type of chemical used in the past years. Some ODOT districts had used calcium magnesium acetate (CMA), until they successfully switched to the use of MgCl₂ over the past five to ten years. One district (D10) used CMA both in liquid and solid forms during 1998 to 2001, which did not work well with the colder climate. Consequently, a transition to MgCl₂ was made in 2002.

All eight ODOT districts had observed an increased usage of chemicals and attributed this change to the following facts: better understanding of advantages of the chemicals over sanding, higher level of service expectations, higher traffic volumes, and colder weather. Table 2-1 provides a comparison of winter maintenance practices of four selected districts based on the 2011 survey results.

Table 2.1: Winter Maintenance Practices of Selected Four ODOT Districts

Region/District	Primary Deicer Products	Maintained Lane miles	Typical Application Rates	Typical Winter Maintenance Season	Estimated Annual Deicer Usage/Cost*
R5/D12	MgCl ₂	1785 miles	Anti-icing and Deicing: 15-60 gal/ln-mi	November-April	500,000-750,000 gal/\$750,000
R3/D8	MgCl ₂	1700 miles	Anti-icing and Deicing: 9-30 gal/Ln-mi	November-April	608,695 gal/\$675,178
R1/D2B	MgCl ₂	1000 miles	Anti-icing and Deicing: 20-40 gal/ln-mi	November-March	300,000 gal/NA
R5/D13	MgCl ₂	1250 miles	Anti-icing and Deicing: 15-60 gal/ln-mi	November-April	300,000 gal/\$420,000

* Note that these are estimates provided by the survey respondents, which may deviate significantly from the actual numbers.

Most winter maintenance managers (seven out of the eight districts) did not consider chloride deicers to pose a significant risk or negative impact on the durability of concrete bridge decks. Only one district (D2B) reported moderately negative effect observed for concrete pavement and bridge decks. Most districts had observed little negative effect of ice control chemicals on the asphalt concrete or PCC pavements or concrete bridge decks. One district (D8) commented that ice control chemicals used correctly can provide safety and mobility benefits for the travelling public and are wonderful options in the toolbox (for highway winter maintenance operations).

2.3.2 Stakeholder Perspective Regional Bridge Managers

The 2011 bridge management survey was designed and distributed to understand the ODOT current and past winter maintenance practices in managing their concrete bridge infrastructure. The ODOT regional bridge managers oversee the design, construction, operation, and maintenance of the bridges located in the State of Oregon highway system using a centralized bridge management system. They regularly conduct inspections, assessment of condition and strength, repairs, and rehabilitation. As such, the bridge managers of the ODOT headquarters, Region 3, Region 4, and Region 5 were approached to achieve a high-level understanding of ODOT bridge management practices, with a focus on the potential effects of deicer exposure and freeze-thaw cycling on bridges decks. Among the five ODOT construction regions, Regions 1 and 2 did not respond to the survey as they featured mostly mild climate and rarely used deicers except on mountain passes

The bridge managers were asked about which external factors influenced the premature deterioration of concrete bridge decks in Oregon, including cracking, spalling, delamination or other forms of deterioration related to the concrete itself and/or rebar corrosion. A majority of ODOT bridge managers responded that freeze-thaw damage and chloride deicers contribute to the premature deterioration of ODOT bridge decks, while a consensus could not be reached on the level of influence posed by the chloride deicers. In addition, cracking caused by traffic loading, natural calamities (earth quake, fire, storm surge, flood, and excessive rain), spalling, and tire studs were also considered as external factors that contributed to the premature deterioration of ODOT bridge decks.

The ODOT bridge managers had started to consider chloride contamination as a factor in influencing the decision making for the maintenance, repair, and rehabilitation of bridge decks. In addition, the ODOT had changed the guidelines for concrete design and construction practices for concrete decks in the effort to prevent their premature deterioration. In the recent past, the following changes had been made:

- Adopted high-performance concrete mix with silica fume for decks,
- Increased use of thin bonded overlays and deck sealers, and
- Increased curing effort and time required for covering wet concrete (extended the total cure time from seven to fourteen days).

2.3.3 A Method of Developing Exposure Maps: ODOT Case Study

The results from the aforementioned ODOT surveys revealed a discrepancy in the perceived risk of chloride deicers to concrete bridge decks, between the winter maintenance managers and the bridge managers. This highlighted the need for a systematic study to investigate this issue, as it has lasting economic and environmental implications. Using the ODOT as a case study, this section presents a streamlined method of developing exposure maps that can be used to better understand the potential effects that deicer usage and other relevant variables may have on an agency's concrete infrastructure.

Bridge Selection: A total of 12 categories were identified through the bridge selection process described earlier (also shown in Figure 2-1). Then one representative concrete bridge deck from each identified category was selected to showcase the methodology of developing exposure maps. Table 2.2 lists the characteristics of 12 selected bridges, including their bridge number, geolocation, district, year built, ADT, and the nearby MesoWest station name.

Table 2.2: List of 12 Selected ODOT Highway Bridges

Deck Category	Bridge	Latitude	Longitude	Elevation	District	Year_Built	ADT_2008	MesoStation
1	19268	42.06269	-123.707	1700	2B	2005	003100	ODT25
2	19681	45.34397	-118.122	2900	13	2003	005454	ODT18
3	18940	45.61778	-122.807	100	2B	2002	020600	ODT06
4	18525	42.34202	-122.889	1360	8	2002	013500	ODT26
5	16534	45.54495	-122.678	270	2B	1985	009793	ODT10
6	16440	45.92242	-119.324	190	12	1985	008332	MWQUM
7	16358	45.54353	-122.674	270	2B	1986	012801	ODT10
8	16844	42.4294	-123.319	915	8	1990	029440	C5474
9	08958F	45.54397	-122.675	270	2B	1973	007790	ODT10
10	00576	42.4308	-123.043	1290	8	1927	006450	C3932
11	09268S	45.53261	-122.687	270	2B	1972	056700	ODT10
12	08682	42.28079	-122.815	1491	8	1962	014200	C2551

Mix Design Data:

The mix design of concrete plays a crucial role in its performance and durability in the service environment. As such, this is an important data set for investigating the premature deterioration of concrete bridge decks. An example of an ODOT deck concrete mix design is shown in Figure 2.3, which provides information on concrete proportioning (type and amount of cement and mineral admixtures; gradation, absorption and amount of fine and coarse aggregates; water-to-cement ratio) and properties of fresh concrete (slump and air content) and hardened concrete (density and compressive strength).

Average Compressive Strength: 47.1 Mpa @ 28 days

Cement	308 kg/m3	LEHIGH	Type I Redding CA
Fly Ash	142 kg/m3	HDWTRS	Class F Centralia
Microsilica	19 kg/m3	DEGUSSA/RHEOMAC SF-100	
19-4.75	1130 kg/m3 SSD	Gssd : 2.827 Abs : 1.2 %	Source : 17-103-3
4.75-0	634 kg/m3 SSD	Gssd : 2.779 Abs : 1.5 %	Source : 17-103-3 FM : 2.71
Water	139 kg/m3	W/C Ratio : 0.30	Slump : 150 mm
Air Content	6.0 %		
Density	2376.0 kg/m3		
	Air Entrainment Agent : Degussa/AE-90		
	Water Reducer :		
	HRWR Admixture : Degussa/Glenium 3000NS		

Figure 2.3: Example of ODOT Deck Concrete Mix Design

ADT Data:

The most recent annual ADT data were obtained from the ODOT bridge management system (as shown in Table 2.2). In addition, the data on the percent of (heavy) truck traffic in the ADT were collected, which do not include vans, pickup trucks, or other light delivery trucks.

Availability of Deicer Usage Data:

Complete records of ice control chemical applications were necessary to assess the relative level of deicer exposure for a given concrete deck. In this case study, manually recorded daily deicer rate data along with the relevant air temperature data were collected and checked for consistency in order to calculate the annual deicer application rate total for each bridge site. The ODOT deicer usage data were only available in daily records and in paper form, ranging from fiscal year (FY) 2000 to FY2011. The deicer most commonly used by the ODOT was shown to be magnesium chloride and it is still used exclusively statewide from FY2006. The log had application date/time, application rate (gallons/lane mile), pavement condition, and air temperature by the time of application recorded.

Quality of Deicer Usage Data: Proper chemical application rates for snow and ice control vary as a function of the pavement temperature characteristics and the type and volume of precipitation as well as the target level of service and the traffic volume. Application rates are determined by the current road conditions as well as the anticipated weather and road conditions, as stated by Martinez and Poecker (*Martinez and Poecker 2006*). According to the ODOT survey results, typical application rates for anti-icing and deicing ranged from 15 to 50 gallons per lane mile (9.6 to 32.2 mL/m²). As such, a preliminary range check was made to identify the extreme values for further examination. Less than 1% of the data were found problematic. Suspect values were then identified manually, and several approaches were employed to verify the values. For instance, the high application rates (e.g., 60 gallons/lane mile) might occur before a large snow event or freezing rain. When the air temperature was slightly below 32°F, there could often be wet snow, sleet, freezing rain, or a mix of all. In such worst icing conditions, the value for daily application rate might go up as needed. When the air temperature was very cold (e.g., below 19°F), the ice/snow was less slick and the traction could be better, hence requiring lower application rates of chemicals. Once validated, the daily application rate data were summarized to obtain the total deicer usage for each winter season.

Infilling the Missing Deicer Usage Data:

In this case study, a large number of missing deicer usage data occurred for four of the 12 selected bridge sites. These four bridges had six out of twelve years' deicer usage data missing. Under the assumption that all bridges were treated with MgCl₂ liquids since FY2006, incompleteness of the data would be a major barrier before a complete picture of deicer use on these bridge decks could be obtained. To address this challenge, the district level deicer usage data were obtained from the ODOT maintenance management system from FY2000 to FY2011. The districts of concern were Districts 2B, 8, 12, and 13.(Figure 2.4) These data were employed to determine the temporal trends of MgCl₂ use by these ODOT Maintenance Districts.

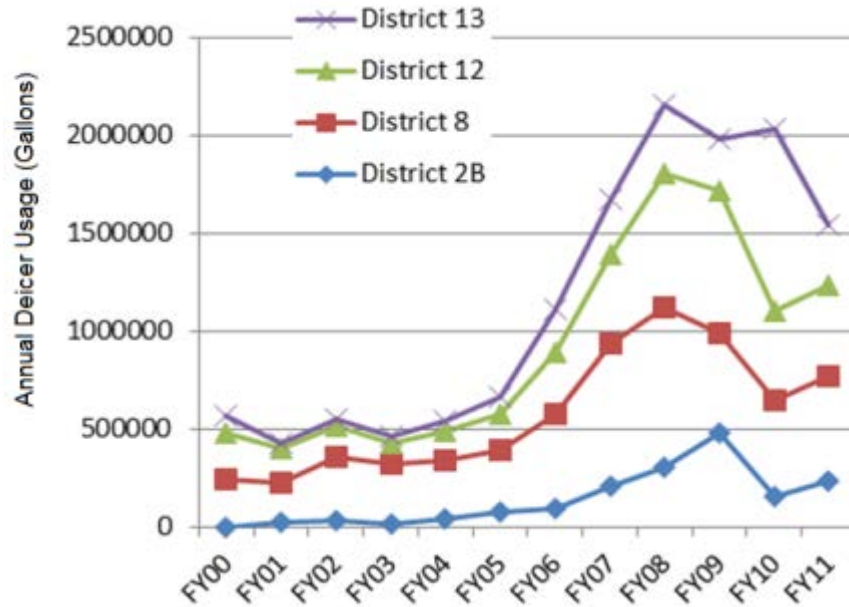


Figure 2.4: Annual Deicer Usage Data for the ODOT District 13, 12, 8 and 2B

Assumptions had to be made to address missing data for certain bridge decks: Figure 2.4 shows that the deicer usage in these four districts generally followed the same trend, with a gradual increase in the first six years (FY 2000 to FY 2005), followed by a sharp increase in the next four years (FY2006 to FY2009) and subsequent fluctuations in the recent years. Assuming that the temporal evolution of application rates on specific bridge decks followed the district-level trend, the deicer usage data for the missing years were infilled from the data from the existing years. Note that the chemical application rates are site-specific and depend on a variety of factors including type of deicer used, air and pavement temperatures, amount of snow on the ground, and steepness of the roadway (*Fischel 2001*). As such, the district deicer usage data should be considered as correlated information and not a statistical representation for the bridge site's actual deicer usage.

Freeze/Thaw Cycles Data:

Yet another influential factor is the number of freeze/thaw cycles that bridge decks were exposed to. The freeze/thaw cycling can pose a significant risk to the durability of concrete bridge decks; as such, cycling can lead to the physical deterioration of the concrete microstructure (*Shi et al. 2009b*). Laboratory studies have shown that the presence of deicers can aggravate the freeze/thaw damage of the concrete and chemically attack the cement paste and aggregate phases.

The severity of freeze/thaw exposure varies with different areas of Oregon. Local climatic records can help determine the severity of such exposure. In this case study, a total of nine MesoWest weather stations were close enough to the 12 selected bridge sites. Over a period of eleven years, more than 2.5 million records of historical air temperature data were collected from these weather stations. The reporting frequencies for these air temperature sensors were every

10, 15 or 20 minutes. The amount of missing data for all these selected weather stations was less than 5%.

Table 2.3 presents the summary of freeze/thaw cycles data of all the 12 bridges from FY2005 to FY2011, along with some other relevant data. To align with the other ODOT data, the freeze/thaw cycles data were estimated for each fiscal year. Based on the results, the freeze-thaw cycles tended to increase dramatically for areas with higher elevation (>1000 feet). For a missing winter season, the data could be infilled by the values calculated from a similar winter. More data and research would be warranted to potentially establish the annual number of freeze/thaw cycles as a function of geolocation (latitude, longitude, elevation). If such a function was established, it would greatly facilitate the infilling of missing data for a given bridge site with known geolocation.

Note that this method of using ambient air temperature to estimate the number of freeze/thaw cycles has its own caveats. It tends to substantially overestimate the actual number of freeze/thaw cycles that occurred inside the concrete, especially when the presence of deicer solution significantly reduced the freezing point temperature of the pore solution.

Bridge Deck Exposure Maps:

The exposure map for FY2011 was developed to provide a snapshot of the statewide exposure conditions for the 12 selected ODOT decks (see Figure 2.5). The underlying data structure was composed of bridge geolocation (latitude, longitude, and elevation), built year, category, ADT along with percent truck traffic, annual deicer usage in gallons per lane mile at the specific bridge, and estimated annual number of freeze/thaw cycles, as well as annual precipitation total. A table of deicer usage per year for each bridge is presented in Appendix A.

Table 2.3: Estimated Freeze/Thaw Cycles for Fiscal Years 2005 – 2011, along with Other Data for the Select Bridge Decks

Bridge No.	Elev. (ft)	2005	2006	2007	2008	2009	2010	2011	Average F/T Cycles*	Total Deicer Usage (gallons)	ADT (2008)
00576	1290	NA	NA	57	61	28	32	48	102	265	645
08958F	270	4	18	13	17	14	9	13	26	870	7790
08682	1491	39	37	49	79	76	54	55	119	4720	14200
09268S	270	4	18	13	17	14	9	13	26	870	56700
16844	915	NA	NA	52	60	41	22	49	90	1010	29440
16358	270	4	18	13	17	14	9	13	26	995	12801
16440	190	82	85	85	101	85	81	71	170	2315	8332
16534	270	4	18	13	17	14	9	13	26	1035	9793
18525	1360	38	60	49	66	70	47	23	93	1145	13500
18940	100	15	33	29	22	20	13	19	41	1600	20600
19268	1700	65	69	74	96	89	47	71	132	3405	3100
19681	2900	143	123	121	155	125	100	117	248	7145	5454

* Some bridge decks have historical weather data available for the years of 2003, 2004, and 2012, which are also utilized in calculating the number of F/T cycles.

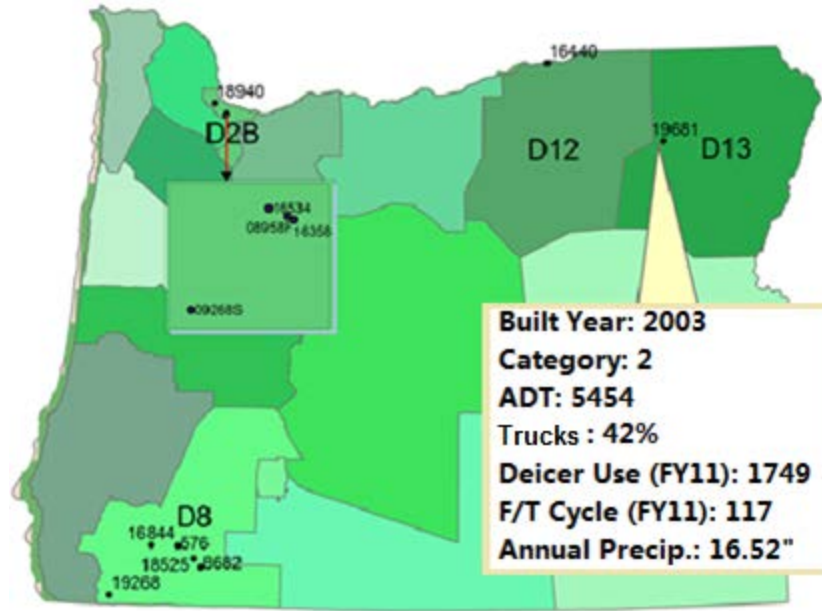


Figure 2.5: FY2011 Exposure Map for the 12 selected ODOT Bridge Decks

2.4 CONCLUDING REMARKS

Anti-icing strategy with $MgCl_2$ liquids has been widely used by ODOT districts and is believed to be very successful by participating winter maintenance survey respondents. Usage of ice control chemicals has generally been increasing during the past ten years due to colder weather, higher traffic volumes and higher level of service. This trend seems to be continuing and has raised some concerns regarding its negative effects on existing highway infrastructure. Nonetheless, the vast majority of the participating ODOT winter maintenance managers did not think that there has been any significant deteriorating effect of $MgCl_2$ on the ODOT concrete bridge decks. In contrast, a majority of bridge managers believed that freeze-thaw damage and chloride deicers both contribute to the premature deterioration of bridge decks, even though they disagreed on the level of influence. To address this potential risk, a few changes have been made by the ODOT in the concrete mix design and in the construction, maintenance, or rehabilitation practices for concrete decks.

This study, while focusing on examining the relevant data from Oregon, has demonstrated the general approach that other agencies could implement or adopt in developing exposure maps for their infrastructure. In order to investigate the root cause of premature deterioration of concrete bridge decks in cold climate, it is important to develop their exposure maps over time. Nonetheless, this study has revealed that currently agencies may not have complete and well-defined records of the relevant data. It is highly recommended that deicer type and application rate, traffic volume and truck traffic volume, road weather conditions (deck temperature, air temperature, precipitation, etc.), concrete mix design, and deck maintenance records be archived into an integrated bridge preservation program. Alternatively, such data should be added to the existing bridge management system. The inventory of such data would then enable agencies to

investigate the role of such variables in the durability of their concrete bridge decks and potentially alter their approach to winter maintenance operations and/or other practices accordingly.

This work unravels great challenges in data collection. Significant amount of historical air or deck temperature data are required to calculate the number of freeze/thaw cycles. Ideally, more detailed records on precipitation and traffic volumes would also facilitate the understanding of how weather, deicer, traffic, etc. might contribute to the premature deterioration of concrete bridge decks. Future study should examine how such exposure maps would facilitate decision-making, once sufficient data become available for data mining and statistical analyses.

3.0 EFFECTS OF DEICER EXPOSURE ON CONCRETE BRIDGE DECKS: A COMPARATIVE STUDY OF FIELD CORES EXPOSED TO POTASSIUM ACETATE, SODIUM CHLORIDE, OR MAGNESIUM CHLORIDE

Little research has been published on how the deterioration of concrete bridge decks in cold climate is affected by their exposure to deicers. Prior to this study, it remained unclear whether the chemical and/or physical attack of chemical deicers would lead to significant degradation of concrete infrastructure in the field environment, where the deicer/concrete interactions are complicated by many other factors at play (e.g., deicer dilution by precipitation, temperature cycling, wet/dry cycling, and mechanical loadings). Sodium chloride (NaCl) is the most commonly used freezing point depressant found in roadway deicers, whereas potassium acetate (KAc) is commonly found in airfield deicers and also used in fixed anti-icing systems on bridge decks (*Shi 2008; Li et al. 2013*). Prior to this study, NaCl-based deicers were known to pose a great risk in their corrosivity to metals (*Shi 2008; Li et al. 2013; Shi et al. 2013*), whereas KAc-based deicers were known to be non-corrosive to mild steel yet corrosive to galvanized steel (*Fay et al. 2013*), potentially cause depletion of oxygen in the water and soil (*Fay et al. 2011*) and may induce alkali silica reaction (ASR) in reactive aggregates (*Balachandran et al. 2011; Sujay et al. 2011; Truschke et al. 2011*). Following the SHRP H205.8 laboratory test, the diluted KAc deicer was found to cause less severe freeze/thaw damage in the PCC specimens than the diluted NaCl deicer (*Shi et al. 2010*).

In this context, this work reports a comparative study of field cores taken from bridge decks in three different states that have been exposed to different deicers.

3.1 METHODOLOGY

3.1.1 Field Sampling

For each state, a few field bridge decks were examined for possible concrete coring to support this investigation. The selection process considered factors such as deck age, cumulative deicer usage, traffic volume, and data availability. As detailed in Chapter 2, 12 concrete decks were selected for the State of Oregon. For Utah and Nebraska, two concrete decks were selected for each State. In all three states, the concrete coring and part of the data collection were conducted by the staff of the departments of transportation. For each selected deck, six to twelve concrete cores were extracted. Note that these decks feature significantly different deicer usage and climatic conditions. By design, this helps to shed light on the effects of deicer type and other factors on the durability of concrete decks in different service environments. For the state of Oregon, the coring occurred in randomly selected deck locations and avoided locations with severe cracking so as to ensure reasonable structural integrity of core specimens. For the state of Utah, the cores were taken in the shoulders of the two decks to avoid travel lane damage and not

directly at locations with apparent signs of surface distress. For the state of Nebraska, the coring generally focused on deck locations with signs of surface distress.

The condition of the concrete cores was assessed following procedures for performing petrographic examination of hardened concrete samples (e.g., ASTM C856-2013). For the majority of the deck cores, no significant deterioration was apparently visible other than surface scaling. In other words, there were generally no signs of significant longitudinal, transverse or diagonal cracking and no evidence of visible precipitates. The only exception was for the Nebraska deck cores, which showed signs of microcracking due to ASR.

3.1.2 Laboratory Testing

Compressive strength:

The compressive strengths of the cored concrete cylinders were determined following the standard test method ASTM C39-2014 for Compressive Strength of Cylindrical Concrete Specimens. For the ODOT specimens, the linear portion of the stress-strain curve from this test was also used to calculate the modulus of elasticity (a.k.a., Young's modulus) of the concrete cores. In general, compressive strength tests are used for quality control, acceptance of concrete and estimating concrete strength for the specified length.

Before testing, the cored concrete cylinder was surface-ground on both ends and then polished with fine silicon carbide paper, so as to ensure a uniform surface finish (and thus a uniformly distributed compressive load). The flattened cylinder was then placed in a hydraulic Material Testing System (MTS Model 880) equipped with two spherical bearing blocks with hardened surface. A compressive load of 100 pounds per second was applied uniformly until the failure of concrete core. During the loading process, the load and displacement data were automatically recorded with a frequency of 1Hz. The ultimate compressive strength was then calculated by dividing the load at failure by the cross-sectional area resisting the load. The test results are the average of three cores taken from the same bridge deck.

Splitting tensile strength:

The tensile strength is very important with respect to cracking, shear capacity, anchorage capacity, and durability. The splitting tensile strengths of the concrete cylinders cored from the three states were determined following the standard test method ASTM C496-2011 for Splitting Tensile Strength of Cylindrical Concrete Specimens. This method was performed to evaluate the shear resistance provided by concrete.

The test method consisted of applying a diametrical compressive force along the longitudinal axis of the cylindrical concrete cores at a rate of 25-50 pounds per second. Two thin pieces of plywood were placed along the longitudinal axis of the concrete cylinder and the compressive load was evenly distributed.

Figure 3.1 shows the setup of the splitting tensile strength test. The load was applied uniformly until the failure of concrete core (typically split in half) and the maximum load at the failure was recorded and used to calculate the splitting tensile strength as follows.

$$STS \text{ (psi)} = \frac{P \cdot C}{\pi \cdot L \cdot D} \quad (1)$$

Where:

P = Load at failure (lb)

C = Estimated length of contact on the top and bottom (for un-scaled specimens, C = 2; but significantly scaled specimens would feature lower contact areas)

L = Length of specimen (in.)

D = Diameter of specimen (in.)

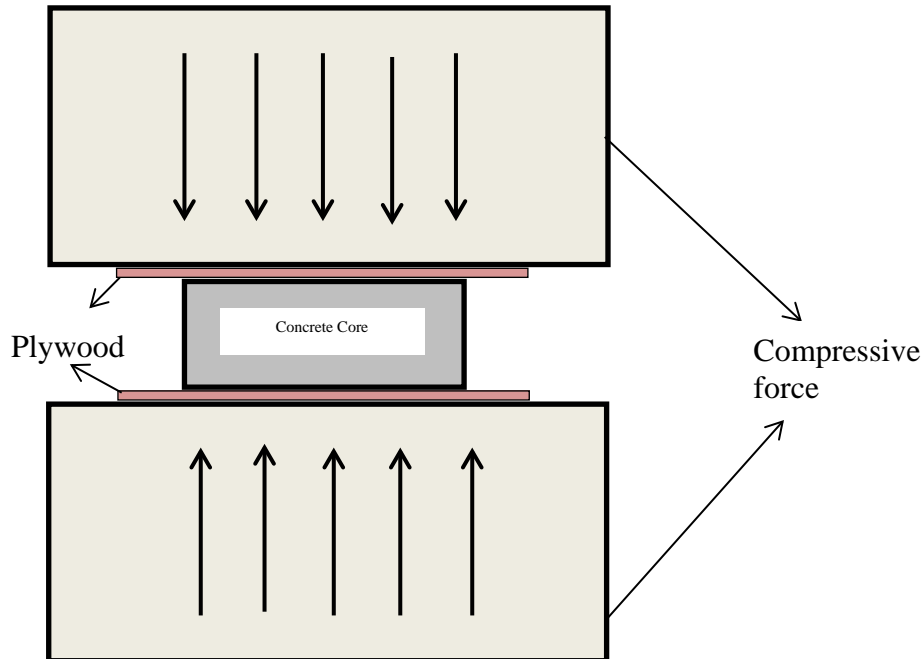


Figure 3.1: The setup of the splitting tensile strength test.

Microhardness:

Microhardness is an approach to evaluating the mechanical properties of brittle materials from a microstructural perspective. This technique entails applying a static load on a polished specimen surface for a certain period of time followed by measuring the size of the indented marks to evaluate the microhardness of the tested spot on the specimen. In this study, small specimens of $36 \times 12 \times 12 \text{ mm}^3$ were cut from the original cores extracted from the bridge decks using a water-cooled saw. Subsequently, the specimens were placed in an oven at 60°C for 24 h. Then, the surfaces were polished using #320, #600, #1000, and #1500 grit sandpapers, respectively. A Digital Vicker's Microhardness Tester (Shanghai Highwell Opto-electronic Technology-HXS-1000AY) was utilized for the measurements. During the loading process, 0.25N was applied and held for 10 s. For each sample, four depth levels, 2-5mm, 15-20mm, 25-30mm and 50-60mm from the deck's driving surface were chosen for testing in order to examine the microhardness of

paste and interfacial transition zone (ITZ) as a function of concrete depth. By design, this aims to illustrate the potential effect of deicer exposure and other factors on the microhardness of the concrete phases. For each depth level, the microhardness was measured for at least 60 spots randomly selected from 3 different paste areas. Similarly, a coarse aggregate with diameter larger than 5mm was selected at each depth, and the microhardness was then measured for at least 60 spots randomly selected from the ITZ around this aggregate.

Chloride penetration:

Chloride penetration resistance is important to bridge decks as the reinforcing steel is susceptible to chloride-induced corrosion. The rebar is often placed with a minimum clear cover of concrete to limit the chloride contact. Over time the chloride ions from marine environment or snow and ice control operations can penetrate into the concrete and initiate the corrosion of rebar once their concentration at the rebar depth exceeds the threshold limit.

To measure the depth of chloride penetration, the Mautzsch procedure (*Baroghel-Bouny 2007*) was utilized. To reveal the depth of chloride penetration, the concrete core sample was first stained with silver nitrate (0.1N AgNO₃) solution followed by potassium chromate. After staining, the relatively yellow areas indicate the presence of high chloride concentration (as shown in Figure 3.2), whereas the relatively red or brown areas indicate little chloride concentration. As such, this semi-quantitative method allows the measurement of the depth of chloride penetration.



Figure 3.2: Example of chloride penetration in an ODOT concrete sample

Alkali-Silica Reactivity detection:

In order to detect the presence of possible ASR in the concrete cores, the concrete samples were stained with sodium cobaltinitrite and rhodamine-B solutions. After the staining, the yellow color represents the K-rich or Na-rich areas of higher alkali concentration (more ASR), whereas the

pink color represents the Ca-Si-rich areas of lower alkali concentration (less ASR). A significant yellow color near a coarse aggregate would suggest the presence of ASR. The test procedure involves cutting the concrete sample into two-halves using a saw-blade cooled with de-ionized water. The samples were subsequently polished with #50, #100, #120, #250, #400, and #600 grit sandpapers. The polished concrete samples were then sprayed with sodium cobaltinitrite solution and held for 30 to 60 s. Subsequently, the surface was rinsed with de-ionized water and dried with a paper towel until the surface saturated condition was achieved. Then the surface was stained with Rhodamine-b solution for 30 to 60 s. After this process, the surface was rinsed with de-ionized water and blotted.

Carbonation determination:

The carbonation of the concrete cores was determined by the phenolphthalein test. This procedure entails the staining of concrete samples with a phenolphthalein solution that in turn converts the concrete surfaces into pink color. The dark pink color indicates the absence of carbonation and light pink color indicates the presence of carbonation. The phenolphthalein solution was prepared by mixing isopropanol with 0.5% of phenolphthalein. The test procedure involves cutting the concrete sample into two-halves using saw-blade cooled with de-ionized water. The samples were subsequently polished with #50, #100, #120, #250, #400, and #600 grit sandpapers. The polished concrete samples were then sprayed with phenolphthalein solution and held for 20 s. The surfaces were then blotted with paper towel.

Air voids test and petrographic analysis:

The air-void characteristics of the polished concrete cores were assessed in accordance with the Standard Test Method ASTM C457-2012 for Microscopical Determination of Parameters of the Air-Void System in Hardened Concrete. In this process, the concrete cores were cut into two-halves and polished as mentioned in the phenolphthalein test. A black color permanent marker was used to dye the entire polished surface. Once the surface was dyed with black color, a white color powder (cornstarch) was applied on the surface to fill the air voids. The surfaces were then scanned with a 4800-dpi high resolution scanner. Subsequently, a stereo-optical microscope coupled with a movable stage was utilized to determine the volumetric fraction of the air voids and other phases in the concrete. A customized MATLAB program was developed and utilized to analyze the image records, from which the key parameters of the air-void system (spacing factor, specific surface area, and volumetric air content) were determined for each tested concrete core sample.

Water absorption:

The concrete samples extracted from the bridge decks were cut parallel to the road surface at a depth of 38 mm (1.5 inch) as shown in Figure 3.3. This was designed to assess how the deicer contamination in the concrete affects its water absorption capacity. The water absorption properties of the concrete cores were determined following the Standard Test Method ASTM C642-2013 for Density, Absorption, and Voids in Hardened Concrete.

In general, the concrete core sample was dried in an oven to obtain its oven-dry mass. The saturated-mass after immersion was obtained by immersing dried cores into room temperature

water followed by immersion into boiling water and subsequently natural cooling. The immersed apparent mass was determined by weighing the concrete core sample immersed into the water by wire. These different mass data were used to calculate the water absorption of each tested concrete core sample.

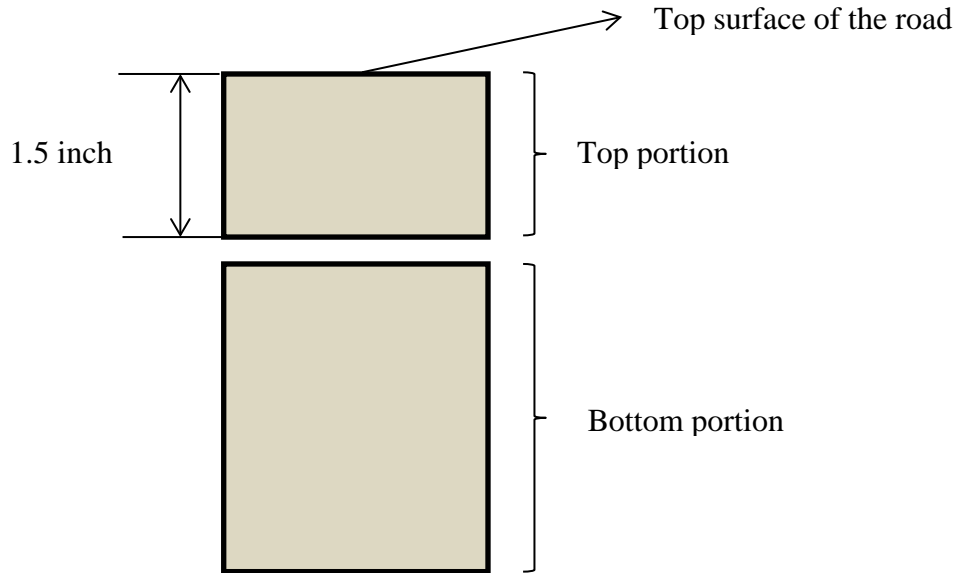


Figure 3.3: Cutting of Samples for Absorption Test.

Gas permeability test:

The gas permeability test was performed using liquid methanol as the gas source to determine the gas transport properties of select ODOT core samples. The test was also performed for select concrete samples fabricated in the laboratory and exposed to the combined effect of F/T cycles and chloride deicers. A schematic of the gas permeability test setup and the associated calculations for the gas permeability coefficient k (m^2/s) are detailed in Chapter 6.

Microscopic characterization:

The surface morphology of select ODOT core samples was observed by scanning electron microscopy (SEM), performed on an FEI-Quanta 200F scanning electron microscope. SEM was conducted under an accelerating voltage of typically 20 kV. The SEM was coupled with an energy-dispersive X-ray spectroscopy (EDS) analyzer. For EDS, a micro-analytical unit was employed to detect the small variations in trace element content, using an accelerating voltage of typically 15-20 kV and a scan time of 60 s per sampling area.

3.2 RESULTS AND DISCUSSION: A COMPARATIVE STUDY OF UTAH AND NEBRASKA DECKS

In the field environment, the deicer effects may vary widely with conditions, such as curing condition, moisture, mix design, and type of deicer (*Rónning 2001*). These conditions will affect not only the degree of saturation condition of the concrete, but also the pore structure and its transport properties. The deterioration of the concrete is governed by multiple factors such as the deicer concentration, temperature variations, and specific traffic loading. Julio- Julio-Betancourt (*Julio-Betancourt 2009*) also claimed that the combination of the chemical attack and mechanical loading are the most likely mechanism underlying the field deterioration of concrete structures.

This case study sheds some light on this complex issue of concrete durability in cold climate and raises the awareness over the risk of using KAc deicers on concrete.

3.2.1 Historical Information of the Bridges

Table 3.1 lists the historical data of the bridge decks in this study. As can be seen in this table, in the State of NE, the annual quantity of the liquid KAc deicers applied in the past three years was 0.19 gallon/ft² (7,606 mL/m²) on the bridge 18181L and 0.31 gallon/ft² (12,631 mL/m²) on the bridge 20100L. In the State of UT, the annual quantity of the solid NaCl deicers applied on bridge 744 and 749 over the past three years were 0.74 and 0.92 lbs/ft² (3,613 and 4,491 g/m²) respectively. The average annual number of freeze/thaw cycles in the past three years was about 108 and 262 for NE and UT decks, respectively. Note that the number of freeze/thaw cycles was estimated from the number of times the ambient air temperature crossed the 0°C threshold (divided by two). This method may overestimate the actual number of freeze/thaw cycles that occurred inside the concrete, especially when the presence of deicer solution significantly reduced the freezing point of the pore solution.

Table 3.1: Historical information of the decks exposed to different deicers in UT and NE

Bridge Deck Core ID	Year built	Year reconstructed	Average F/T cycles in recent 3 years	Average deicer usage in recent 3 years	Average Daily Traffic	Condition rating
NE-SO80 18181L ⁺	1964	1989	114	0.19 gallon/ft ²	7,098	8
NE-SO80 20100L ⁺⁺	1964	2000	102	0.31 gallon/ft ²	7,085	7
UT-744 [*]	1989	-	229	0.92 lbs/ft ²	4,145	7
UT-749 ^{**}	1999	-	295	0.25 lbs/ft ²	5,560	6

The NE cores were taken at deck locations with signs of surface distress. ⁺ North Platte Interchange with the mix design: type I cement, w/c ratio 0.41, average air content 5.3%, 28-day compressive strength of 4000 psi; ⁺⁺ 2E Brady Interchange with the mix design: type I/II cement with 17% class C fly ash, w/c ratio 0.41, average air content 5.8%, 28-day compressive strength of 4000 psi. Both NE decks used 30% Ledge rock aggregate (limestone, no ASR risk) and 70% North Platte river sand and gravel aggregate (highly ASR reactive).

The UT cores were taken in the shoulders of the two decks to avoid travel lane damage and not directly at locations with apparent signs of surface distress. The aggregates used in UT decks are not typically reactive and the specifications also require a minimum of 20% fly ash to mitigate any potential risk of ASR. * Cores 742-747 came from deck shoulders of our Bridge ID: 0C-751, SR-248 MP 14.19, Weber-Provo Diversion Canal Bridge, Kamas. ** Cores 748-753 came from deck shoulders of our Bridge ID: 0F-608, SR-140 MP 0.41, Jordan River Bridge on 14600 South, Bluffdale.

3.2.2 Mechanical Properties

Compressive and splitting tensile strengths:

The compressive and splitting tensile strengths of the bridge deck cores are listed in Table 3.2. As can be seen from this table, the average splitting tensile strength of the UT samples, 7.0 MPa (1000 psi), was about twice as high as those of NE, 3.4 MPa (500 psi). The average compressive strength of the UT samples, 31.0 MPa (4500 psi), was also much higher than those of NE, 22.8 MPa (3300 psi). These results suggest that the UT decks exposed to NaCl deicers feature minimal strength loss in locations without apparent sign of surface distress. In contrast, the NE decks exposed to KAc deicers feature significant strength loss in locations with signs of surface distress.

Table 3.2: The compressive and splitting tensile strengths of the cored bridge deck samples

<i>Compressive strength</i>											
NE-SO 80 18181L						UT-744					
Sample	Load (lbs)	Length (in)	L/D	Correction Factor	Strength (psi)	Sample	Load (lbs)	L (in)	L/D	Correction Factor	Strength (psi)
1	8360	3.852	1.94	1.00	2689	1	43080	4.924	2.48	1.00	3428
2	14430	3.832	1.93	0.99	4637	2	66310	3.806	1.92	0.99	5277
NE-SO80 20100L						UT-749					
Sample	Load (lbs)	Length (in)	L/D	Correction Factor	Strength (psi)	Sample	Load (lbs)	L (in)	L/D	Correction Factor	Strength (psi)
1	10790	3.989	1.99	1.00	3484	1	54400	5.043	1.26	0.93	4329
2	7900	3.979	1.98	1.00	2550	2	60260	4.875	1.22	0.92	4796
<i>Splitting tensile strength</i>											
NE-SO80 18181L						UT-744					
Sample	Load (lbs)	Length (in)	Diameter (in)	Strength (psi)	Sample	Load (lbs)	L (in)	D (in)	Strength (psi)		
1	6380	3.285	2.000	618	1	14690	3.956	3.945	1169		
2	5200	3.707	2.000	447	2	12320	3.975	3.796	980		
NE-SO80 20100L						UT-749					
Sample	Load (lbs)	Length (in)	Diameter (in)	Strength (psi)	Sample	Load (lbs)	L (in)	D (in)	Strength (psi)		
1	6350	3.981	2.000	508	1	15800	4.718	4.001	1258		
2	5060	3.982	2.000	404	2	16570	4.322	3.975	1319		

Microhardness: Figure 3.4 demonstrates box plots of the microhardness distribution of the interfacial transition zone (ITZ) and paste zone of the concrete cores extracted from NE and UT. As can be seen from this figure, the average value of the microhardness in the ITZ area of the UT cores was about 18% higher than the microhardness of the NE cores at the top of the samples (2-5 mm). Due to the high variability in each group of microhardness values, the difference in their

top surface ITZ microhardness may not be statistically significant. The microhardness values in the paste of the UT cores were significantly higher than those found in the paste of the NE cores in this area and remained a relatively stable average around 60 MPa (8,700 psi) from the top down to more than 50 mm deep into the concrete. In contrast, for the NE cores the average value of the microhardness sharply increases from about 40 to 65 MPa (5,801 to 9,427 psi) from the top down to about 15 mm and then remains relatively stable deep into the concrete. These results suggest that the exposure to KAc deicers negatively affected the microstructure and integrity of the top surface of the NE concrete decks, especially the cement paste phase.

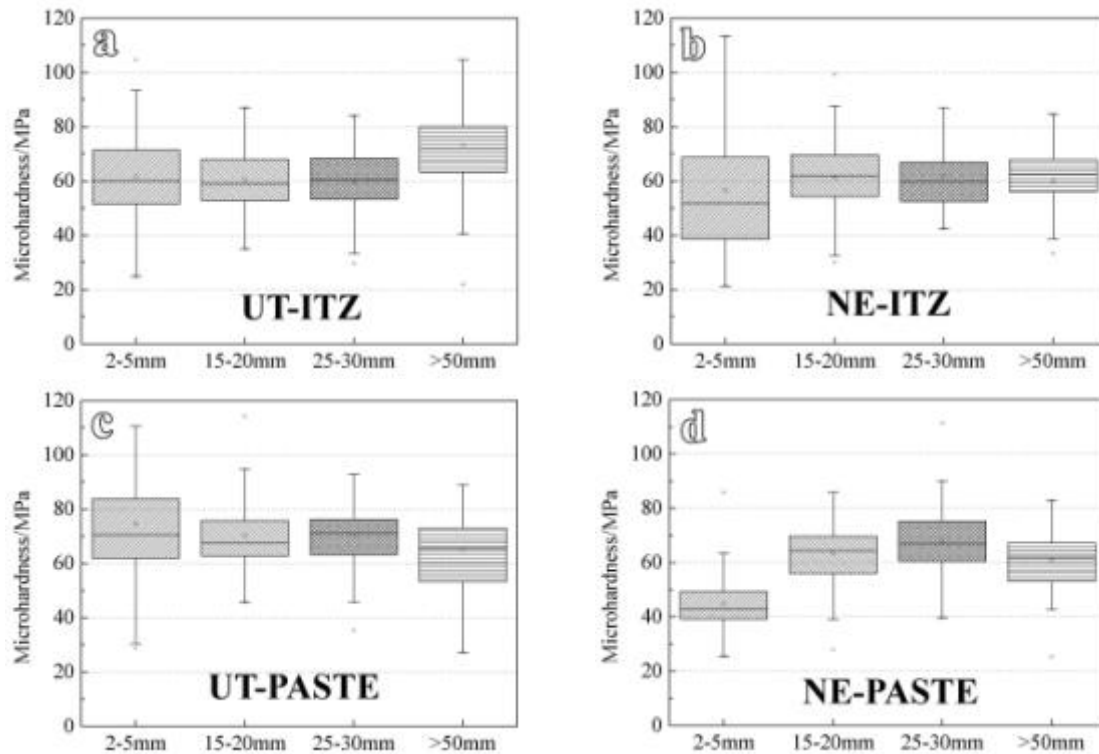
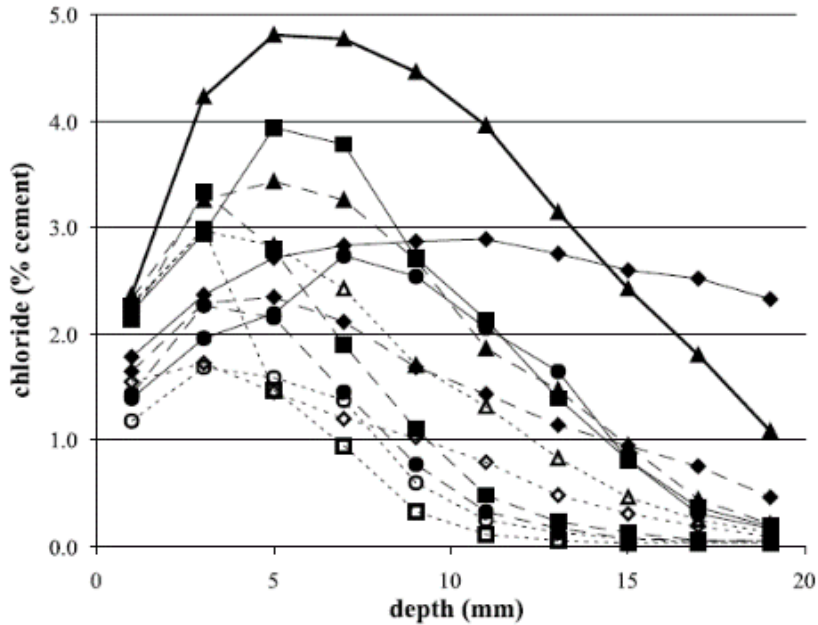
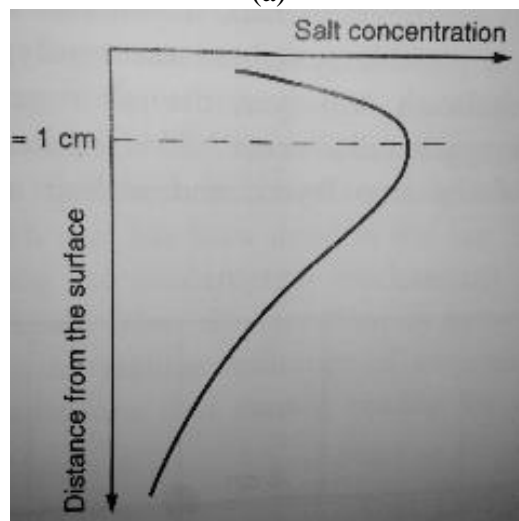


Figure 3.4: The microhardness distribution of the core samples from the concrete bridge decks: a) ITZ area (UT), b) ITZ area (NE), c) paste area (UT), and d) paste area (NE)

Note that the deicer chemical concentration gradient from the surface to the center is governed by two factors. First, the chemically bound deicer (e.g., bound chloride) can be released as a result of surface carbonation and/or diluted by the wetting of the concrete surface. As such, the highest deicer concentration is often not observed on the very top surface of concrete but often 5 to 10 mm beneath it (see Figure 3.5). As with further increase of concrete depth, the concentration of the deicer chemicals will decrease due to the diffusion gradient. Second, during the summer time, the chemical reaction rate will be faster than in winter season, which leads to more serious ASR reactions in the bridge decks using KAc as deicer.



(a)



(b)

Figure 3.5: Typical chloride concentration in profile in (a) laboratory concretes after 26 weekly cycles of 24-h wetting in 3% NaCl solution and 6-d drying in 20°C, 50% RH (*Polder and Peelen 2002*); (b) field concretes subjected to periodical salt applications (*Rösli and Harnik 1980*).

3.2.3 Transport Properties of Cored Concrete Decks

Chloride penetration:

The depth of the chloride penetration is related to the pore structure of the concrete paste matrix (*Stanish 1997*). The main pathway for chloride to enter the concrete structure is through the capillary pores or microcracks when the surface of the concrete is repeatedly wetted and dried.

After the chloride has penetrated into the concrete due to the above mentioned mechanism, diffusion allows for deeper penetration.

Figure 3.6 shows the image of the concrete samples that represents the extent of chloride penetration in the cores extracted from NE and UT, respectively. Table 3.3 further quantitatively lists the chloride penetration depth of the samples from the two states. As demonstrated in Figure 3.6, there is a clear difference between these two samples, and from the quantitative analysis, the chloride penetration depth is much higher in UT than in NE. The chloride penetration in the NE deck cores may be attributed to the chloride deicers applied on the roadways adjacent to the bridge deck and carried on to the deck by traffic.

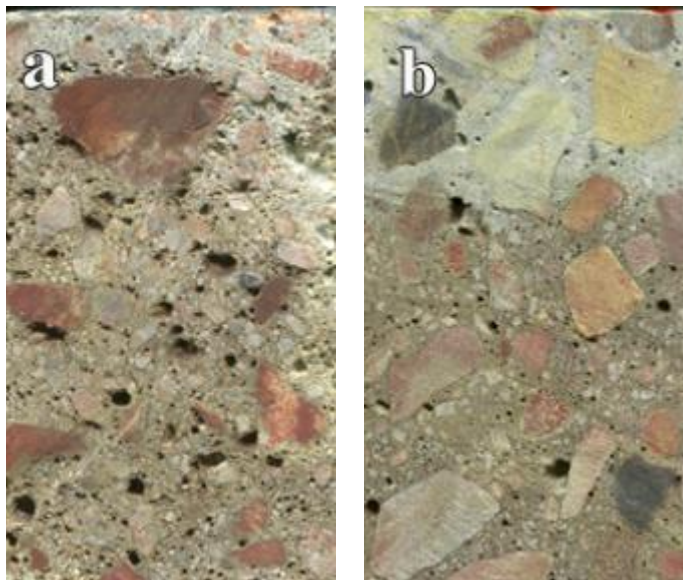


Figure 3.6: Cl⁻ penetration staining test results of cores from a) NE and b) UT

Table 3.3: Chloride penetration depth of the bridge decks in UT and NE

Bridge Deck Core ID	Cl ⁻ penetration depth
NE-18181L	0 & 0.65 inches
NE-20100L	0 inch
UT-744	1.40 inch
UT-751	1.25 inch

Carbonation and air void characteristics:

The phenolphthalein test did not reveal any significant sign of carbonation for the core samples extracted from the two UT decks and the two NE decks.

Figure 3.7 shows the original scanned and after treated images of a typical sample. The contrast difference of the air-voids (white color), cement paste, and aggregates (black color) were illustrated clearly. The images were processed using a customized MATLAB program to find the percentage of the air-content and other parameters associated with the air-void system. Note that these parameters were obtained from a limited number of 2D profiles and thus may not accurately represent the actual characteristics of the 3D concrete microstructure in each bridge deck investigated.

Table 3.4 provides the parameters calculated using the air-void test based on the images such as those shown in Figure 3.7. The quantitative analysis showed that the paste content was about 39% in UT and 63% in NE. The spacing factor was about 0.0020 ± 0.0001 inches (51 ± 3 microns) for all decks, implying similar resistance to F/T of their air void systems. All the cored decks exhibited a proper air-void system for freeze-thaw resistance as their spacing factor remained well below 200 microns per the ASTM C457 test method. The spacing is a simplified measure of the theoretical maximum distance from any point in the paste to the nearest void. The F/T resistance of a concrete sample is directly related to the amount of paste that is located in the beneficial zone of influence, the area near and around the air voids, of one or more air voids (*Hover 2006*).

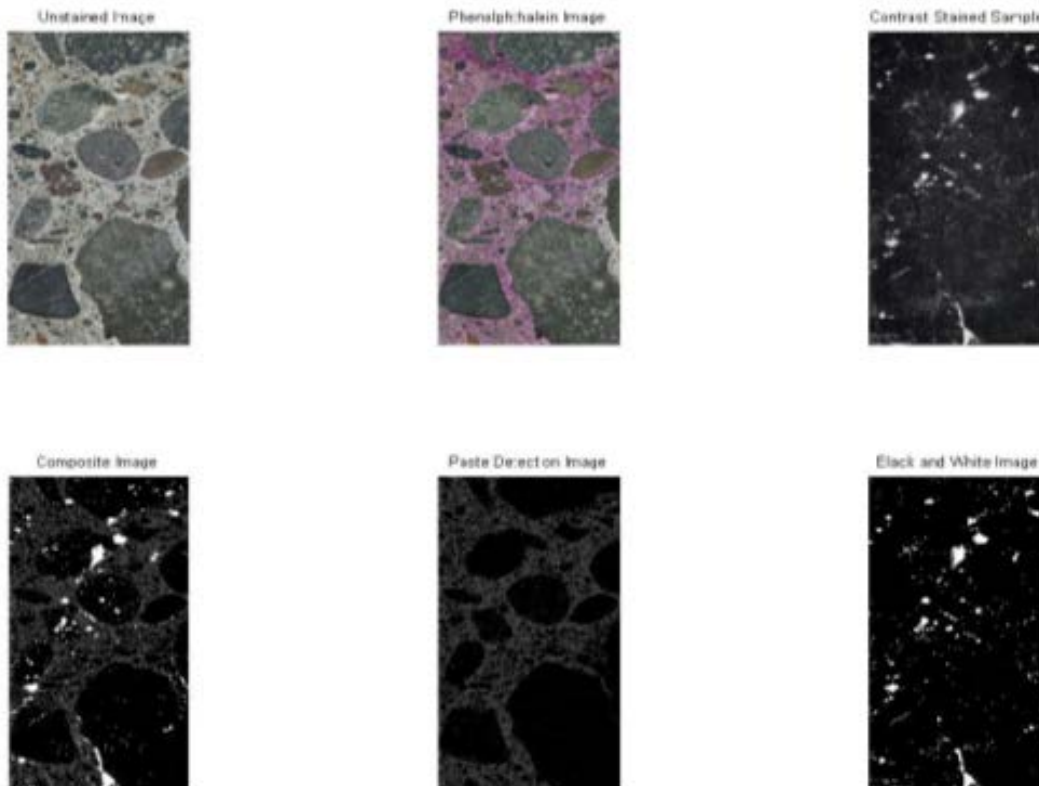


Figure 3.7: the image of a core sample processed for phenolphthalein and air-void tests

Table 3.4: The air void characteristics of the bridge deck samples from UT and NE

Bridge Deck Core ID	Air Content	Paste Content	Spacing Factor (inches)	Paste to air ratio	Specific surface (inch ⁻¹)
NE-SO80 18181L	8.2 %	61.4 %	0.0020	7.5	2743
NE-SO80 20100L	7.5 %	63.9 %	0.0022	8.6	2743
UT-744	7.5 %	39.0 %	0.0015	5.2	3200
UT-749	2.5 %	38.3 %	0.0032	15.4	2400

It is interesting to note that while the cores from the two NE bridge decks featured similar air void characteristics (in terms of air content, paste content, spacing factor, and specific surface as shown in Table 3.4), the cores from deck NE-SO80 20100L exhibited a significantly lower average gas permeability coefficient (1.68×10^{-16} m²/s) than those from deck NE-SO80 18181L (6.90×10^{-16} m²/s). This may be attributed to the presence of less ASR-induced cracking in the former, which used type I/II cement with 17% class C fly ash in place of type I cement.

The difference in the paste to air ratios of UT and NE deck cores was not statistically significant (10.3 ± 5.1 vs. 8.0 ± 0.6). The paste to air ratio can be used as an index for the strength of the concrete. Concrete with higher paste to air ratio tends to have higher strength whereas concrete with lower paste to air ratio tends to have lower strength if all other characteristics can be neglected (*Hover 2006*).

The results show that the specific surfaces were 2743 and 2800 ± 400 inch⁻¹ and the air contents were 7.9 ± 0.3 % and 5 ± 2.5 % for NE and UT decks, respectively. In other words, there was no significant difference between their specific surfaces, but one UT deck (UT-749) might have had less entrapped air. The specific surface is a measure of the size of the air voids. This measure is based on the ratio of total air void surface area to total air volume, and its limitations lie in the use of one single value to characterize the total range of air void sizes throughout the concrete sample.

Water absorption:

The water absorption performance is considered an indicator of the degradation resistance of concrete under various exposure conditions, as much of this degradation is associated with the ingress of moisture into the hardened concrete. Spragg et al. (*Spragg 2011*) found that the presence of deicers in field samples affected the absorption performances when field samples were tested in a laboratory scale.

Table 3.5 lists the water absorption and pore parameters of the bridge deck samples from UT and NE. As demonstrated in this table, the values of the dry bulk density were about $2.2 \pm 0.1 \text{ g/cm}^3$ in all tested samples. The absorption of water through immersion ranged from 4.95 % to 6.76 % by mass. These values increased after the specimens were placed in boiling water. After the samples were immersed in boiling water, the absorption increased about 0.05% in UT samples and about 0.10% in NE samples. The apparent density of the specimens was about $2.5 \pm 0.1 \text{ g/cm}^3$ in all tested samples. By combining the dry bulk density and the apparent density, it was possible to calculate the volume of permeable pore space. The values calculated were about $12.5 \pm 0.5 \%$.

Table 3.5: Water absorption and pore parameters of the UT & NE bridge deck cores

Bridge ID	Side	Absorption after Immersion (room temperature water)	Absorption after Immersion (boiling water)	Dry Density (g/cm^3)	Apparent Density (g/cm^3)	Volume of permeable pore space (voids)
UT-744	Top	5.66%	5.70%	2.211	2.530	12.6%
	Bottom	5.74%	5.77%	2.152	2.456	12.4%
UT-749	Top	5.60%	5.50%	2.212	2.518	12.2%
	Bottom	6.76%	6.80%	2.238	2.639	15.2%
NE-SO80 18181L	Top	4.95%	5.10%	2.254	2.547	11.5%
	Bottom	5.10%	5.21%	2.195	2.478	11.4%
NE-SO80 20100L	Top	5.19%	5.31%	2.311	2.634	12.3%
	Bottom	6.13%	6.19%	2.133	2.458	13.2%

3.2.4 ASR

ASR is a chemical reaction that may occur in concrete because of the alkali environment. Reactive forms of silica present within aggregate particles react with free alkali in the concrete pore solution to produce potentially expansive alkali-silica gel. ASR leads to swelling or cracking of concrete with the absorption of moisture. In order to initiate and sustain ASR, three essential factors must be satisfied namely, the aggregates are potentially reactive; the alkali concentration is high in the concrete pore solution; and the concrete is exposed to high humidity conditions (*Hover 2006*).

Figure 3.8 shows the stained image of the bridge deck samples cored from NE and UT respectively. It is clearly visible that the ASR distress was more obvious in the samples from NE than UT. This phenomenon further helps to explain why the mechanical properties of the NE samples were lower than the UT samples.

In the field, more ASR occurred in NE bridge decks. This is attributable to the use of 70% North Platte riversand and gravel aggregate (highly ASR reactive) in both NE decks. This is also consistent with the recent findings by Clemson University that the acetate-based deicers could induce increased levels of expansion in concrete with aggregates susceptible to ASR, and could trigger ASR in concrete that previously did not show susceptibility to ASR (*Rangaraju et al. 2005, 2006, Rangaraju and Desai 2006*). It was proposed that such deicers react with one of the major cement hydration products, Portlandite, which leads to higher pH of the concrete pore solution (*Rangaraju and Olek 2007*). Furthermore, the concrete specimens exposed to KAc deicer showed presence of certain secondary reaction products, the effect of which on the durability of concrete merits further investigation (*Rangaraju 2007*). Other factors that may have influenced the ASR occurrence include: the annual precipitation (as rain may mitigate deicer accumulation inside the concrete pavement) and the average temperature of the service environment (as higher temperature generally accelerates the chemical attack process).

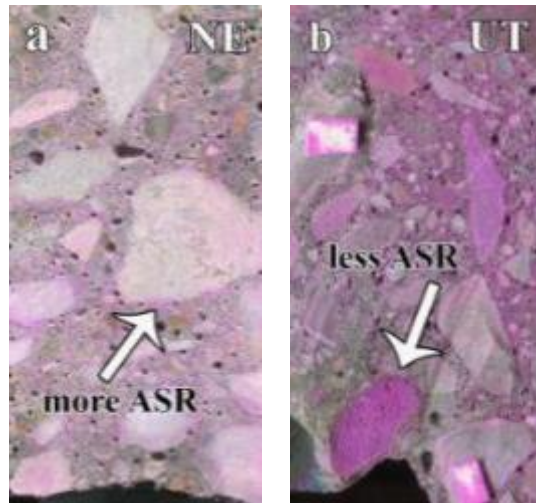


Figure 3.8: Staining image illustrating the presence of ASR in concrete samples from a) NE and b) UT

3.3 RESULTS AND DISCUSSION: A CASE STUDY OF ODOT DECKS

This case study sheds light on the complex issue of concrete durability exposed to cold climate and $MgCl_2$ deicer. The Oregon data for the study were acquired from the 12 ODOT bridge decks described in Table 2.2 and they are summarized in Table 3.6.

3.3.1 Statistical Correlations

Despite the limited number of data points available, efforts were made to explore the statistical correlations between the various parameters (mix design, service environment, properties of hardened concrete) of the 12 ODOT bridge decks described in Table 2.2 using the average data summarized in Table 3.6.

The following pairs of parameters exhibited relatively strong statistical correlation, with the absolute value of Pearson correlation higher than 0.36. The truly relevant correlations were identified after further examination and are highlighted in bold below.

- Total deicer usage & paste-to-air ratio: -0.46
- Average annual number of F/T cycles & paste-to-air ratio: -0.39

Note: Increased deicer usage may have contributed to the decalcification of cement paste and the subsequent coarsening of the air voids. Increased number of F/T cycles may aggravate the coarsening of the air voids.

- *w/c* ratio of fresh concrete & splitting tensile strength: -0.67
- Air content in fresh concrete & splitting tensile strength: -0.38
- A regression equation is obtained as follows.

$$\text{Splitting tensile strength} = 1316 + 154 \text{ Air_in_Fresh_Mix} - 3987 \text{ w/c}$$

$$(\text{Adjusted } R^2=0.36)$$

Note: Under the investigated conditions, higher *w/c* ratio and higher air content in fresh concrete generally corresponded to lower splitting tensile strength of hardened concrete. The detrimental effect of higher air content to strength may be attributed to the presence of entrapped air.

- *w/c* ratio of fresh concrete & paste-to-air ratio: -0.37
- Air content in fresh concrete & paste-to-air ratio: 0.52
- *w/c ratio* of fresh concrete & paste content: 0.69

Note: Under the investigated conditions, lower *w/c* ratio and higher air content in fresh concrete generally corresponded to higher paste-to-air ratio of hardened concrete. The positive effect of higher air content to paste-to-air ratio may be partially attributed to the presence of entrapped air and the benefits of air voids in mitigating F/T attack. The other possible reason is that this is not a cause-and-effect relationship as there is also a strong Pearson correlation between air content and paste content (0.57). A regression equation is obtained as follows, which implies the unreliability of the historical data of the specified (instead of measured) air content in fresh concrete.

$$\text{Air_in_Hardened_Concrete} = 0.124 - 0.0597 \text{ Air_in_Fresh_Mix} + 0.658 \text{ w/c}$$

$$(\text{Adjusted } R^2=0.55)$$

(3.1)

Among the 12 selected bridge decks, lower w/c ratio in fresh concrete generally corresponded to lower paste content (i.e., higher aggregate content) of hardened concrete. Again this may not be a cause-and-effect relationship.

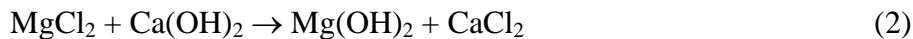
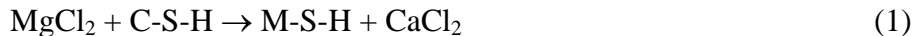
- Maximum depth of chloride penetration & paste-to-air ratio: 0.41

Higher paste-to-air ratio generally corresponded to higher depth of chloride penetration, suggesting that the presence of more cement paste phase in place of air voids facilitated the ingress of external chlorides into the concrete. Or, this may not be a cause-and-effect relationship.

- Total deicer usage & spacing factor: 0.41
- Average annual number of F/T cycles & paste content: -0.62
- ADT in 2008 & spacing factor: -0.46

Note: Increased deicer usage may have contributed to the decalcification of cement paste and the subsequent coarsening of the air voids (and thus the decrease in paste content and the increase in spacing factor). The higher daily traffic volume put the concrete under more compression and likely helped to slow down the ingress of detrimental chemical deicers into the concrete (and thus slow down the increase in spacing factor).

The aforementioned findings obtained from the cored field concrete decks are consistent with existing laboratory studies that reported the detrimental effect of $MgCl_2$ on Portland cement concrete (*Moukwa 1990; Cody et al. 1994; Deja and Loj 1999; Lee et al. 2000; Sutter et al. 2008*) and with some limited field studies (*Cody et al. 1996*). As shown in Equation (1), $MgCl_2$ can react with the cementitious calcium silicate hydrate (C-S-H) present in the cement paste and turn it into non-cementitious magnesium silicate hydrate (M-S-H). As shown in Equation (2), $MgCl_2$ can also react with another type of cement hydration product, Portlandite ($Ca(OH)_2$), and produce a crystal known as brucite ($Mg(OH)_2$). The formation of brucite in confined concrete pores induces great expansive forces and may lead to cracking of the concrete (*Helmy et al. 1991; Wakeley et al. 1992; Rechenberg and Sylla 1996*).



A recent laboratory study reported the formation of another potentially detrimental phase, calcium oxychloride ($3CaO \cdot CaCl_2 \cdot 15H_2O$), formed in cement mortars exposed to 15% $MgCl_2$ solutions for 84 days, as confirmed by optical microscopy, scanning electron microscopy (SEM), and microanalysis (*Sutter et al. 2006*). The proposed mechanism was based on Equations (2) and (3):



The petrographic evidence indicated that plate calcium oxychloride crystals and their carbonate-substituted phase precipitated in air voids and cracks by consuming Portlandite. In addition,

Friedel's salt ($3\text{CaO}\cdot\text{Al}_2\text{O}_3\cdot\text{CaCl}_2\cdot 10\text{H}_2\text{O}$) was detected in the specimens analyzed (*Sutter et al. 2006*). In another laboratory study by the same group, the structures of brucite were also observed in the outer layers of the PCC specimens exposed to concentrated MgCl_2 (*Sutter et al. 2008*).

3.3.2 Mechanical Properties

Splitting tensile strength of core samples:

The splitting tensile strengths for the cores from the 12 ODOT bridge decks ranged between 2.8 to 6.2 MPa (400-990 psi, see Table 3.7), which was lower than the typical value of about 6.9 MPa (1000 psi) for new concrete that has not been compromised. As such, one can conclude that the exposure to service environments in the State of Oregon had significantly degraded the splitting tensile strength and thus the shear resistance of concrete bridge decks. As reported earlier, the average splitting tensile strengths of UT and NE samples were 6.9 MPa (1000 psi) and 3.4 MPa (500 psi), respectively. Considering the similarity in traffic conditions and similar maturity (compressive strength ≥ 27.6 MPa or 4000 psi) requirements across states, the observed considerable strength reduction in the ODOT and NE bridge decks is more likely due to the exposure to MgCl_2 and KAc deicers (in combination with F/T cycles).

Figure 3.9 demonstrates the relationship between the gas permeability coefficient and the splitting tensile strength of all field samples from the ODOT bridge decks built in different years. Figure 3.9a, Figure 3.9b and Figure 3.9c show the relationship for the concrete decks built in the years of 2000-2005, 1985-1990, and before 1980, respectively. As can be seen in Figure 3.9a and Figure 3.9b, the splitting tensile strength increased with a decrease of gas permeability. However, this trend was not observed in Figure 3.9c with two bridges having lower splitting tensile strengths at lower gas permeability levels.

Table 3.6: Average data for the 12 selected ODOT bridge decks

Bridge No.	Total Deicer Usage (gln)	Average Annual No. of F/T Cycles	2008 ADT	Air Content in Fresh Concrete (%)	w/c Ratio	Cl Penetration (inches)	Compressive Strength (psi)	Splitting Tensile Strength (psi)	Paste-to-Air Ratio in Hardened Concrete	Air Content in Hardened Concrete	Paste Content	Spacing Factor (inches)
576	265	102	645	*	*	1.83	3101	648	7.12	3.31%	23.6%	0.003
8682	4720	119	14200	*	*	2.18	6096	606	3.29	9.75%	32.1%	0.009
08958F	870	26	7790	*	*	0.02	1602	721	2.86	9.23%	26.4%	0.016
09268S	870	25	56700	*	*	1.64	2186	847	5.25	5.27%	27.6%	0.002
16358	995	26	12801	5.6	0.4	0.52	2028	589	6.39	4.72%	30.2%	0.003
16440	2315	174	8332	5.6	0.4	0.19	2784	570	3.89	4.85%	18.9%	0.012
16534	1035	26	9793	5.6	0.4	1.45	*	*	10.41	3.97%	41.3%	0.003
16844	1010	90	29440	5.43	0.397	0.47	1902		5.35	6.16%	33.0%	0.002
18525	1145	93	13500	4.6	0.37	0.12	3498	523	2.98	9.04%	27.0%	0.012
18940	1600	41	20600	5.7	0.42	0.1	2812	422	3.89	8.14%	31.7%	0.009
19268	3405	133	3100	4.5	0.28	0.84	2360	876	3.21	4.39%	14.1%	0.013
19681	7145	248	5454	6	0.4	0.14	4798	664	*	*	*	*

Table 3.7: Parameters of splitting tensile test

Sample No	Bridge No	Max. Load	Length	Diameter	Strength
		(lbs)	(in)	(in)	(psi)
1	09268S	7710	4.112	1.694	705
		9440	3.585	1.694	990
2	576	7050	4.199	1.634	654
		6830	4.134	1.641	641
3	08958F	3820	2.48	1.707	574
		5010	2.763	1.707	676
		6840	2.795	1.707	913
		4660	2.19	1.710	792
4	8682	6050	3.689	1.635	639
		6050	4.112	1.635	573
5	18940	3310	3.128	1.685	400
		3860	3.265	1.694	444
6	16440	5010	3.475	1.727	531
		7010	4.243	1.726	609
7	19681	7660	3.313	1.745	844
		5360	4.065	1.736	484
8	18525	3920	3.602	1.629	425
		6960	4.372	1.634	620
9	19268	10830	4.649	1.678	884
		9670	4.336	1.635	868
10	16358	4850	3.579	1.708	505
		5750	3.866	1.708	554
		5850	3.079	1.708	708
11	16534	4600	3.680	1.710	465
12	16844	7170	3.42	1.65	809

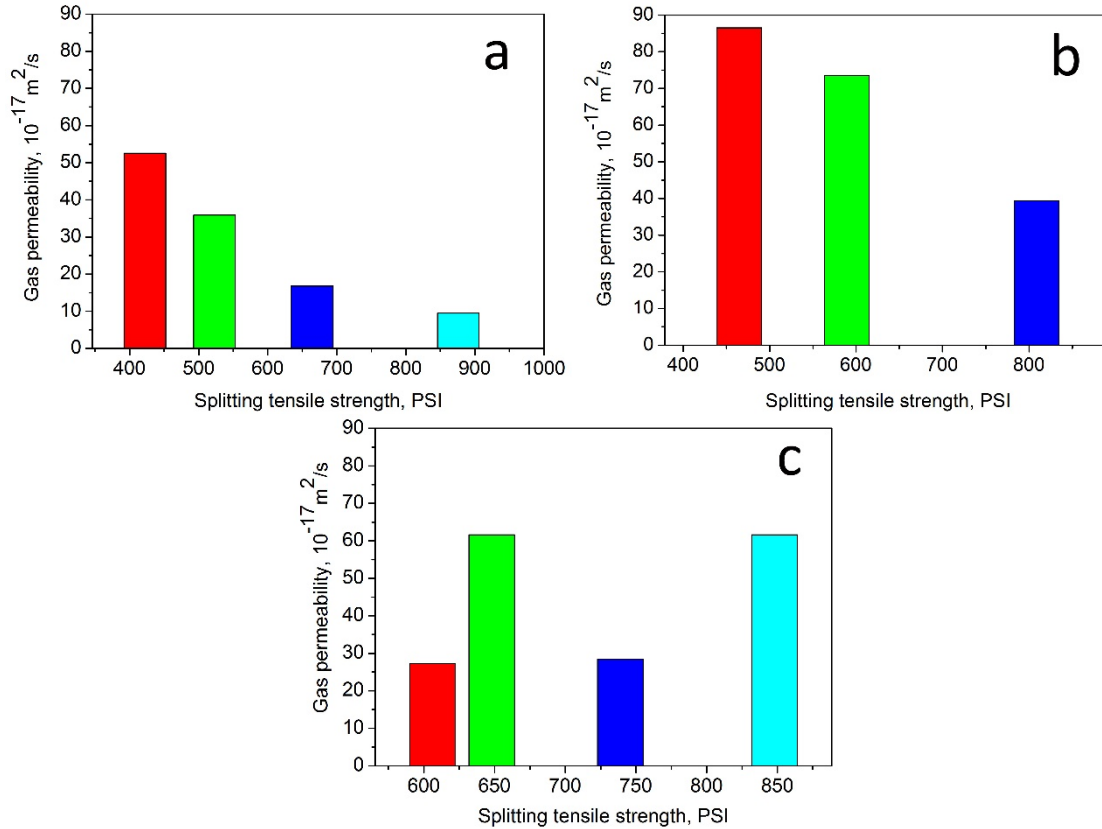


Figure 3.9: The gas permeability as a function of the splitting tensile strength of the decks built in different years a) 2000-2005, b) 1985-1990, and c) before 1980.

The deterioration mechanisms of bridge decks exposed to coupling effects can be divided into physical and chemical ones. The physical damage is mainly associated with F/T cycles and/or external mechanical loadings. Depending on the specific road weather scenarios, the presence of dilute or concentrated MgCl_2 deicer may increase or decrease the number of F/T cycles inside the concrete matrix, as the deicer solution reduces the freezing point temperature of the concrete pore solution. The chemical damage is mainly associated with the chemical reaction of MgCl_2 and other additives in the deicer solution with the cement hydrates, generally degrading its physicochemical integrity (e.g., the bond strength of the cementitious phase and the interfacial transition zone at the surface of coarse aggregates). Figure 3.9a and Figure 3.9b showed that for the concrete decks built during 1985-2000, the reduction of splitting tensile strength (indicator of shear resistance) followed the same trend with the reduction of gas permeability (indicator of physical microstructure). In contrast, Figure 3.9c showed that for the concrete decks built before 1980, the change in splitting tensile strength differed from the trend in gas permeability. This implies that their splitting tensile strength is no longer mainly determined by physical microstructure but also other parameters (potentially the level of chemical contamination).

Figure 3.10 illustrates the splitting tensile strength for core samples from two different groups of bridge decks, with deicer usage higher or lower than 2000 gallons per lane mile (1286 mL/m²) per fiscal year (FY). The results reveal that the average splitting tensile strength of concrete decks with deicer usage over 2000 gal/in-mi/FY was lower than those with lower deicer usage. This implies the potentially deleterious role of MgCl₂ deicer in the splitting tensile strength of ODOT concrete decks.

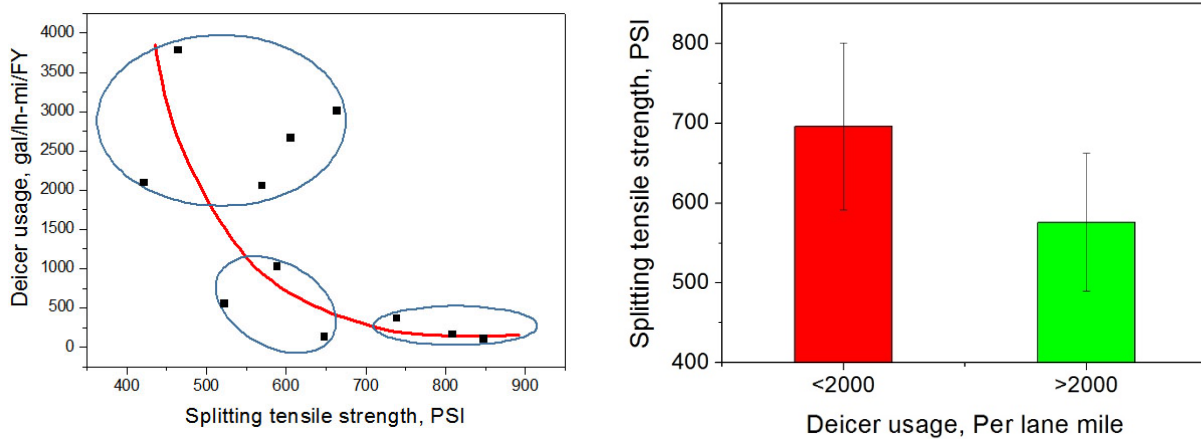


Figure 3.10: The splitting tensile strength as a function of annual deicer usage.

Compressive strength of core samples:

Note that the correlations related to compressive strength of small (typically D2"×H4", i.e., D 5.1 cm × H 10.2 cm) cored concrete cylinders were discarded. The measured data seem to suggest that increased deicer usage or higher number of F/T cycles would correspond to generally higher compressive strength of the hardened concrete. Similarly, higher compressive strength generally corresponded to lower splitting tensile strength. These are very difficult to explain from a mechanistic perspective and unlikely cause-and-effect relationships. As detailed in this section, the measured *compressive strength and Young's modulus* values featured very high variability across the multiple cores from the same bridge deck and thus deemed unreliable and excluded for in-depth analysis.

The compressive strengths for the cores from the 12 ODOT bridge decks ranged between 6.7 to 42.0 MPa (978 – 6096 psi) (see Table 3.8). Some of the core samples exhibited compressive strengths less than 10.3 MPa (1500 psi), partly due to the presence of large aggregate in the relatively small sample sizes. In some cases, the coarse aggregate in the edge of the flattened surface chipped off with relatively less load; as such, the measured compressive strength was lower than the actual value. As such, the compressive strength data were less reliable than the splitting tensile strength data. Nonetheless, much of the observed reduction in compressive strength could be attributed to the inherent deterioration of the concrete.

Table 3.8 also presents the Young's modulus of some core samples. It was not feasible to derive the Young's modulus from the stress-strain curve of the compressive test of some samples as there was no apparent linear zone. This incomplete set of Young's modulus data still indicated

great variability among the different concrete decks, likely due to their difference in exposure conditions.

Table 3.8: Parameters from the compressive strength test

Category	Bridge No	Max. Load	Length (L)	Diameter (D)	L/D Ratio	Correction Factor	Compressive Strength (psi)	Young's Modulus (psi)
		(lbs)	(in)	(in)				
1	09268S	2271	3.21	1.7	1.89	0.98	996	276319
		7906	3.1	1.7	1.83	0.98	3448.6	471985
2	00576	4688	3.09	1.63	1.9	0.98	2224.9	894902
		9659	3.67	1.65	2.23	1	4623.2	
		5380	2.8	1.65	1.7	0.98	2455.1	
		6610	2.77	1.65	1.68	0.97	3011.9	
3	08958F	4337	2.98	1.71	1.75	0.98	1856.6	176883
		3044	2.94	1.71	1.72	0.98	1300.5	131058
		3959	2.52	1.71	1.48	0.96	1655.4	
		6380	3	1.7	1.82	0.99	2940.4	
4	16844	4121	3.68	1.65	2.23	1	1930.8	482612
		4680	3.4	1.65	2.06	1	2184.7	464400
5	08682	14289	2.93	1.64	1.79	0.98	6539.6	51970
		4560	3.22	1.63	1.98	0.99	2165.2	
6	18940	6317	2.56	1.69	1.51	0.96	2704.7	424284
		6997	2.88	1.7	1.69	0.98	2993.9	346743
7	16440	6449	3.39	1.74	1.96	1	2719.2	399075
8	19681	11065	3.46	1.74	1.99	1	4661.9	
9	18525	11724	3.2	1.65	1.94	1	5486.5	907067
		4467	3.15	1.64	1.91	0.99	2091.3	
10	19268	5696	2.57	1.64	1.57	0.97	2614.7	443493
		5422	3.22	1.65	1.95	1	2520.7	613654
11	16358	7330	4.04	1.71	2.37	1	3199	755228
		2462	3.54	1.71	2.07	1	1075	357007
		4223	3.02	1.71	1.77	0.98	1809	
12	16534	12439	3.5	1.8	1.94	1	4866	921959
		12054	3.5	1.8	1.94	1	4716	

Microhardness analyses of core samples:

This section is devoted to the use of microhardness measurements to shed light on the observed strength reduction in the concrete cores and explore their potential linkage to the exposure to MgCl₂ deicer usage and F/T cycles. Microhardness measurements offer a spatial distribution of properties across the concrete matrix instead of a single value for the entire concrete specimen.

Out of the 12 ODOT bridge decks, a few representative cores were chosen to examine the microhardness of concrete specimen as a function of historical exposure, sample depth, and sample area (paste vs. ITZ).

Figures 3.11a and 3.11b present the microhardness gradients for two concrete decks (bridge 09268S, exposed to 105 gal/l_n-mi (67.5 mL/m²) and 25 F/T cycles per year and 56700 ADT in 2008; and bridge 16534, exposed to 3784 gal/l_n-mi (2434 mL/m²) and 26 F/T cycles per year and 9793 ADT in 2008). These two decks were selected as they present the two extreme ends of the annual deicer usage spectrum and both experienced low number of F/T cycles per year. While the bridge deck exposed to less MgCl₂ deicer (and more traffic) generally featured a higher average microhardness value at various concrete depth than the one exposed to more MgCl₂ deicer, the only statistically significant differences are *at the interior (25-30 mm) for cement paste* and *at the very top surface (2-5 mm) for ITZ*. This shows that higher deicer exposure alone (in absence of substantial F/T cycling) may not induce significantly more degradation across the entire matrix of the field concrete. Yet, the deck with higher deicer exposure exhibited higher average splitting tensile strength (848 psi or 5.8 MPa vs. 465 psi or 3.2 MPa).

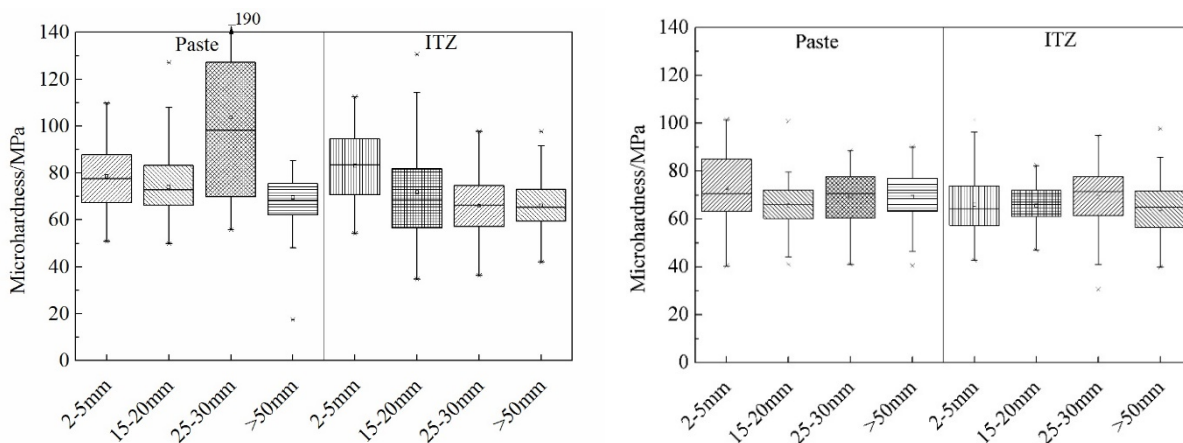


Figure 3.11: The microhardness of concrete specimens from two ODOT bridge decks, exposed to a) 105 and b) 3784 gal/l_n-mi/FY, respectively

To further explore the effect of deicer usage on the microhardness of field concrete, Figure 3.12 presents the microhardness gradients of bridges 19681, 8682, and 18940, all of which experienced MgCl₂ deicer at over 2000 gal/l_n-mi/FY (1286 mL/m²/year). Specifically, these three bridges were exposed to 3006 gal/l_n-mi (1933 mL/m²) and 248 F/T cycles per year, 2263 gal/l_n-mi (1455 mL/m²) and 119 F/T cycles per year, and 2091 gal/l_n-mi (1345 mL/m²) and 41 F/T cycles per year, respectively. They also had an ADT of 5454, 14200, and 20600 in 2008, respectively. Two of these field core samples exhibit lowest microhardness values about 15 to 25 mm inside the concrete. This observed trend corresponds well with the chloride concentration profile typically seen in field concretes subjected to periodical salt applications (Figure 3.5b). For one of the field core samples (bridge 8682), the microhardness at the deck surface (2-5 mm) remained mainly in the range of 70 to 80 MPa, which was consistent with the values of concrete

that was not chemically degraded (such as the data shown in Figure 3.4 for the Utah DOT deck, or the data shown in Figure 3.11a for the ODOT deck). Yet the microhardness decreased to the range of mainly 40 to 50 MPa at the deck depth of 50 mm. This is likely attributable to the accumulation of $MgCl_2$ inside the concrete over time and the dilution of surface chloride content by carbonation and precipitation (as shown in Figure 3.5). Note that for all these cored bridge decks, the microhardness values in the ITZ were slightly lower than that in the paste and such difference was not statistically significant.

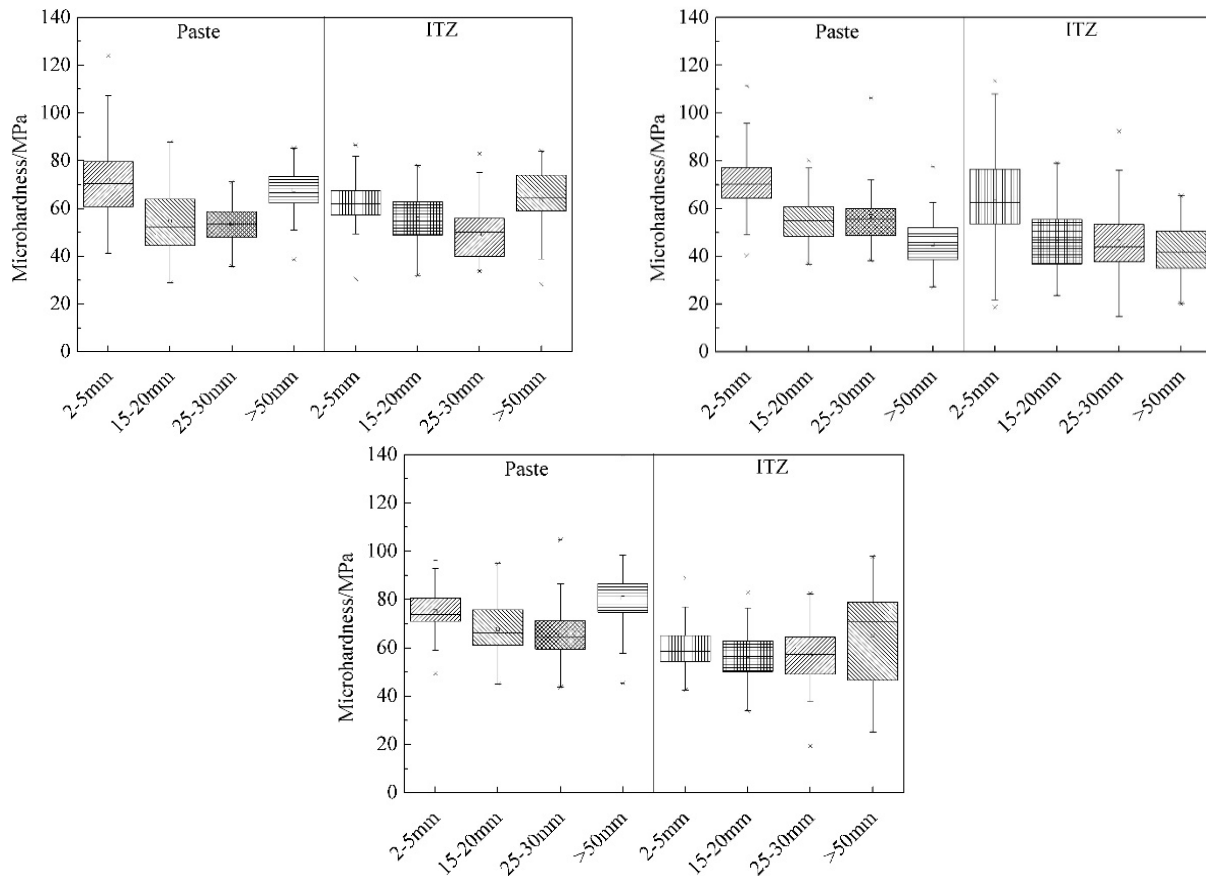


Figure 3.12: The microhardness of three concrete decks experienced $MgCl_2$ deicer at over 2000 per lane mile per year: a) bridge 19681; b) bridge 8682; c) bridge 18940

Figure 3.12 reveals that concrete exposed to significant amount of $MgCl_2$ could be degraded subsurface, yet does not exhibit observable distress or damage on its surface. This phenomenon was confirmed in the accelerated laboratory tests described in Chapter 6 as well. As detailed in Chapter 6, the exposure to $NaCl$ deicer and F/T cycles typically leads to visible scaling, spalling and significant mass loss of concrete, whereas the exposure to $MgCl_2$ deicer and F/T cycles may not lead to any of these visible symptoms but gradual decalcification of the binder phase, degradation of the overall microstructure, and strength loss of the concrete. These three ODOT bridge decks exhibited splitting tensile strength of 664 ± 255 psi (5.6 ± 1.8 MPa), 606 ± 47 (4.2 ± 0.3 MPa), and 422 ± 21 psi (2.9 ± 0.1 MPa), respectively. All of these decks' splitting tensile strengths

were far lower than 1000 psi (6.9 MPa), the typical value of concrete that was not chemically compromised.

Validation by laboratory-fabricated concrete samples:

To validate some of the observations in the field core samples, concrete samples of the same mix design were fabricated and exposed to the combined effect of F/T cycles and chloride deicers under well-controlled laboratory conditions. Figures 3.13 and 3.14 illustrate the external morphologies of laboratory-fabricated concrete cylinders exposed to MgCl₂ and NaCl solutions with various concentrations after 5 and 10 F/T cycles, respectively. The concrete samples exposed to NaCl exhibited significant surface scaling after 5 F/T cycles; however, all the concrete samples exposed to MgCl₂ solutions exhibited no surface distress even after 10 F/T cycles. As a result, to accelerate the salt scaling phenomenon of the concrete samples in MgCl₂ solution, the concentration of the solutions were fixed to 15% in both NaCl and MgCl₂ solutions from the 11th to 15th F/T cycles.





Figure 3.13: Lab concrete samples exposed to 5 F/T cycles in $MgCl_2$ and $NaCl$ solutions, respectively





Figure 3.14: Lab concrete samples exposed to 10 F/T cycles in MgCl₂ and NaCl solutions, respectively

Figure 3.15 shows the splitting tensile strength results of a separate set of concrete specimens exposed to 15 F/T cycles in MgCl₂ and NaCl solutions. In this F/T cycling process, the MgCl₂ and NaCl concentrations were 2.54% and 3%, respectively, from the 1st to the 10th F/T cycles after which all the solution concentrations were changed to 15% for the following 5 F/T cycles. The 2.54% and 3% concentrations were used to achieve the same molar concentration of Cl⁻ ions. It can be seen in this figure that the splitting tensile strengths of the samples that experienced F/T in MgCl₂ solution showed lower values than those in NaCl solution after 15 F/T cycles. Again, in this case, the visual inspection would be misleading for assessing the condition of concrete bridge decks exposed to MgCl₂ deicer, as the chemical attack by MgCl₂ did not exhibit apparent signs of distress until severe disintegration of the concrete occurred.

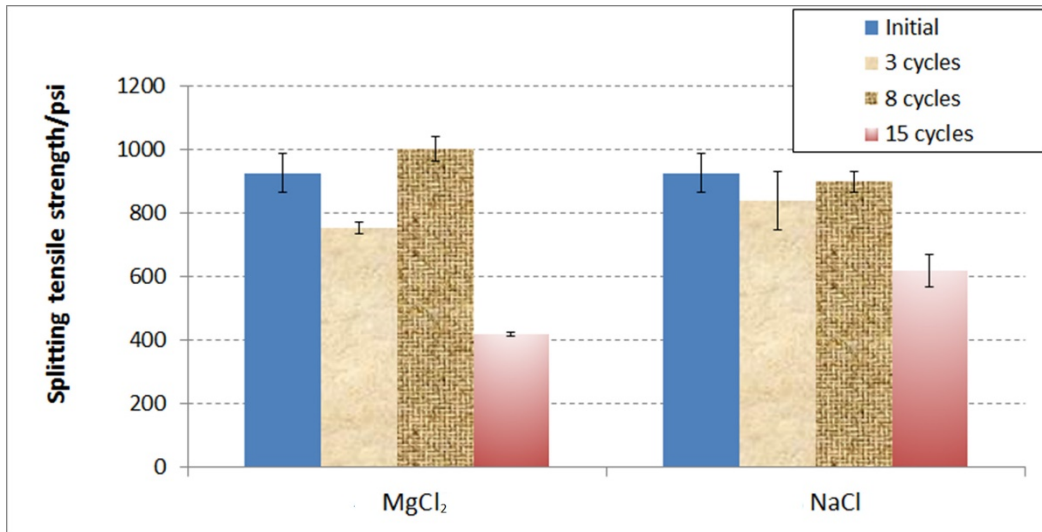


Figure 3.15: Splitting tensile strength of lab concrete samples exposed to F/T cycles in NaCl and MgCl₂ solution.

(Note: The solution concentration of MgCl₂ was 2.54% and NaCl was 3% during the first 10 F/T cycles. The solution concentration was changed to 15% for both MgCl₂ and NaCl solutions in the 11th to 15th cycles)

3.3.3 Transport Properties

Chloride penetration:

The chloride penetration into the field concrete decks was assessed using a AgNO₃ solution spray method, which entailed the observation of the discolored area on a fractured surface of each deck core. The chloride penetration depths of the twelve ODOT bridge deck cores is given in Table 3.9, of which only one (08682) had chloride penetration greater than 2 inches. This was similar to the chloride penetration measured from cores obtained from the two Utah DOT bridge decks, which were predominantly exposed to NaCl deicer. The American Concrete Institute (ACI) requires clear cover of two inches for any concrete that is exposed to the weather (ACI Committee 302, 1996). It is cautioned, however, this study has demonstrated that even if the AgNO₃ spray method shows a chloride penetration as little as 0.1 inches (2.5 mm), this does not guarantee the integrity of the concrete exposed to MgCl₂ deicer. As shown in Table 3.9, the splitting tensile strength of the ODOT deck cores did not show any significant correlation with the maximum chloride penetration depth. For instance, the highest splitting tensile strength values were observed in the ODOT deck showing a chloride penetration depth of 1.64 inches (4.2 mm), whereas the lowest splitting tensile strength values were observed in the ODOT deck showing a chloride penetration depth of 0.10 inches (2.5 mm).

The discrepancy between the splitting tensile strength and chloride penetration can be explained by the facts that the strength reduction is mainly caused by the attack of Mg²⁺ cations to the cement paste and the ingress of Mg²⁺ cations into the concrete differs from that of Cl⁻ anions. In

addition, there is one caveat with the AgNO₃ solution spray method as it is unable to detect the chloride ingress front unless it exceeds the threshold level for color change, typically a soluble Cl⁻ concentration of 0.15% by weight of cement (*Otsuki et al. 1992*). The threshold level of total chlorides to induce the corrosion of rebar in mortars and concretes may vary greatly as a function of the specific experimental conditions, in the range of 0.15% to 2.5% by weight of cement, according to a review of multiple field and laboratory studies (*Glass and Buenfeld 1997*).

Table 3.9: Maximum chloride penetration vs. splitting tensile strength of the 12 ODOT concrete decks

Sample	Max. Depth of chloride Penetration (inches)	Splitting Tensile Strength (psi)
00576	1.83	648±9
08682	2.18	606±47
08958F	0.02	739±146
09268S	1.64	848±202
16358	0.52	589±106
16440	0.19	570±55
16534	1.45	465
16844	0.47	809
18525	0.12	523±138
18940	0.10	422±31
19268	0.84	876±11
19681	0.14	664±255

The age of the concrete is a concern with respect to chloride penetration. The older the concrete is, the longer time it has had to allow the chloride anions to enter the void spaces and cracks inside the concrete matrix. With a larger number of wetting and drying cycles, the concrete would have been exposed to more chloride ingress due to water transport (a.k.a., “wick action”).

The quality of the concrete when it was initially placed also plays an important role in the concrete’s resistance to chloride penetration. If the concrete was improperly consolidated, it could have an increased amount of void space and thus higher susceptibility to chloride penetration (*Stanish 1997*).

Carbonation and air void characteristics:

Table 3.10 provides the parameters calculated using the phenolphthalein and air-void tests, for 11 ODOT concrete decks. The data for the ODOT bridge 19681 were not available. The results of phenolphthalein test revealed the presence of some surface carbonation in the bridge decks 00576, 08682, 16440, 19268, and 16358. These did not correspond to the decks with higher usage of MgCl₂ deicer, suggesting that the role of MgCl₂ in the carbonation of field concrete, if any, is not significant. Carbonation of the concrete is associated with the corrosion of steel reinforcement and with shrinkage. However, carbonation increases both the compressive and

tensile strength of the concrete. Depth of carbonation is less on areas exposed to heavy rain than the sheltered faces.

Table 3.10: The parameters calculated using the phenolphthalein and air-void tests

Bridge No.	Air Content	Paste Content	Spacing Factor	Distance between stops (in)	Void Frequency	Paste to air ratio	Avg. chord length	Specific surface
09268S	5.27	0.2764	0.002	0.002	3.626	5.25	0.015	2400
00576	3.31	0.236	0.003	0.002	5.075	7.12	0.007	1920
16534	3.97	0.4126	0.003	0.002	2.286	10.40	0.017	1920
08958F	9.23	0.2637	0.016	0.002	4.087	2.86	0.023	2133
08682	9.75	0.321	0.009	0.002	9.002	3.29	0.011	2400
16844	6.16	0.3295	0.002	0.002	2.212	5.35	0.028	1920
18940	8.14	0.3166	0.009	0.002	8.474	3.89	0.01	2133
16440	4.85	0.1888	0.012	0.002	3.958	3.89	0.012	1920
18525	9.04	0.2695	0.012	0.002	5.687	2.98	0.016	2133
19268	4.39	0.1409	0.013	0.002	2.774	3.21	0.016	2133
16358	4.72	0.3015	0.003	0.002	4.464	6.39	0.011	1920

The air contents from the linear traverse method did not match those determined through the absorption test. The air contents determined by the linear traverse method ranged from 3.31 to 9.75 percent for the 11 ODOT bridge decks (see Table 3.11), which are similar to those of the Utah and Nebraska decks. The absorption tests gave a volume of permeable pore space with a range from 12.2 to 17.6 percent for the 12 ODOT bridge decks (see Table 3.11). With the linear traverse method, the air voids were measured across the cross-section of the sample on the surface of the cut. With the absorption by immersion method, the entire sample was used to determine the parameters of the sample. The absorption method is able to measure the large voids and the small capillary pores that will absorb water. With the linear traverse method the minimum measurable air void size is limited by the magnification of the microscope or the resolution of the scanner in this case.

A caveat of the air content measurement is that no distinction is made between entrained air and entrapped air. Entrained air is preferable air that can improve the freeze thaw resistance of the concrete and is often times in the form of small or fine bubbles evenly dispersed throughout the concrete matrix. Entrapped air is often large air voids that degrade the strength of the concrete and occur at random locations throughout the concrete matrix.

The spacing factor ranged from 0.002 to 0.016 for the 12 ODOT bridge decks, some of which were considerably higher than that of the Utah and Nebraska bridge decks (0.002 ± 0.0001). As shown in Table 3.11, six out of the 11 ODOT bridge decks exhibited a spacing factor higher than 200 microns (0.008 inches) per the ASTM C457 test method. This suggests that *they no longer have a proper air-void system for freeze-thaw resistance.*

The paste content of the ODOT core samples ranged from 14.1% to 41.3%. Little to no correlation existed between the air content and the paste content or between the air content and the spacing factor. For the ODOT core samples, the paste to air ratio ranged from 2.86 to 10.40, some of which were considerably lower than that of the Utah and Nebraska bridge decks (10.3 ± 5.1 and 8.01 ± 0.56 , respectively).

The ODOT bridge decks featured generally smaller air voids, relative to those of the Utah and Nebraska bridge decks investigated in this study, which might have contributed to better F/T resistance. For the ODOT core samples, their specific surface ranged from 1920 to 2400 inch^{-1} , which is significantly lower than that of NE (2743 inch^{-1}) and UT ($2800 \pm 400 \text{ inch}^{-1}$). Note that this method has its limitations in the use of one single value to characterize the total range of air void sizes throughout the concrete sample.

One limitation in the linear traverse method is related to the maximum aggregate size to size of sample ratio. Ideally, the diameter of the sample should be at least three times greater than the maximum aggregate present in the sample. Due to the inability to core large diameter samples from bridges that are in service, this caveat was ignored. With large aggregate present in some of the core samples, it is possible that some of the data are inaccurate.

Water Absorption:

The water absorption performance is often looked as an indicator of the degradation resistance of concrete under various exposure conditions, as much of this degradation is associated with the ingress of moisture into the hardened concrete.

Table 3.11 presents the water absorption and pore parameters of the bridge deck samples from ODOT. As demonstrated in this table, the values of the dry bulk density ranged between 2.06 to 2.41 g/cm^3 , which was similar to those seen in the Utah and Nebraska deck samples. The dry bulk density is often used to calculate the overall porosity and void space within the concrete specimen.

For the ODOT core samples, the absorption of water through immersion ranged from 4.58 to 8.20 percent by mass. These values increased after the specimens were placed in boiling water and allowed to absorb a greater amount of water. The absorption after boiling ranged from 5.07 to 8.47 percent. The apparent density of the ODOT core samples ranged from 2.53 to 2.72 g/cm^3 , some of which were slightly higher than that of the Utah and Nebraska bridge decks ($2.5 \pm 0.1 \text{ g/cm}^3$). The apparent density is the density of the specimen minus the volume contribution from the air voids.

Using the dry bulk density and the apparent density it is possible to calculate the volume of permeable pore space. This measurement does not count the void space that may not be connected to any of voids. For the ODOT core samples, their volume of permeable pore space ranged from 12.2 to 17.6 percent, some of which were significantly higher than that of the Utah and Nebraska bridge decks ($12.5 \pm 0.5 \%$).

The combination of air void and water absorption data suggest that relative to the Utah and Nebraska bridge decks some of the ODOT decks featured higher amount of permeable voids, smaller air voids, higher apparent density (possibly less impermeable voids) and higher spacing factor.

Table 3.11: Parameters from the absorption test for the ODOT bridge decks

Sample No	Bridge Number	Side	Absorption After Immersion	Absorption after Immersion and Boiling	Bulk Density, Dry (g/cm^3), (g_1)	Bulk Density After Immersion (g/cm^3)	Bulk Density After Immersion and Boiling (g/cm^3)	Apparent Density (gm/cm^3), (g_2)	Volume of permeable pore space (voids)
1	09268S	Top	6.43%	6.85%	2.236	2.379	2.389	2.64	15.3%
		Bottom	6.76%	7.17%	2.2	2.348	2.358	2.612	15.8%
2	576	Top	4.58%	5.69%	2.33	2.437	2.463	2.687	13.3%
		Bottom	4.79%	5.07%	2.413	2.529	2.536	2.75	12.2%
3	16534	Top	6.74%	7.26%	2.14	2.284	2.295	2.533	15.5%
		Bottom	5.83%	6.41%	2.22	2.349	2.362	2.588	14.2%
4	08958F	Top	6.98%	7.17%	2.163	2.314	2.318	2.56	15.5%
		Bottom	8.20%	8.40%	2.086	2.257	2.262	2.53	17.5%
5	8682	Top	5.92%	6.93%	2.266	2.4	2.423	2.688	15.7%
		Bottom	7.01%	7.91%	2.171	2.323	2.343	2.621	17.2%
6	16844	Top	6.93%	7.16%	2.175	2.326	2.331	2.576	15.6%
		Bottom	5.46%	5.75%	2.271	2.394	2.401	2.612	13.1%
7	18940	Top	7.39%	7.52%	2.214	2.378	2.381	2.657	16.7%
		Bottom	6.41%	6.60%	2.244	2.388	2.392	2.634	14.8%
8	16440	Top	7.20%	7.80%	2.172	2.329	2.341	2.615	16.9%
		Bottom	6.10%	6.39%	2.264	2.402	2.409	2.647	14.5%
9	19681	Top	7.36%	8.47%	2.06	2.212	2.235	2.496	17.4%
		Bottom	6.80%	8.08%	2.174	2.321	2.349	2.637	17.6%
10	18525	Top	7.04%	7.67%	2.154	2.306	2.319	2.581	16.5%
		Bottom	7.34%	7.96%	2.155	2.314	2.327	2.602	17.2%
11	19268	Top	6.17%	6.47%	2.261	2.4	2.407	2.648	14.6%
		Bottom	6.02%	6.22%	2.27	2.407	2.411	2.643	14.1%
12	16358	Top	5.74%	6.08%	2.335	2.469	2.477	2.721	14.2%
		Bottom	6.26%	6.81%	2.261	2.402	2.415	2.673	15.4%

Figure 3.16 shows that no trends were present when the absorption characteristics of the top and bottom of the ODOT deck core samples were compared.

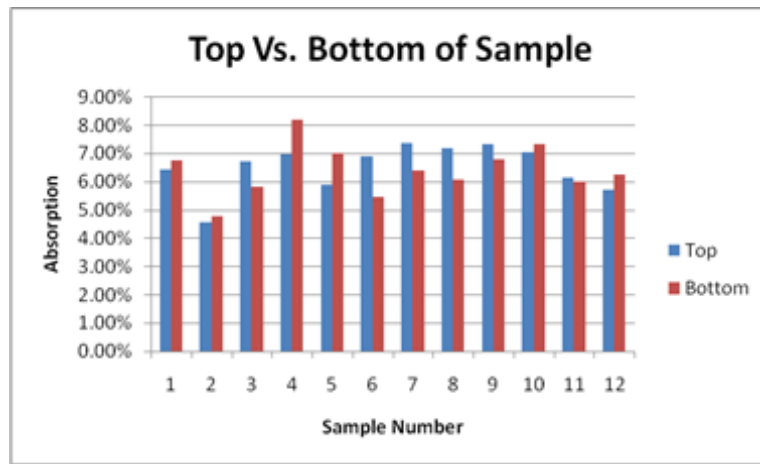


Figure 3.16: Water absorption as a function of deck number and sample depth

3.3.4 ASR

Figure 3.17 shows the stained image of the samples cored from select ODOT bridge decks. The staining test revealed the presence of ASR (yellow color) around coarse aggregates in some bridge deck cores. This is more likely attributable to the presence of reactive aggregates. Similar to carbonation, the presence of ASR did not correspond to the decks with higher usage of $MgCl_2$ deicer, suggesting that the role of $MgCl_2$ in the ASR of field concrete, if any, is not significant.

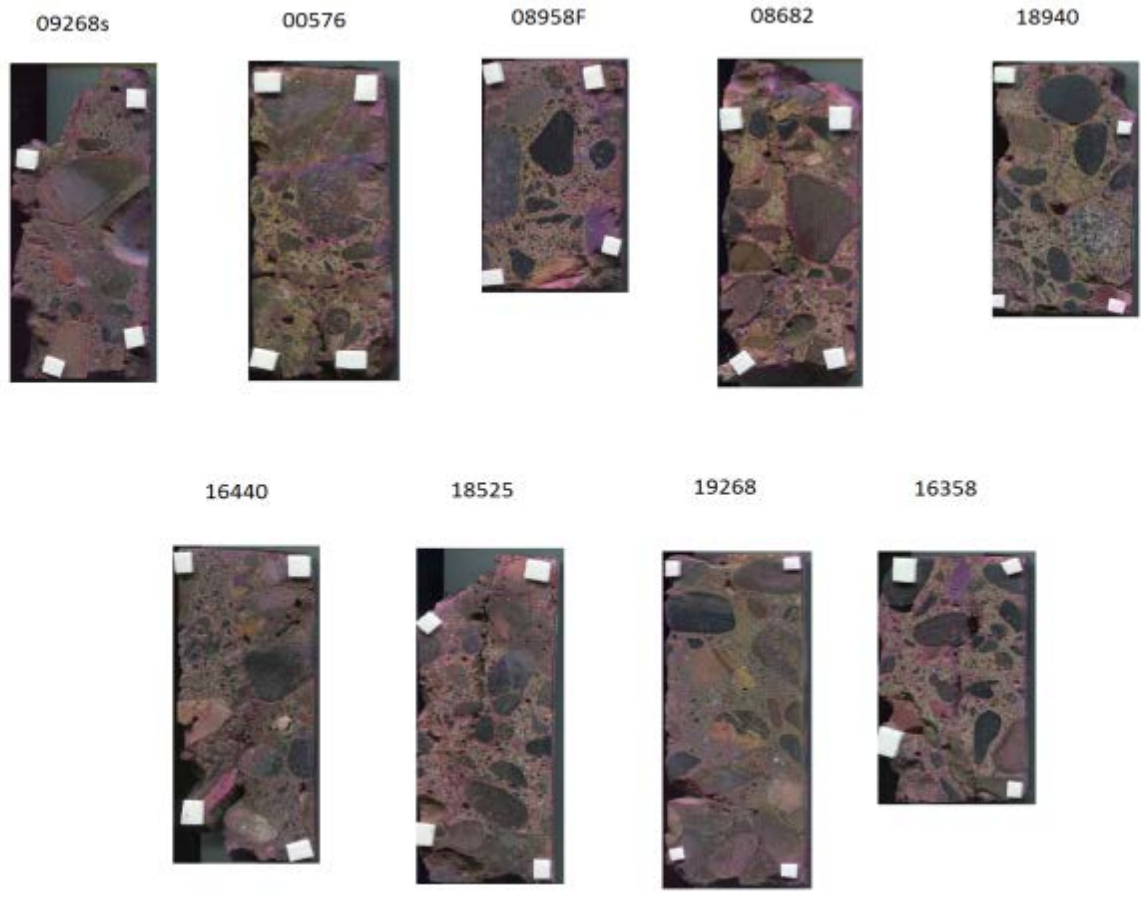


Figure 3.17: Images from ASR test of select ODOT core samples

3.4 MICROSCOPIC ANALYSIS OF SELECT ODOT CORE SAMPLES

The microscopic characterization of select ODOT core samples was conducted using SEM and EDS, in order to help interpret the observed engineering properties of the concrete at macroscopic level. The results shed light on the mechanisms by which the $MgCl_2$ deicer deteriorates the concrete in the field environments in the State of Oregon. Out of the 12 ODOT bridge decks, a few representative cores were chosen to help illustrate the consistency and discrepancy of some concrete decks when their condition is rated by the current ODOT method or by the proposed CSIL method detailed in Chapter 5.

3.4.1 SEM Analysis

Figure 3.18 and Figure 3.19 show the low and high magnification SEM images of the core samples from ODOT bridges 16844 and 08682, which were evaluated as SATISFACTORY by ODOT and 90-92% by CSIL, and POOR by ODOT and 36-37% by CSIL, respectively. Figure 3.20, Figure 3.21 and Figure 3.22 demonstrate the low and high magnification SEM images of the core sample from ODOT bridges 16440, 19681 and 16534, respectively. These three bridge decks were evaluated by ODOT as GOOD, GOOD, and SATISFACTORY and by CSIL as 36-37%, 53-57%, and 26-34%, respectively.

As demonstrated in the low magnification image (Figure 3-18a), the sample cored from the ODOT bridge 16844 featured a high density of cement hydrates (likely calcium silicate hydrates, C-S-H) and very few observable pores in the paste. In addition, as can be seen from the high magnification image (Figure 3-18b), the typical lamellar shape C-S-H phase was well maintained, the surfaces of the C-S-H phase were smooth, and little other precipitates or crystals were observed. This favorable microstructure corresponded very well with the high rankings by both ODOT and CSIL for its macroscopic engineering properties. This sample served as a positive reference to evaluate the physical condition of a concrete deck from the microstructure perspective.

As demonstrated in Figure 3.19, the sample cored from the ODOT bridge 08682 exhibited a drastically different microstructure than that of the core from bridge 16844. The microstructure of core 08682 featured a highly porous microstructure and absence of high density cement hydrates. It can be seen from the high magnification image (Figure 3.19b) that the microstructure of the C-S-H phase was no longer a dense lamellar structure but a penetrable porous structure. This deleterious microstructure corresponds very well with the low rankings by both ODOT and CSIL for its macroscopic engineering properties. This sample served as a negative reference to evaluate the physical condition of a concrete deck from the microstructure perspective.

Figure 3.20 shows the SEM micrograph of the core sample from the ODOT bridge 16440. The microstructure of this sample exhibited typical porous structure and the presence of some precipitates on the surfaces of the C-S-H phase. The evidence suggested that the C-S-H structure had been compromised to some extent, likely by the chemical attack of $MgCl_2$. The surface of the lamellar shaped C-S-H structure was not very smooth compared with that seen in the core from the bridge 16844 (Figure 3.18b).

Figure 3.21 shows the SEM micrograph of the core sample from the ODOT bridge 19681. The microstructure of this sample exhibited obvious microcracks on most of the pore surfaces but not around the pores. This implied cracks being induced by internal forces, most likely due to F/T damage in the presence of $MgCl_2$. Small amount of crystalline precipitate phases were observed (Figure 3.21b). The

microscopic evidence further suggested that the concrete in the field environment had been affected by both physical and chemical damages.

Figure 3.22 shows obvious crystalline precipitates in the core sample from the ODOT bridge 16534. Compared with the microstructure of 19681, there were more obvious crystalized phases that had precipitated (Figure 3.22a). From the high magnification observation shown in Figure 3.22b, the precipitate phases were needle-shape with diameter of about 1 μm and length of 10-20 μm . The precipitation process and the chemical analysis of these precipitates need to be further investigated in future studies.

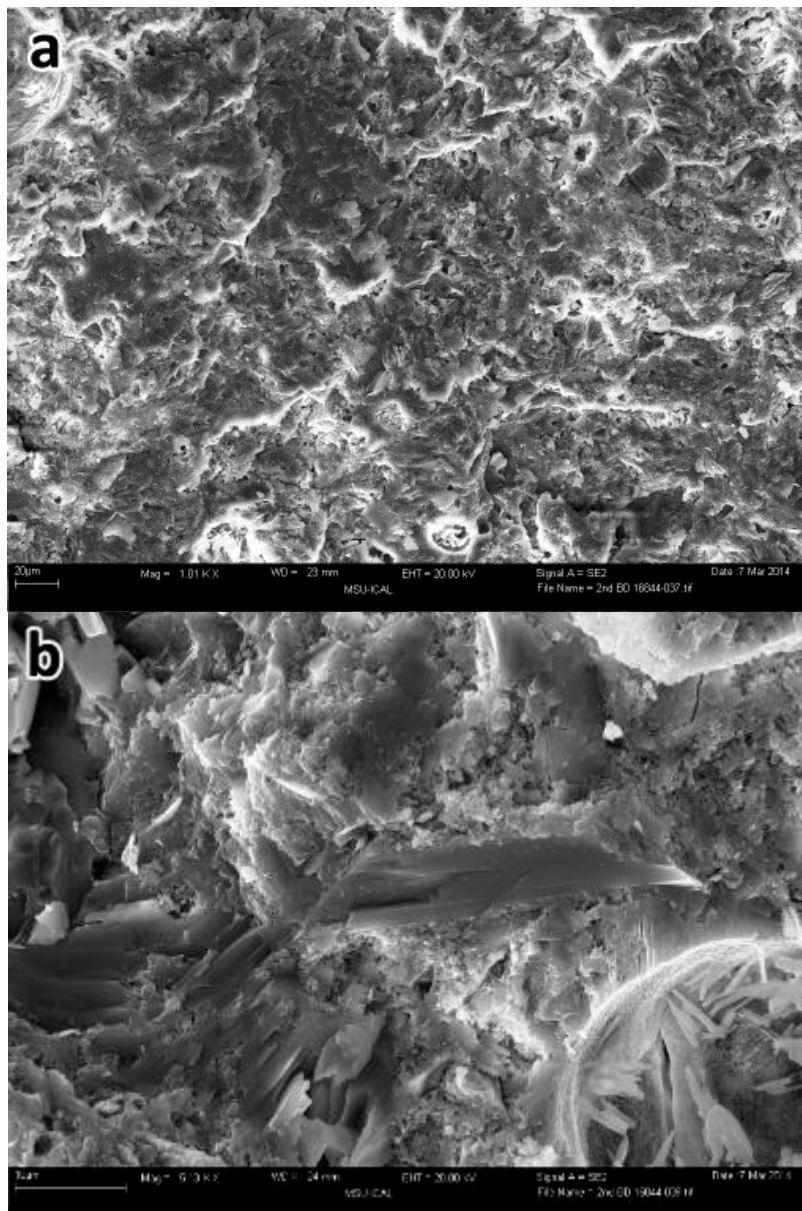


Figure 3.18: SEM micrographs of ODOT bridge deck 16844: a) low magnification and b) high magnification

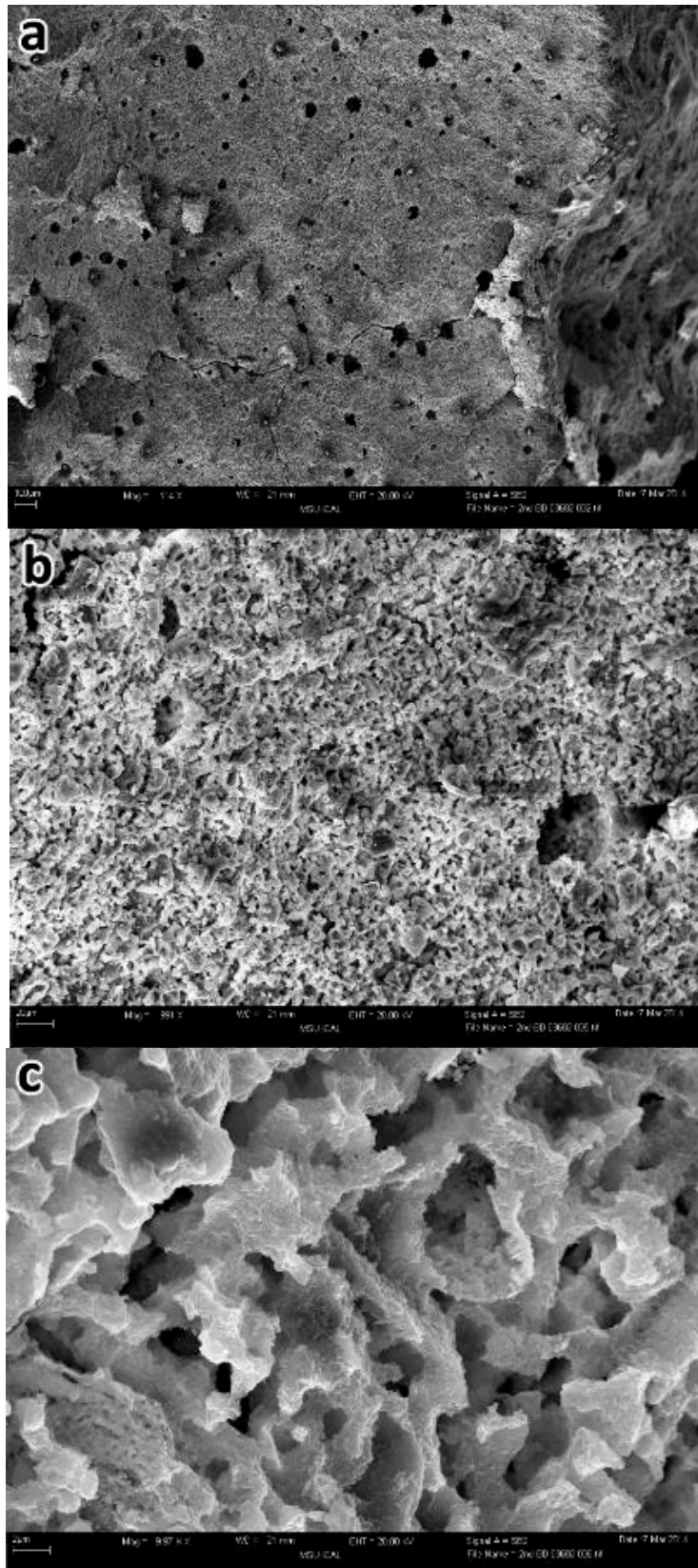


Figure 3.19: SEM micrograph of ODOT bridge deck 08682:
a) low magnification, b) high magnification, and c) ultrahigh magnification

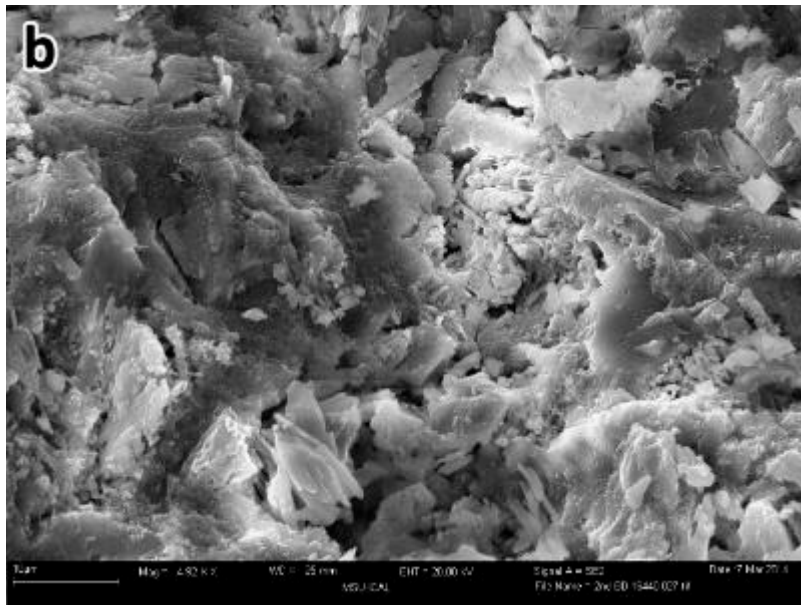
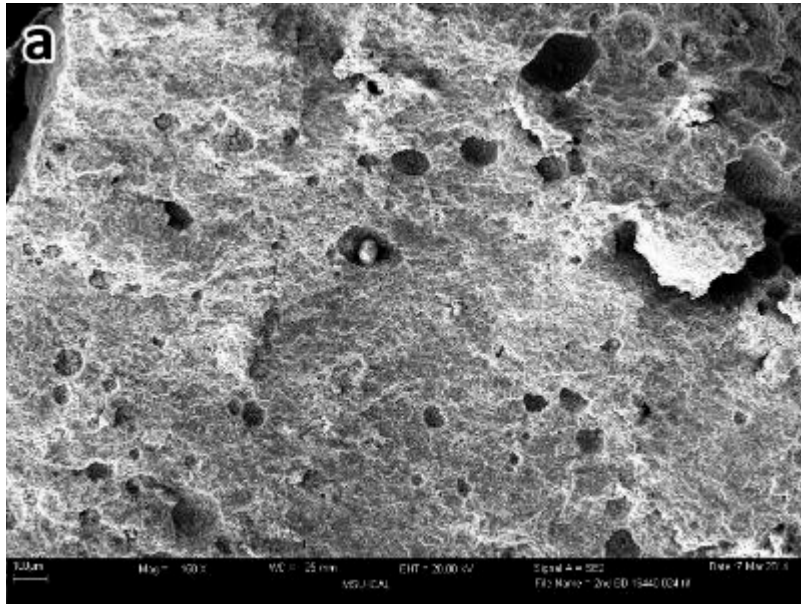


Figure 3.20: SEM micrographs of ODOT bridge deck 16440:
a) low magnification and b) high magnification

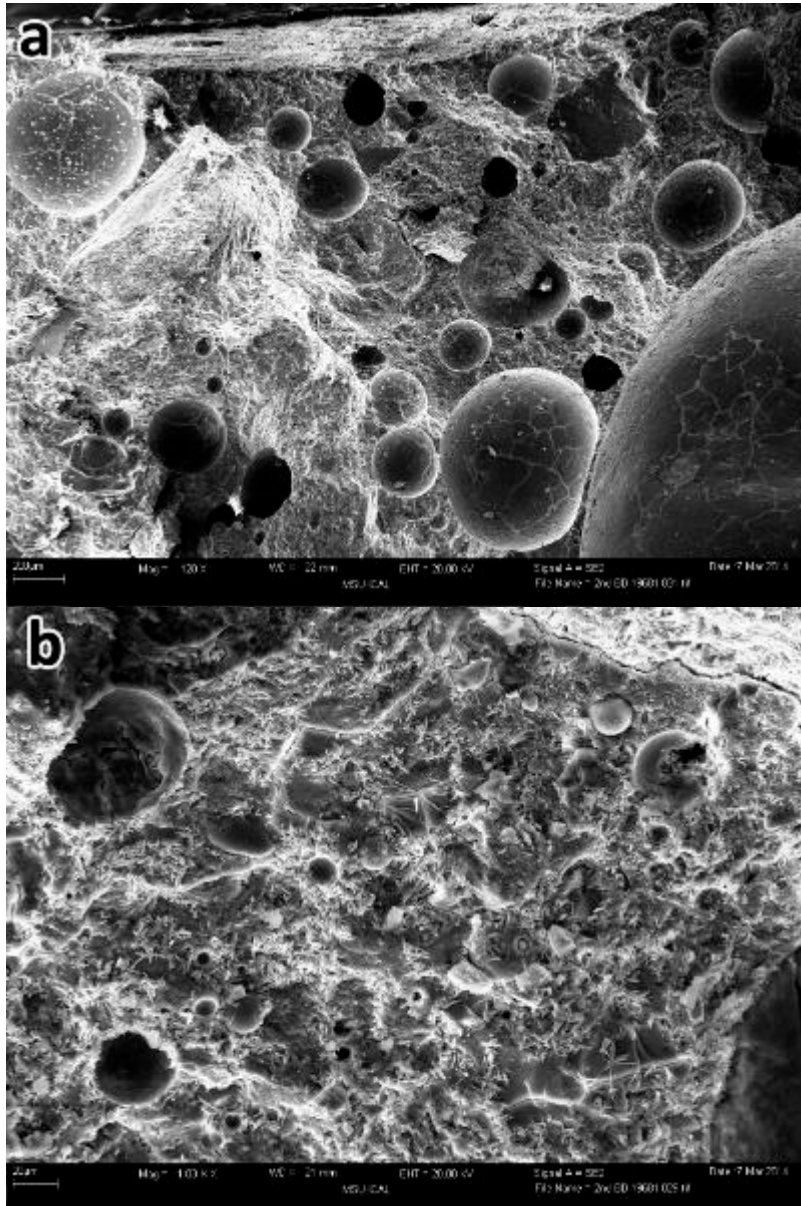


Figure 3.21: SEM micrographs of ODOT bridge deck 19681:
a) low magnification, b) high magnification

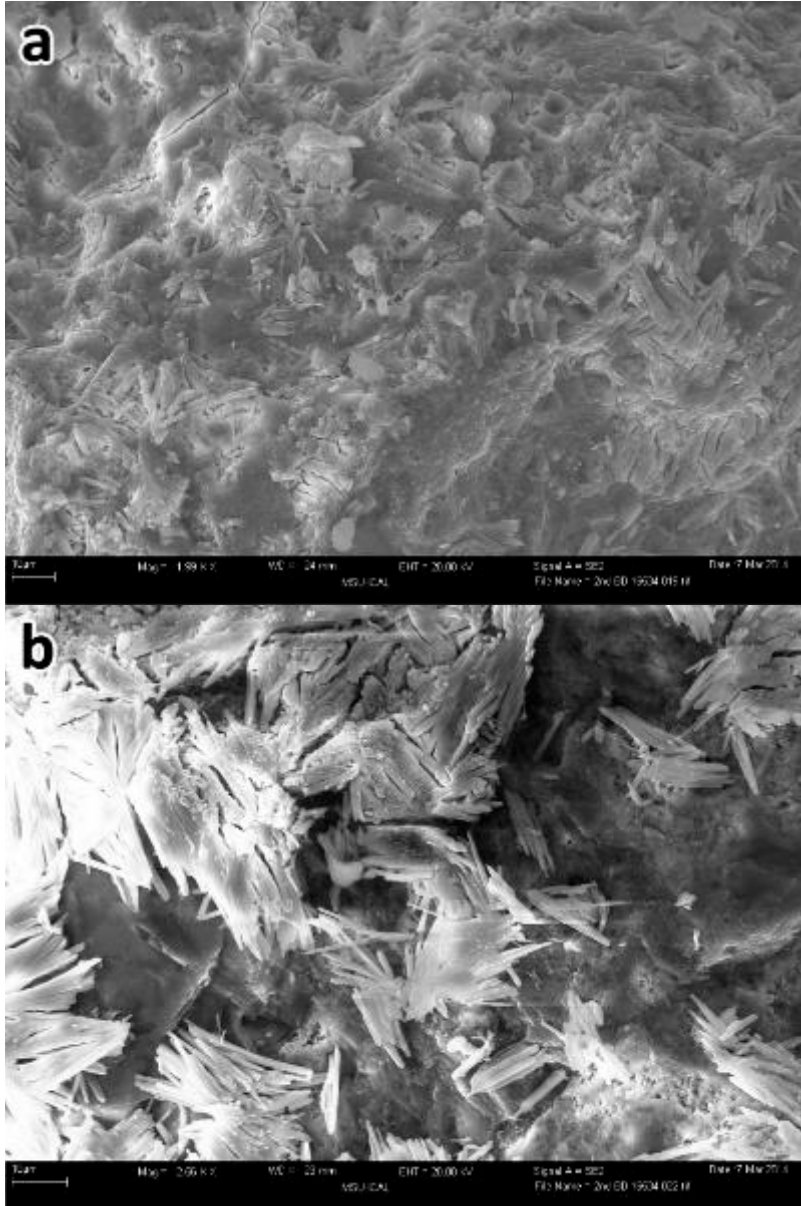


Figure 3.22: SEM micrographs of ODOT bridge deck 16534:
a) low magnification and b) high magnification

3.4.2 SEM/EDS Analysis

Figure 3.23 and Figure 3.24 give the SEM/EDS analysis results of bridge decks 16844 and 08682, which represent good and poor concrete conditions, respectively, by both ODOT and CSIL rankings. It can be seen that the Mg content was higher in deck 08682 than in deck 16844 (0.78 wt.% vs. 0.60 wt.%). The Ca content was lower in deck 08682 than in deck 16844 (21.8 wt.% vs. 23.9 wt.%). This confirms the leaching of Ca^{2+} out of cement paste caused by the chemical reaction of MgCl_2 with Ca-rich cementitious phases, as reported in our previous laboratory studies.

Figure 3.25 gives the SEM/EDS analysis results of bridge deck 19681, which was ranked as GOOD by ODOT while 53-57% by CSIL. In this sample, the Mg content was as high as 0.83 wt.% and the Ca content was as low as 19.2 wt.%, which suggested more severe Ca^{2+} leaching than the bridge deck 08682.

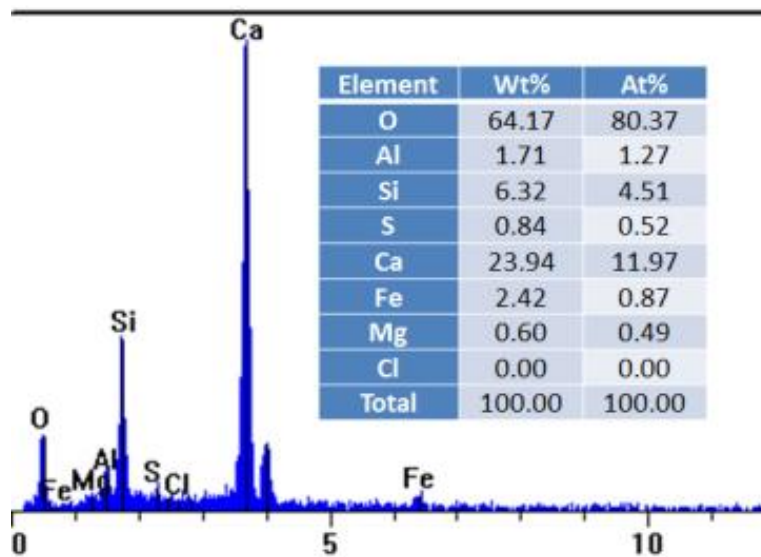
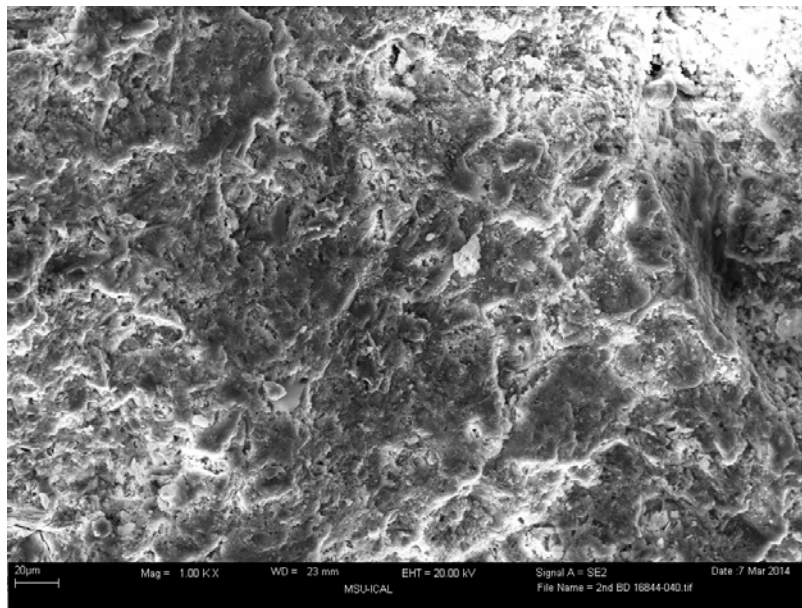


Figure 3.23: SEM/EDS analysis of 16844 bridge deck

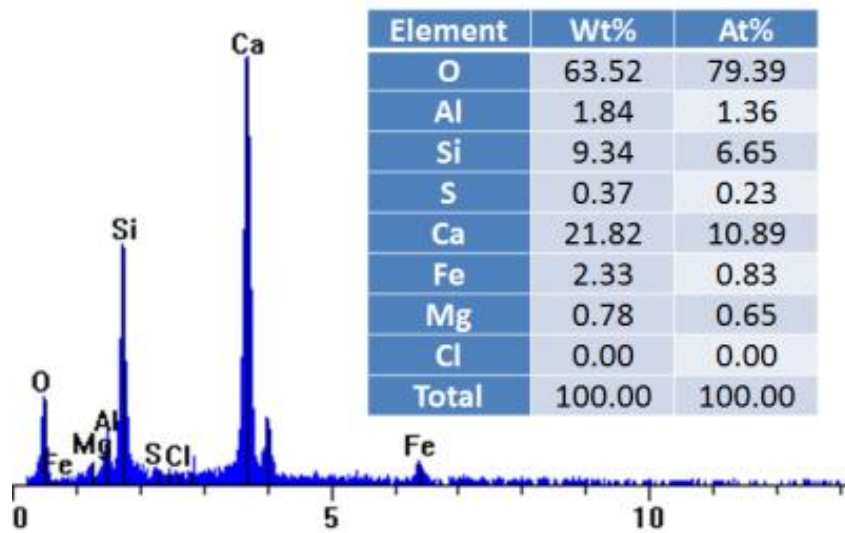
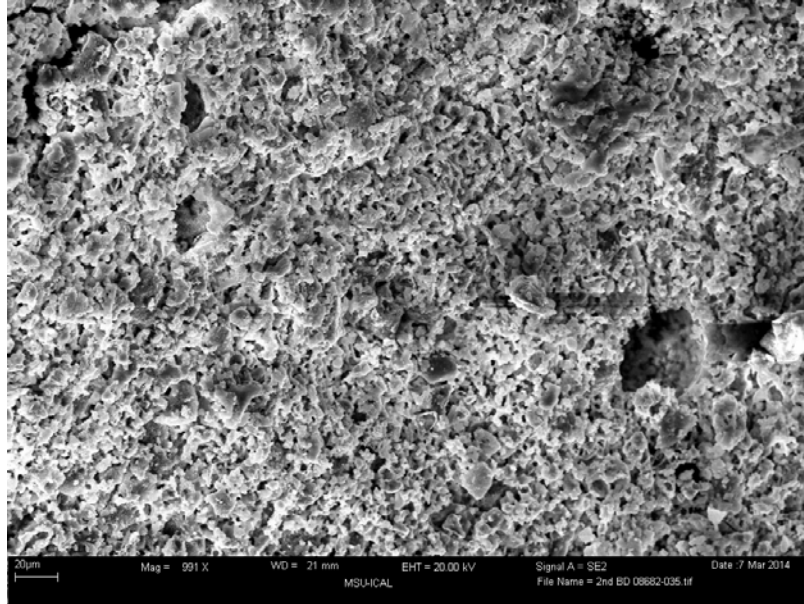


Figure 3.24: SEM/EDS analysis of 08682 bridge deck

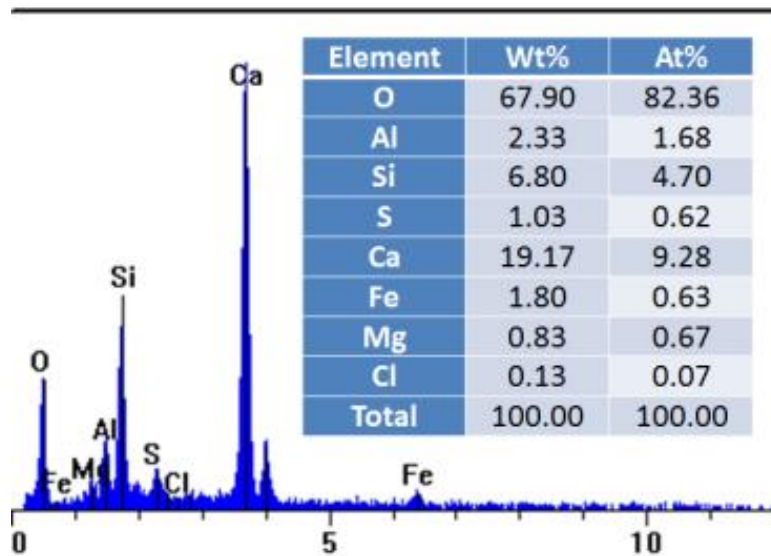
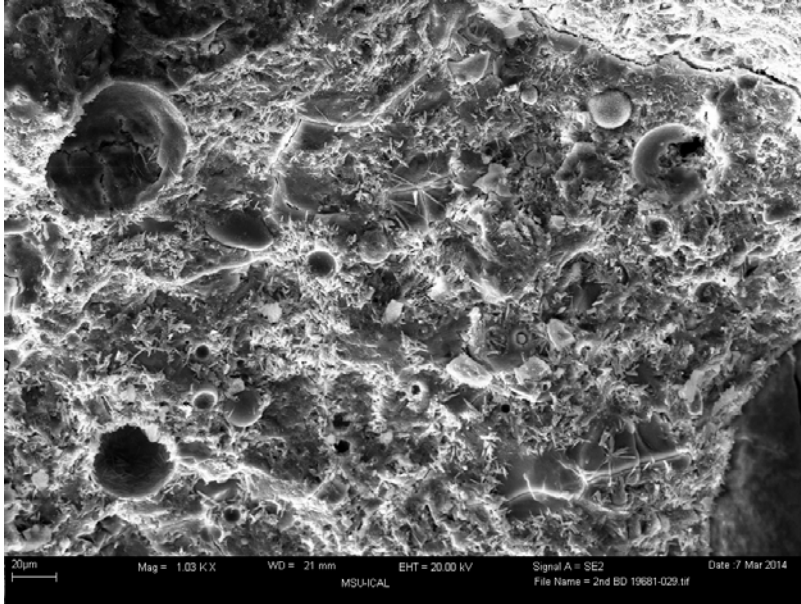


Figure 3.25: SEM/EDS analysis of 19681 bridge deck

As discussed earlier, the deck cores for the microstructural analysis were chosen to help illustrate the consistency and discrepancy when their condition is rated by the current ODOT method or by the proposed CSIL method detailed in Chapter 5. Table 3.12 summarizes the key findings from the SEM/EDS analysis, along with the deicer usage, F/T cycles, tensile strength, gas permeability of the selected ODOT decks and their rankings by the two different methods.

Table 3.12: Summary of microstructure analysis of the select ODOT bridge decks, along with other key parameters and rankings

Bridge ID	Average annual no. of F/T cycles vs. ADT in 2008	Annual deicer Usage (gal/ln-mi)	Splitting tensile strength, psi	Gas permeability, $10^{-16} \text{ m}^2/\text{s}$	ODOT rating	CSIL rating	Microstructural analysis by SEM/EDS
<i>ODOT and CSIL Ratings In Agreement</i>							
16844	90 vs. 29440	166	809	3.94	Satisfactory	83% - 85%	A high density of cement hydrates (well-maintained CSH) & very few observable pores in the paste. Ca: 23.9 wt.%; Mg: 0.60 wt.%
08682	119 vs. 14200	2663	606±47	2.73	Poor	36%-37%	A highly porous microstructure (penetrable porous CSH) and absence of high density cement hydrates. Ca: 21.8 wt.%; Mg: 0.78 wt.%
<i>ODOT and CSIL Ratings In Disagreement</i>							
16440	174 vs. 8332	2058	570±55	3.91	Good	36%-37%	Porous structure and the presence of some precipitates on the CSH surfaces
19681	248 vs. 5454	3006	664±255	1.68	Good	53%-57%	Obvious microcracks on most of the pore surfaces but not around the pores. Small amount of crystalline precipitate phases. Ca: 19.2%; Mg: 0.83 wt.%.
16534	26 vs. 9793	3784	465	8.65	Satisfactory	26%-34%	More obvious crystalline, needle-shaped precipitates

3.5 CONCLUSIONS

This chapter reports the collection, examination and testing of field concrete cored from 12 selected ODOT bridge decks (predominantly exposed to $MgCl_2$ deicer, at random locations without severe cracking), as well as those of field concrete cored from two Utah DOT bridge decks (predominantly exposed to $NaCl$ deicer at locations without apparent surface distress) and two Nebraska Department of Roads bridge decks (mainly exposed to KAc deicer, at locations with apparent surface distress). These decks generally specified a w/c ratio of about 0.40 (between 0.37 to 0.42, except 0.28 for the ODOT bridge 19268), air content of 5% to 6%, and a compressive strength of about 27.6 MPa (4000 psi) to 30 MPa (4350 psi). The reactivity of aggregates in Oregon decks was unknown. The aggregates used in Nebraska decks were 30% non-reactive and 70% reactive, while the aggregates used in Utah were not typically reactive. The field cores were tested for their mechanical properties and transport properties. They were also subjected to staining tests to detect possible chloride penetration, carbonation, and ASR, and subjected to petrographic analysis to characterize their paste and air contents. For the ODOT bridge decks, additional microscopic investigation was conducted to better understand the concrete deterioration in the presence of $MgCl_2$ deicer.

The following are the key findings from the field investigation:

1. For the vast majority of the deck core, no significant deterioration was apparently visible other than surface scaling. In other words, there were generally no signs of significant longitudinal, transverse or diagonal cracking and no evidence of visible precipitates. The only exception was for the Nebraska deck cores, which showed signs of microcracking due to ASR.
2. The concrete bridge decks exposed to KAc or $MgCl_2$ deicer showed significant reductions in their splitting tensile strength and microhardness, whereas surface-distress-free decks exposed to $NaCl$ deicer did not.
3. The observed considerable strength reduction in the ODOT and NE bridge decks is likely due to the exposure to $MgCl_2$ and KAc deicers (possibly in combination with F/T cycles).
4. The visual inspection would be misleading for assessing the condition of concrete bridge decks exposed to $MgCl_2$ deicer as the chemical attack by $MgCl_2$ generally does not exhibit apparent signs of distress (until severe disintegration of the concrete occurs).
5. Even if the detectable chloride penetration per the $AgNO_3$ spray method is as little as 0.1 inches (2.5 mm), this does not guarantee the integrity of the concrete exposed to $MgCl_2$ deicer.
6. The role of $MgCl_2$ in the carbonation and ASR of field concrete, if any, was not significant, but KAc may play a significant role in contributing to ASR in concrete containing reactive aggregate.
7. The microscopic evidence further suggested that the concrete in the field environment had been affected by both physical and chemical attack by F/T cycles and $MgCl_2$.

In addition, the accelerated cold lab testing results demonstrated that the influences of the MgCl_2 deicer to the concrete samples were different from the NaCl deicer. NaCl can lead to observable physical damage (e.g., F/T damage in the form of surface scaling), whereas MgCl_2 can lead to chemical degradation (mainly Ca-leaching and formation of new crystalline phases) below the surface of the concrete.

4.0 DEVELOPING DEICER EXPOSURE MEASUREMENT METHOD

This chapter describes the development of a method to measure the deicer exposure at a specific site. The ideal method would be inexpensive to deploy, and the output from the method would be an exposure rank that correlates with the cumulative chloride exposure at the surface of the concrete in the target area (e.g., a specific bridge deck).

Instead of extracting chlorides from weathered concrete surfaces, one alternative may be akin to the wire-on-bolt test that measures atmospheric galvanic corrosion (ASTM G116). The following sections detail the development of a method to quantify cumulative deicer exposure at a given site, using mortar, metallic, or polymeric specimens. The focus was placed on mortar specimens since the other two types of specimens were found inappropriate for this intended application.

4.1 MOTAR SPECIMENS

4.1.1 Materials and Methods

Preparation of mortar specimens:

The mix design of mortar specimens was specified following the ASTM C 672-91 standard. An ASTM specification C150-07 Type I/II low-alkali Portland cement (Holcim-Trident Plant, Three Forks, MT) was used in this study. The fine aggregates used were clean, natural silica sand acquired from Kenyon Noble, classified as SP (i.e., sand Poorly Graded per the United Soil Classification System). The mix designs had a water-to-cement ratio (w/c) of 0.48, 0.53, or 0.58, and an aggregate-to-cement ratio of 2.0. The fine aggregates' moisture content, prior to batching, was measured to be 5.67%. A moisture correction was applied to the batch mix based on a fine aggregate absorption of 1.28%. Prior to batching, the mixing drum was lightly coated with water to minimize water loss during mixing process. The air entraining agent was added to the water prior to mixing. The fine aggregates and the water were then added to the mixing container and the mixing process started. The Portland cement was then quickly added in large subsequent fractions of total batch cement. The mix was mixed per ASTM C192 standard. After sufficient mixing, the mortar mix was placed into a dampened wheelbarrow to allow access for testing and casting cylinders. Temperature and air test per ASTM C231 standard were then conducted on the wet mix to ensure the quality of the mix. After mixing, the fresh mixture was cast into polyvinyl chloride piping molds to form cylinders of D2"×H4" (D 51 mm × H 102 mm), D3"×H6" (D 76 mm × H 142 mm), or D4"×H8" (D 102 mm × H 203 mm) per ASTM C192 standard. The batch was remixed periodically during the casting of the test specimens. For each combination of w/c ratio and cylinder size, at least eighteen specimens were made. In the first 24 h of molding, the mortar specimens were placed on a rigid surface and stored at room temperature. Next, the

specimens were de-molded and cured in a moist cure room at room temperature and relative humidity (RH) of 95% for 27 days. Once fully-cured, the mortar specimens were allowed to be air-dried for 24 h at $23 \pm 1.7^\circ\text{C}$ (73.4°F), RH 45–55% and weighed, before being subjected to the tests.

Freeze-thaw cycling in the presence of deicers:

The impacts of magnesium chloride deicers on concrete were assessed by conducting freeze-thaw tests of mortar samples in the presence of diluted deicers (with 30% MgCl_2 diluted at 100:1, 100:3 and 100:5 respectively). The test evaluates the combined effects of chloride brine and freeze-thaw cycling on the structural integrity of specimens of poorly air-entrained concrete. For all the mixes, the dosage of air entraining agent was MicroAirTM at 0.006% by weight of cement, designed to achieve less than 6% air content typically seen in air-entrained concrete so as to accelerate the potential freeze/thaw damage. Depending on the statistical design of the experiments detailed later, 10, 20 or 30 exposure cycles were used to simulate the temperature and wet/dry cycles experienced by field concrete in an accelerated manner. Each cycle consisted of 48 hours of fully immersing the mortar specimens in the diluted MgCl_2 solution at $-27 \pm 5^\circ\text{F}$, RH $50 \pm 5\%$ followed by 24 hours of thawing and 12 hours of exposing the mortar specimens in dry air at room temperature ($73.4 \pm 3^\circ\text{F}$, RH $25 \pm 5\%$). For the deicer exposure, each mortar specimen was placed in a Ziploc bag containing sufficient chloride brine to avoid water evaporation. A thermocouple was embedded in one of the control concrete samples to monitor temperatures during freeze-thaw cycling. The average freezing rate was approximately $0.05^\circ\text{C}/\text{min}$ during the first 5 hours and then approximately $0.05^\circ\text{C}/\text{min}$ during the subsequent 25 hours. The average warming rate was observed to be approximately $0.01^\circ\text{C}/\text{min}$. After exposure cycles, the test specimens were individually rinsed under running tap water and hand-crumbled to remove any scaled-off material during the freeze/thaw cycling. The specimens were air-dried for 24 h at $23 \pm 1.7^\circ\text{C}$ (73.4°F), RH 45–55%. After drying, test specimens are weighed and the final weights recorded.

Periodic measurement of concrete resistivity:

The surface resistivity of mortar specimens were periodically measured after the given number of freeze/thaw (F/T) and wet/dry (W/D) cycles. Such measurements were conducted during the dry stage after the mortar specimen had reached the room temperature. The resistivity was measured using a Resipod Resistivity Meter (Proceq USA, Inc., Aliquippa, PA) with four equally spaced point electrodes that are pressed onto the mortar surface (Wenner or 4-point method). The two outer electrodes induce an alternating current (AC) in the range of 50 to 1000 Hz and the two inner electrodes measure the potential drop, from which the surface resistivity can be calculated (Figure 4.1).

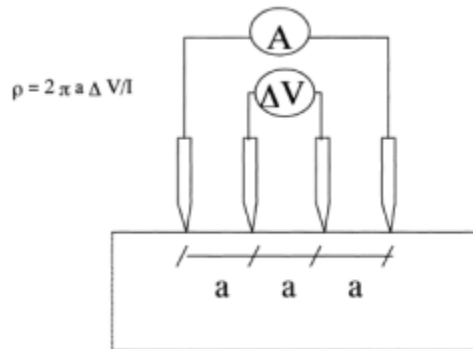


Figure 4.1: Setup of four electrode measurement of concrete resistivity

Note that the surface resistivity measured is significantly affected by the test temperature and relative humidity, which were at $23 \pm 3^\circ\text{C}$ (73.4°F) and $32 \pm 7\%$ respectively in this study. For each type and size of mortar specimen after a given exposure, three measurements were made on each of the two replicate specimens and all six readings were averaged and reported as a single value as they were found to be typically with $\pm 10\%$ of error.

Testing mechanical properties of mortar specimens:

Subsequent to the F/T and W/D cycling, the mortar specimens were tested for weight loss as well as Young's modulus and compressive strength or splitting tensile strength. The compressive strength of mortar cylinders was determined according to ASTM C39 (Standard Test Method for Compressive Strength of Cylindrical Concrete Specimens). Stiffness was another important property of the mortar. The Young's modulus (a.k.a., elastic modulus) was determined from load-deformation measurements made on mortar cylinders tested in uniaxial compression (ASTM C469, Standard Test Method for Static Modulus of Elasticity and Poisson's Ratio of Concrete in Compression). The splitting tensile strengths of the mortars were investigated according to ASTM C496 (Standard Test Method for Splitting Tensile Strength of Cylindrical Concrete Specimens).

Statistical design of experiments (DoE):

- The statistical DoE incorporated four influential factors, each specified at three levels.
- X_1 : w/c (0.48, 0.53, 0.58)
- X_2 : specimen size (D2"×H4", D3"×H6", D4"×H8")
- X_3 : chloride dilution by volume (100:1, 100:3, 100:5; from 30% MgCl_2 solution)
- X_4 : exposure time (10, 20, 30 cycles; each cycle takes 84 hours)
- As shown in Table 4.1, there were three response variables as follows: Y_1 = compressive strength, Y_2 =splitting tensile strength, and Y_3 =Young's modulus.

Table 4.1: Factors and Levels for the Statistical DoE

Factor Level	Factors			
	Exposure Time Cycles	w/c Ratio	Dimensions	Dilution Ratio from 30% MgCl ₂ (by volume)
1	10	0.48	Small: D2"×H4"	100:1
2	20	0.53	Medium: D3"×H6"	100:3
3	30	0.58	Large: D4"×H8"	100:5

An orthogonal fractional factorial design was employed for this investigation. As such, a total of 27 combinations of influential factors (a.k.a., observations) were designed. Note that at least two specimens were used for each combination, one for testing Young’s modulus and then compressive strength and the other for testing splitting tensile strength.

To minimize the potential effect of other variables (e.g., operator and time of the day) on the measured results, the order of preparing and testing the mortar specimens was randomized. Note that during actual preparation and testing, some of the “observations” were grouped together for convenience. For instance, only three batches (w/c ratios) of mortar specimens were made, and the mortar specimens were subjected to F/T and W/D cycling in three batches (10-cycle, 20-cycle, or 30-cycle). Nonetheless, any deviation from the principle of randomization was minimized wherever possible.

4.1.2 Results and Discussion

General trends:

There were three mix designs tested, i.e., mortars with w/c of 0.48, 0.53, or 0.58, and their air content was tested to be 5.0%, 4.0% and 4.5% respectively according to the ASTM C185 – 08 (Standard Test Method for Air Content of Hydraulic Cement Mortar). The 28-day compressive strengths of these mixes were 8652 psi (60 MPa), 8233 psi (57MPa), and 6375 psi (44MPa), respectively, with tests performed on three D4"×H8" cylinders for each mix.

Table 4.2 presents the tested mechanical properties of 27 “observations” that represent the combination of various mortar specimens with various deicer exposure conditions. The accumulated exposure to MgCl₂ is estimated by first multiplying the duration of exposure with the deicer dilution ratio and then dividing it by the exposure mortar specimen surface area. As detailed later, the potential correlation between this cumulative deicer exposure (30% MgCl₂, in hr/m²) and each of the three mechanical properties was explored. The colors in Table 4.2 indicate the cases where the mechanical property is not a good indicator for the cumulative exposure to MgCl₂ deicers.

Table 4.2: Mechanical properties of mortar specimens after various deicer exposure conditions

<i>w/c</i>	Mortar Specimen Dimensions	Deicer Dilution	F/T + W/D Cycles	30% MgCl ₂ exposure (hr/m ²)	Compressive Strength (psi)	Splitting Tensile Strength (psi)	Young's Modulus (psi)
0.48	2"x4"	100:01:00	10	460	8687	797	1114900
0.48	2"x4"	100:03:00	30	4138	8725	735	2840900
0.48	2"x4"	100:05:00	20	4598	8346	773	3158800
0.48	3"x6"	100:01:00	30	613	6918	926	2863600
0.48	3"x6"	100:03:00	20	1226	8831	763	3182700
0.48	3"x6"	100:05:00	10	1022	8252	842	1077400
0.48	4"x8"	100:01:00	20	230	4426	528	2678300
0.48	4"x8"	100:03:00	10	345	4591	810	2935900
0.48	4"x8"	100:05:00	30	1724	4498	557	2993300
0.53	2"x4"	100:01:00	30	1379	8340	468	1947000
0.53	2"x4"	100:03:00	20	2759	8270	997	2687400
0.53	2"x4"	100:05:00	10	2299	4163	572	3072000
0.53	3"x6"	100:01:00	20	409	4993	852	2681700
0.53	3"x6"	100:03:00	10	613	5984	880	2564700
0.53	3"x6"	100:05:00	30	3066	7862	811	3010400
0.53	4"x8"	100:01:00	10	115	5543	600	3638100
0.53	4"x8"	100:03:00	30	1035	4223	754	3039300
0.53	4"x8"	100:05:00	20	1150	3224	958	2260000
0.58	2"x4"	100:01:00	20	920	6213	949	2684800
0.58	2"x4"	100:03:00	10	1379	5551	507	2845200
0.58	2"x4"	100:05:00	30	6897	7105	540	1358200
0.58	3"x6"	100:01:00	10	204	7498	680	3440200
0.58	3"x6"	100:03:00	30	1839	6631	747	2351900
0.58	3"x6"	100:05:00	20	2044	6451	689	3977200
0.58	4"x8"	100:01:00	30	345	4475	722	646900
0.58	4"x8"	100:03:00	20	690	2984	693	2613800
0.58	4"x8"	100:05:00	10	575	3229	478	2665000
					Not sensitive enough		
					No clear trend		
					Mechanistically challenged		

It is interesting to note that no strong correlation was found between the Young's modulus, compressive strength, or splitting tensile strength of these mortars after exposure. For any two of them, the R-square for correlating them was found to be less than 0.05, indicating little

correlation. This suggests that the exposure to deicers and F/T cycles have altered the mortar specimens and affected their modulus, compressive strength, and splitting tensile strength in different ways, depending on the specimen size, dilution ratio, etc.

Figure 4.2 illustrates how the average compressive strength changed as a function of various factors. The average compressive strength of mortar specimens decreased with an increase in the w/c ratio, but this trend is not statistically significant until the w/c ratio increased from 0.48 to 0.53. All the mortar specimens exhibited significant reduction in their initial compressive strength (8652 psi/59.6MPa, 8233 psi/56.8MPa, and 6375 psi/44.0MPa, for w/c of 0.48, 0.53, and 0.58, respectively). The average compressive strength also decreased with an increase in the mortar specimen dimensions, but this trend is not statistically significant until the specimen size increased from D3"×H6" to D4"×H8". One likely explanation is that D4"×H8" specimens were more prone to F/T damage due to the more severe temperature gradients inside them. Statistically speaking, the average compressive strength of mortar specimens did not change significantly with the dilution ratio of the 30% $MgCl_2$ solution or with the number of F/T + W/D cycles; the mechanisms responsible for which remain to be unraveled.

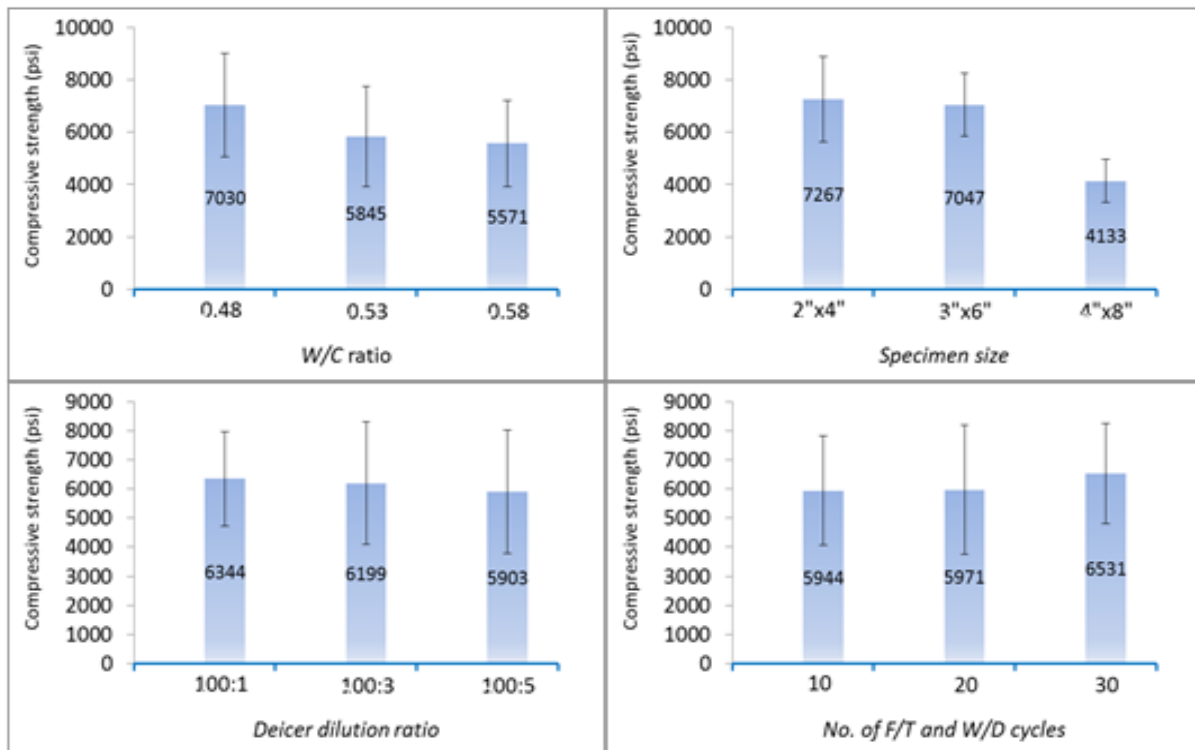


Figure 4.2: Average compressive strength as a function of various factors

Statistically speaking, neither the average splitting tensile strength (STS) nor the average Young's modulus of mortar specimens changed significantly with the four factors shown in Figure 4.3 and 4.4. The average STS and Young's modulus peaked at the w/c of 0.53, with D3"×H6" specimens, at deicer dilution ratio of 100:3, and at the number of F/T + W/D cycles of

20. In other words, there was more than one mechanism at work to affect the STS of exposed mortar specimens, which remain to be unraveled.

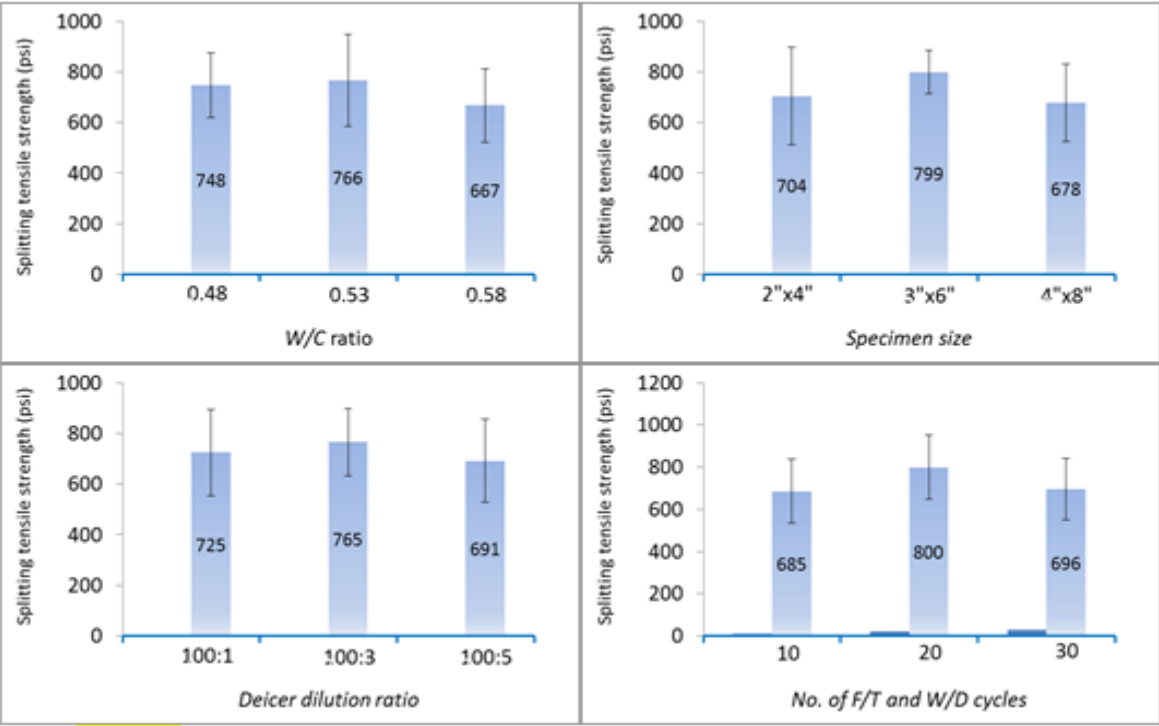


Figure 4.3: Average splitting tensile strength as a function of the influential factors

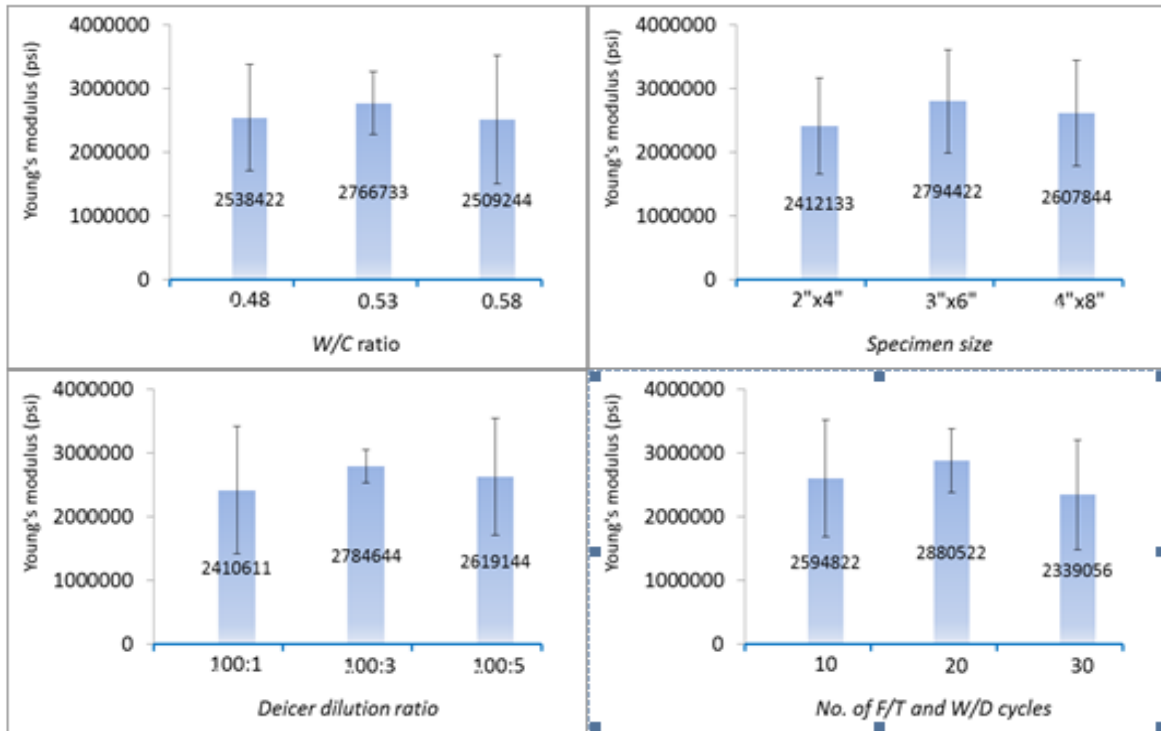


Figure 4.4: Average Young's modulus as a function of the influential factors

Statistical data analyses:

This section presents the results of the statistical data analyses. X_1 , X_2 , X_3 , and X_4 represent w/c ratio, dimensions, deicer dilution ratio, and number of F/T + W/D cycles, respectively. First, the estimated Response Surface Regression model for Y_1 (compressive strength) with all four factors is provided as follows:

$$Y_1 = -19885704 + 3272953 * X_1 - 3368 * X_2 + 38790 * X_3 - 30664 * X_4 + 182366 * X_1^2 - 9 * X_2^2 - 19 * X_3^2 + 3 * X_4^2 + 817 * X_1 * X_2 - 3512 * X_1 * X_3 + 596 * X_1 * X_4 + 4 * X_2 * X_3 - 5 * (X_2 * X_4) + 30 * (X_3 * X_4) \quad (4.1)$$

With adjusted R-square of 68.6%, the number of F/T + W/D cycles (X_4), the square term of dimensions (X_2^2), the interaction term of dimensions with the number of cycles ($X_2 * X_4$), the interaction term of deicer dilution with the number of cycles ($X_3 * X_4$) are the ones that are statistically significant at 90% confidence level and they are highlighted in the regression model above. Interestingly, X_1 (w/c) or its interaction with other factors were not found to be statistically significant, possibly due to unknown competing roles the water/cement ratio played in the deterioration of mortar specimens.

Second, the estimated Response Surface Regression model for Y_2 (STS) with all four factors reveals that none of the terms are statistically significant at 90% confidence level, which indicates that the model was not a good fit. The estimated Response Surface Regression model for Y_3 (Young's modulus) with all four factors reveals that the interaction of w/c ratio and the number of exposure cycles ($X_1 * X_4$) is the only term statistically significant at 90% confidence level.

Finally, a general regression analysis was conducted to investigate the surface resistivity of mortar specimens (Y_4) as a function of the four influential factors. The data in Table 4.3 were utilized in the analysis. Since the surface resistivity measurements were non-destructive and were taken more frequently than the mechanical tests, X_4 (number of cycles) were varied on far more than three levels. In other words, this group of data no longer followed the statistical DoE in Table 4.1. A regression model for Y_4 was estimated by Minitab using the existing data and reveals that surface resistivity generally increases with the decrease in the w/c ratio, the decrease in the mortar specimen dimensions, and the increase in the number of exposure cycles.

Table 4.3: Surface resistivity (in KΩ.cm) as a function of influential factors

w/c	Mortar Specimen Dimensions	MgCl ₂ Deicer Dilution	F/T + W/D Cycles	30% MgCl ₂ exposure (hr/m ²)	Surface Resistivity (KΩ.cm)
0.48	2"x4"	100:1	0	0	8.82
0.48	2"x4"	100:1	3	138	10.10
0.48	2"x4"	100:1	6	276	10.77
0.48	2"x4"	100:1	9	414	10.52
0.48	2"x4"	100:1	10	460	10.50
0.53	2"x4"	100:1	0	0	6.83
0.53	2"x4"	100:1	3	138	7.22
0.53	2"x4"	100:1	6	276	7.62
0.53	2"x4"	100:1	9	414	7.35
0.53	2"x4"	100:1	12	552	7.67
0.53	2"x4"	100:1	15	690	7.57
0.53	2"x4"	100:1	18	828	7.48
0.58	2"x4"	100:1	0	0	5.43
0.58	2"x4"	100:1	3	138	5.95
0.58	2"x4"	100:1	6	276	6.30
0.58	2"x4"	100:1	9	414	6.40
0.58	2"x4"	100:1	12	552	6.50
0.58	2"x4"	100:1	15	690	6.70
0.58	2"x4"	100:1	18	828	6.60
0.48	3"x6"	100:1	0	0	5.82
0.48	3"x6"	100:1	3	61	6.13
0.48	3"x6"	100:1	6	123	6.65
0.48	3"x6"	100:1	9	184	6.68
0.48	3"x6"	100:1	12	245	6.67
0.48	3"x6"	100:1	15	307	6.73
0.48	3"x6"	100:1	18	368	6.32
0.53	3"x6"	100:1	0	0	4.43
0.53	3"x6"	100:1	3	61	4.52
0.53	3"x6"	100:1	6	123	4.87
0.53	3"x6"	100:1	9	184	4.80
0.53	3"x6"	100:1	12	245	4.82
0.53	3"x6"	100:1	15	307	4.67
0.53	3"x6"	100:1	18	368	5.00
0.58	3"x6"	100:1	0	0	3.92
0.58	3"x6"	100:1	3	61	4.22
0.58	3"x6"	100:1	6	123	4.75
0.58	3"x6"	100:1	9	184	4.67
0.58	3"x6"	100:1	10	204	4.33
0.48	4"x8"	100:1	0	0	5.20
0.48	4"x8"	100:1	3	34	5.50
0.48	4"x8"	100:1	6	69	5.68
0.48	4"x8"	100:1	9	103	5.52
0.48	4"x8"	100:1	12	138	5.75
0.48	4"x8"	100:1	15	172	5.85
0.48	4"x8"	100:1	18	207	5.85
0.48	4"x8"	100:1	21	241	5.65
0.53	4"x8"	100:1	0	0	3.53
0.53	4"x8"	100:1	3	34	3.55
0.53	4"x8"	100:1	6	69	3.62
0.53	4"x8"	100:1	9	103	3.73
0.53	4"x8"	100:1	10	115	3.57
0.58	4"x8"	100:1	0	0	3.20
0.58	4"x8"	100:1	3	34	3.47
0.58	4"x8"	100:1	6	69	3.93
0.58	4"x8"	100:1	9	103	3.65
0.58	4"x8"	100:1	12	138	3.73
0.58	4"x8"	100:1	15	172	3.78
0.58	4"x8"	100:1	18	207	4.02
0.48	2"x4"	100:3	0	0	9.17
0.48	2"x4"	100:3	3	414	9.90
0.48	2"x4"	100:3	6	828	10.50
0.48	2"x4"	100:3	9	1242	10.67
0.48	2"x4"	100:3	12	1655	10.82
0.48	2"x4"	100:3	15	2069	11.55
0.48	2"x4"	100:3	18	2483	10.73
0.53	2"x4"	100:3	0	0	6.38
0.53	2"x4"	100:3	3	414	8.57
0.53	2"x4"	100:3	6	828	7.17
0.53	2"x4"	100:3	9	1242	7.55
0.53	2"x4"	100:3	12	1655	7.73
0.53	2"x4"	100:3	15	2069	7.68
0.53	2"x4"	100:3	18	2483	7.63
0.58	2"x4"	100:3	0	0	5.25
0.58	2"x4"	100:3	3	414	5.87
0.58	2"x4"	100:3	6	828	6.22
0.58	2"x4"	100:3	9	1242	6.25
0.58	2"x4"	100:3	10	1379	6.60
0.48	3"x6"	100:3	0	0	5.70
0.48	3"x6"	100:3	3	184	6.20
0.48	3"x6"	100:3	6	368	5.72
0.48	3"x6"	100:3	9	552	6.38
0.48	3"x6"	100:3	12	736	6.50
0.48	3"x6"	100:3	15	920	6.67
0.48	3"x6"	100:3	18	1104	6.40
0.53	3"x6"	100:3	0	0	4.38
0.53	3"x6"	100:3	3	184	4.60
0.53	3"x6"	100:3	6	368	4.97
0.53	3"x6"	100:3	9	552	5.07
0.53	3"x6"	100:3	10	613	4.92
0.58	3"x6"	100:3	0	0	3.62
0.58	3"x6"	100:3	3	184	3.87
0.58	3"x6"	100:3	6	368	3.67
0.58	3"x6"	100:3	9	552	3.90
0.58	3"x6"	100:3	12	736	4.20
0.58	3"x6"	100:3	15	920	4.32
0.58	3"x6"	100:3	18	1104	4.30
0.48	4"x8"	100:3	0	0	5.45
0.48	4"x8"	100:3	3	103	5.98
0.48	4"x8"	100:3	6	207	5.93
0.48	4"x8"	100:3	9	310	6.30
0.48	4"x8"	100:3	10	345	6.00
0.53	4"x8"	100:3	0	0	3.55
0.53	4"x8"	100:3	3	103	3.70
0.53	4"x8"	100:3	6	207	3.78
0.53	4"x8"	100:3	9	310	3.83
0.53	4"x8"	100:3	12	414	3.95
0.53	4"x8"	100:3	15	517	3.98
0.53	4"x8"	100:3	18	621	4.00
0.58	4"x8"	100:3	0	0	3.37
0.58	4"x8"	100:3	3	103	3.60
0.58	4"x8"	100:3	6	207	3.68
0.58	4"x8"	100:3	9	310	3.75
0.58	4"x8"	100:3	12	414	3.88
0.58	4"x8"	100:3	15	517	3.98
0.58	4"x8"	100:3	18	621	3.98
0.48	2"x4"	100:5	0	0	9.13
0.48	2"x4"	100:5	3	690	10.30
0.48	2"x4"	100:5	6	1379	9.98
0.48	2"x4"	100:5	9	2069	10.08
0.48	2"x4"	100:5	12	2759	10.95
0.48	2"x4"	100:5	15	3449	11.03
0.48	2"x4"	100:5	18	4138	10.92
0.53	2"x4"	100:5	0	0	6.55
0.53	2"x4"	100:5	3	690	7.37
0.53	2"x4"	100:5	6	1379	7.08
0.53	2"x4"	100:5	9	2069	7.67
0.53	2"x4"	100:5	10	2299	7.80
0.58	2"x4"	100:5	0	0	5.52
0.58	2"x4"	100:5	3	690	6.13
0.58	2"x4"	100:5	6	1379	6.52
0.58	2"x4"	100:5	9	2069	6.80
0.58	2"x4"	100:5	12	2759	7.02
0.58	2"x4"	100:5	15	3449	7.53
0.58	2"x4"	100:5	18	4138	7.52
0.48	3"x6"	100:5	0	0	5.97
0.48	3"x6"	100:5	3	307	6.20
0.48	3"x6"	100:5	6	613	6.73
0.48	3"x6"	100:5	9	920	6.37
0.48	3"x6"	100:5	10	1022	6.55
0.53	3"x6"	100:5	0	0	4.32
0.53	3"x6"	100:5	3	307	4.62
0.53	3"x6"	100:5	6	613	5.02
0.53	3"x6"	100:5	9	920	5.00
0.53	3"x6"	100:5	12	1226	4.93
0.53	3"x6"	100:5	15	1533	5.33
0.53	3"x6"	100:5	18	1839	5.33
0.58	3"x6"	100:5	0	0	3.73
0.58	3"x6"	100:5	3	307	4.05
0.58	3"x6"	100:5	6	613	4.43
0.58	3"x6"	100:5	9	920	4.32
0.58	3"x6"	100:5	12	1226	4.50
0.58	3"x6"	100:5	15	1533	4.65
0.58	3"x6"	100:5	18	1839	4.68
0.48	4"x8"	100:5	0	0	5.32
0.48	4"x8"	100:5	3	172	5.67
0.48	4"x8"	100:5	6	345	5.70
0.48	4"x8"	100:5	9	517	5.88
0.48	4"x8"	100:5	12	690	6.13
0.48	4"x8"	100:5	15	862	6.15
0.48	4"x8"	100:5	18	1035	6.13
0.53	4"x8"	100:5	0	0	3.50
0.53	4"x8"	100:5	3	172	3.72
0.53	4"x8"	100:5	6	345	3.82
0.53	4"x8"	100:5	9	517	3.92
0.53	4"x8"	100:5	12	690	4.02
0.53	4"x8"	100:5	15	862	3.95
0.53	4"x8"	100:5	18	1035	4.12
0.58	4"x8"	100:5	0	0	3.27
0.58	4"x8"	100:5	3	172	3.87
0.58	4"x8"	100:5	6	345	3.65
0.58	4"x8"	100:5	9	517	4.02
0.58	4"x8"	100:5	10	575	3.75

Methods of using mortar specimens to assess cumulative MgCl₂ deicer exposure:

Close examination of data shown in Table 4.2 and Table 4.3 reveals that in some specific cases, the mortar specimens could serve as reliable sensors to be deployed in the field environment to assess the cumulative MgCl₂ deicer exposure at the given site. This is considering the strong correlation between their readily measurable “response parameters” (compressive strength, splitting tensile strength, Young’s modulus, and surface resistivity) and the cumulative deicer exposure (30% MgCl₂, in hr/m²), as shown in Figure 4.5 and Figure 4.6. Note that these excluded the cases where there is no clear trend between the response parameter and the cumulative deicer exposure or the trend is mechanistically challenged as a result of other complicating factors, or the response parameter is not sensitive to the change in deicer exposure, or when the correlation R-square is less than 0.90.

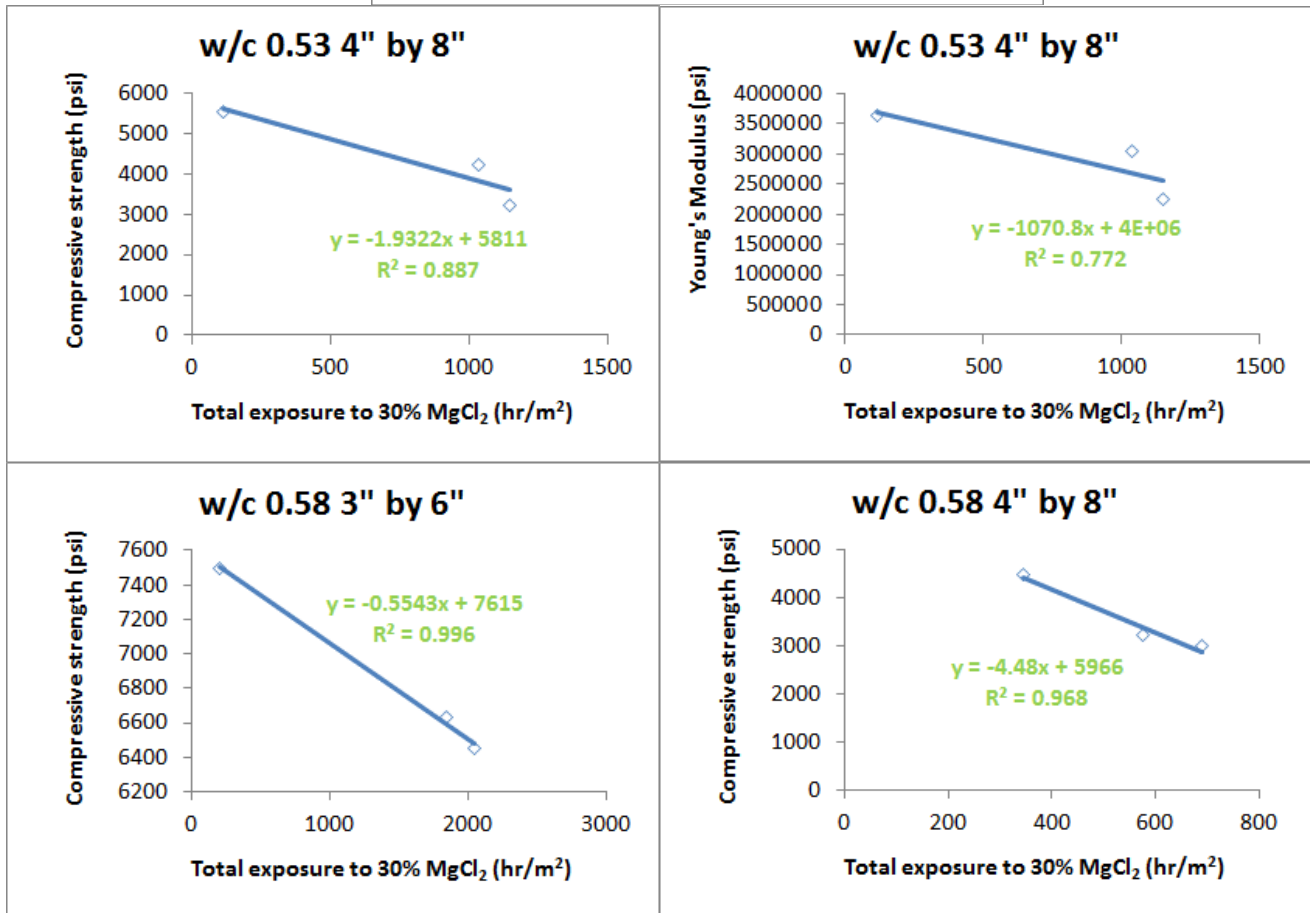
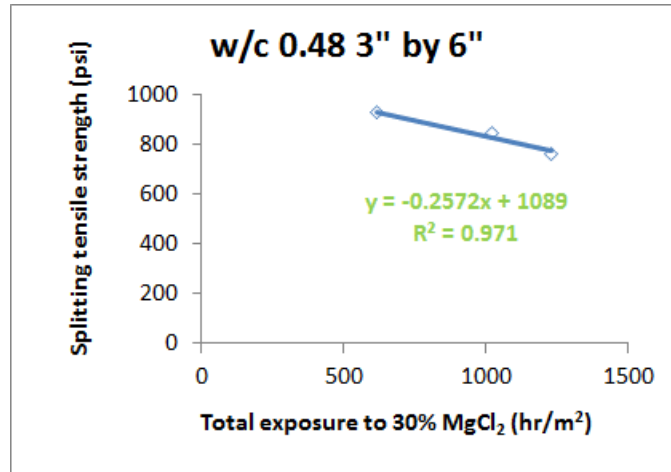
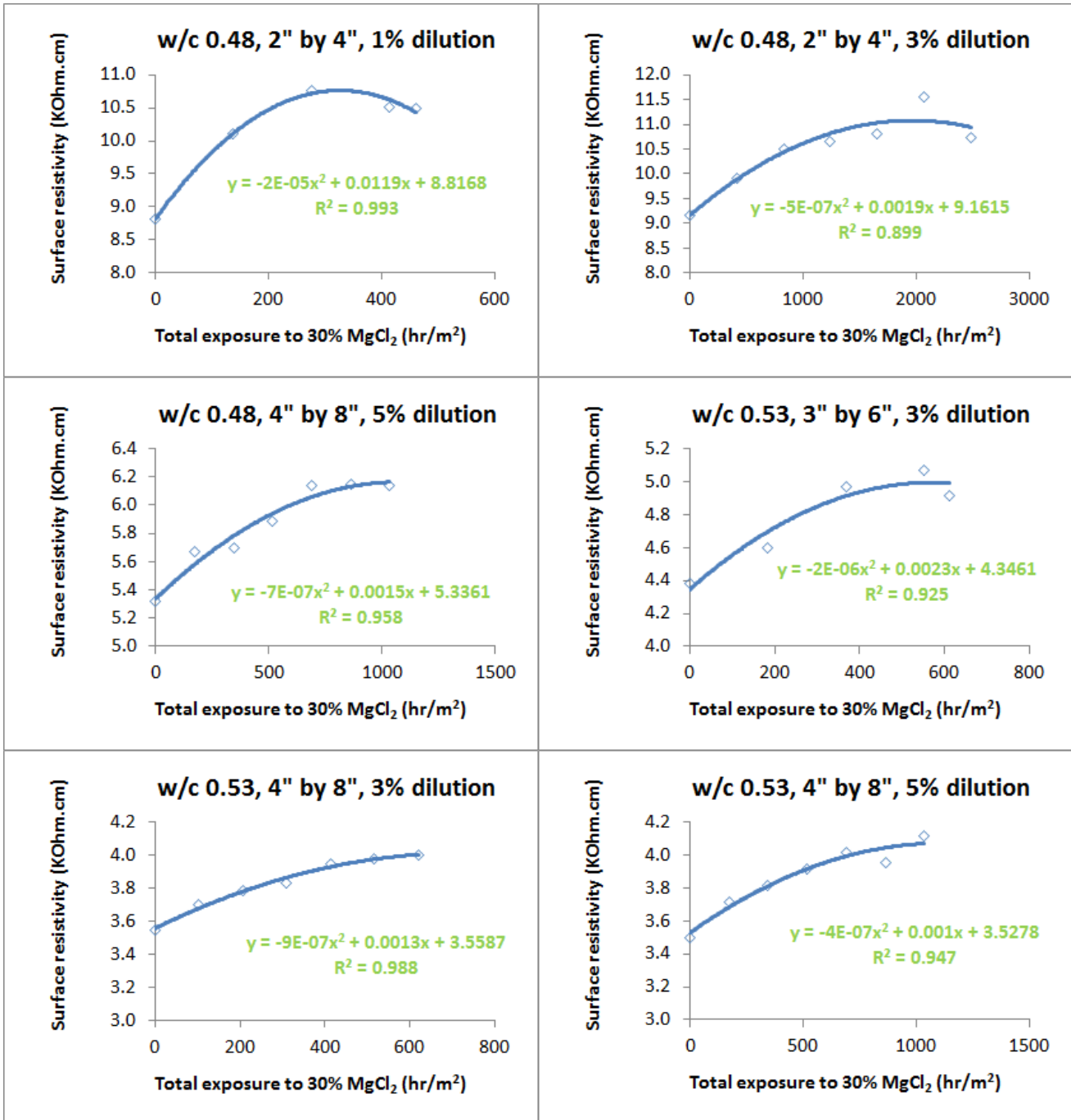


Figure 4.5: Mechanical properties of mortar specimens as reliable indicator of MgCl₂ deicer exposure



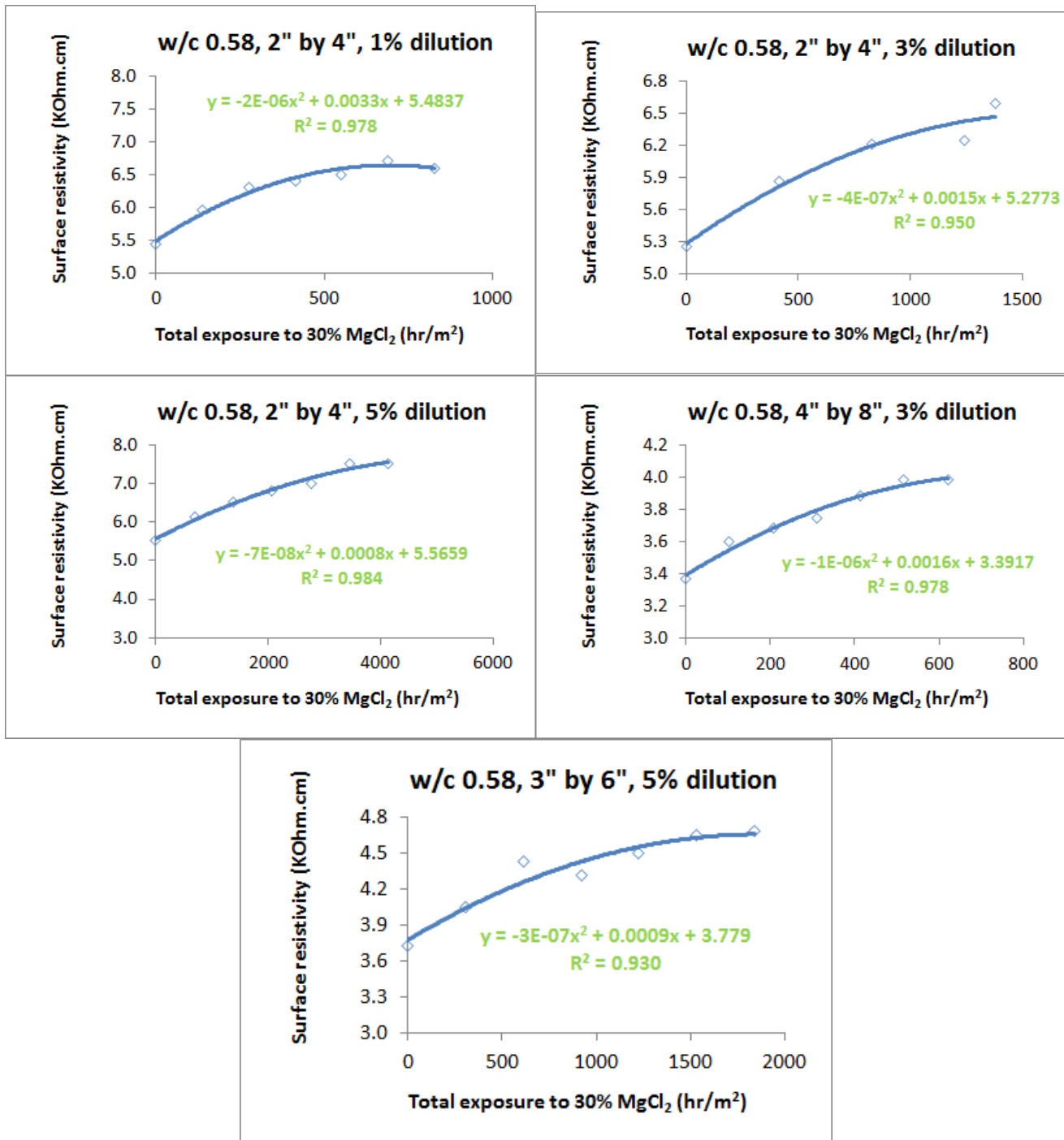


Figure 4.6: Surface resistivity of mortar specimens as reliable indicator of MgCl₂ deicer exposure

To assess the cumulative MgCl₂ deicer exposure over time at a given site, a total of at least 21 mortar samples should be deployed for periodical, non-destructive surface resistivity measurements, as shown in Table 4.4. Each set of mortar specimens should be in triplicates and each specimen should be measured for six surface resistivity reading at the given time. Note that the surface resistivity readings should be taken at room temperature (23±3°C, i.e., 73±5°F) and a

relative humidity of $32 \pm 7\%$. With the average surface resistivity value, the MgCl_2 deicer exposure can be estimated using the equations shown in Figure 4.6. The consensus from different equations on the estimated MgCl_2 deicer exposure (in hr/m^2) should also shed light on the average dilution ratio of the applied deicer at the given site, based on Table 4.4.

Table 4.4: Deploying mortar specimens for periodical surface resistivity measurements

Set No.	w/c	Dimension	Most suitable range of dilution exposure by the applied 30 wt.% MgCl_2 concentration
1	0.48	2" by 4"	1% to 3% (two different equations)
2	0.48	4" by 8"	5%
3	0.53	3" by 6"	3%
4	0.53	4" by 8"	3% to 5% (two different equations)
5	0.58	2" by 4"	1%, 3%, to 5% (three different equations)
6	0.58	4" by 8"	3%
7	0.58	3" by 6"	5%

To assess the cumulative MgCl_2 deicer exposure at a given site, another group of mortar samples can be deployed. This is for periodical sampling (12 mortar specimens for each sampling) followed by surface resistivity readings and destructive mechanical testing, as shown in Table 4.5. Each set of mortar specimens should be in triplicates. With the average mechanical property value, the MgCl_2 deicer exposure can be estimated using the equations shown in Figure 4.5. The consensus from different equations on the estimated MgCl_2 deicer exposure (in hr/m^2) should be adopted, which may further supplement the estimates from surface resistivity measurements.

Table 4.5: Deploying mortar specimens for periodical sampling and mechanical testing

Set No.	w/c	Dimension	Most suitable mechanical property to use for estimating MgCl_2 exposure
1	0.48	3" by 6"	Splitting tensile strength
2	0.53	4" by 8"	Compressive strength and Young's modulus (from the same stress-strain curve of compression test)
3	0.58	3" by 6"	Compressive strength
4	0.58	4" by 8"	Compressive strength

4.2 METALLIC SPECIMENS

4.2.1 Materials and Methods

The metallic coupons included hot rolled low carbon steel (C1010), a tool steel, a magnesium alloy, and an aluminum alloy (Al 1100). After the cyclic exposure to MgCl_2 solutions of various concentrations (detailed later), digital photos of the metallic coupons were taken during the dry stage of each cycle and their dry weight measured following the cleaning procedure described as follows. For carbon steel and tool steel, the coupons are pre-washed under running tap water to remove any loosely adherent corrosion products. Then they are placed into glass beakers containing the cleaning acid, which is composed of concentrated hydrochloric acid (HCl) containing 50 g/L SnCl_2 (stannous chloride) and 20 g/L SbCl_3 (antimony trichloride). Then allow the coupons to soak in the cleaning acid for a total of 15 minutes. Remove the coupons from the acid and rinse with tap water followed by distilled water. Wipe with a paper towel to clean any residual deposit from the coupons. They are then returned to the cleaning acid and the procedure is repeated. For magnesium alloy coupons, they are soaked in tap water for 10 minutes first. Then put them out and lay them on some clean paper towel to dry. After that, use a brush to treat the whole top surface of coupons with a chromic acid solution (10%), which has been added to sulfuric acid by the ratio of 100:1. Allow the chromic acid to remain on the surface for 10 minutes. Repeat this step for another 10 minutes. Then turn coupons over and treat the other surface with the same procedure. Coupons then are rinsed with tap water followed by de-ionized water, finally by acetone. This cleaning cycle is repeated four times for the magnesium alloy coupons. For aluminum coupons, there was generally no visible corrosion after extensive exposure to MgCl_2 . As such, they are rinsed with tap water followed by acetone and then by de-ionized water. After cleaning, the metallic coupons are rinsed in chloroform, air dried for 15 minutes and weighed. The surface resistivity of these metallic specimens were then measured using a Resipod Resistivity Meter (Proceq USA, Inc., Aliquippa, PA) with four equally spaced point electrodes that are pressed onto the metal surface (Wenner or 4-point method, as shown in Figure 4.1). The resistivity measurements were taken at ambient conditions, temperature $23 \pm 3^\circ\text{C}$ (73.4°F) and relative humidity $32 \pm 7\%$. Three measurements were made on each metallic coupon of interest. For some carbon steel coupons, their Rockwell hardness were measured following the ASTM E18 method and using a Digital ME-2 Hardness Tester (New Age Industries, Feasterville, PA) at the “B” scale.

Statistical design of experiments (DoE):

The statistical DoE for each type of metallic coupon incorporated three influential factors, each specified at three levels.

- X_1 : dimension of the metallic coupons (small, medium, large)
- X_2 : type of wet/dry and deicer exposure cycles, all with five 6-hr wet/18-dry days followed by two dry days. (Type 1: 1st day in 30% MgCl_2 , 2nd day in 3% MgCl_2 , 3rd day in 1% MgCl_2 , 4th and 5th day in deionized water; Type 2: 1st and 5th day in

30% MgCl₂, 2nd day in 3% MgCl₂, 3rd and 4th day in deionized water; Type 3: 1st, 3rd, and 5th day in 30% MgCl₂, 2nd and 4th day in 3% MgCl₂).

- X₃: number of weeks (2, 4, and 6)

There were 30 runs for each metal type and each run was with duplicate coupons. The run order was randomized.

4.2.2 Results and Discussion

Figure 4.7 shows the Rockwell hardness of C1010 carbon steel coupons may serve as a possible indicator of cumulative MgCl₂ deicer exposure. There is a relatively good negative correlation between these two, with more deicer exposure leading to lower hardness values. However, the R-square is only 0.70, suggesting that this may not be as reliable as using mortar specimens and their engineering properties (discussed in Section 4.1).

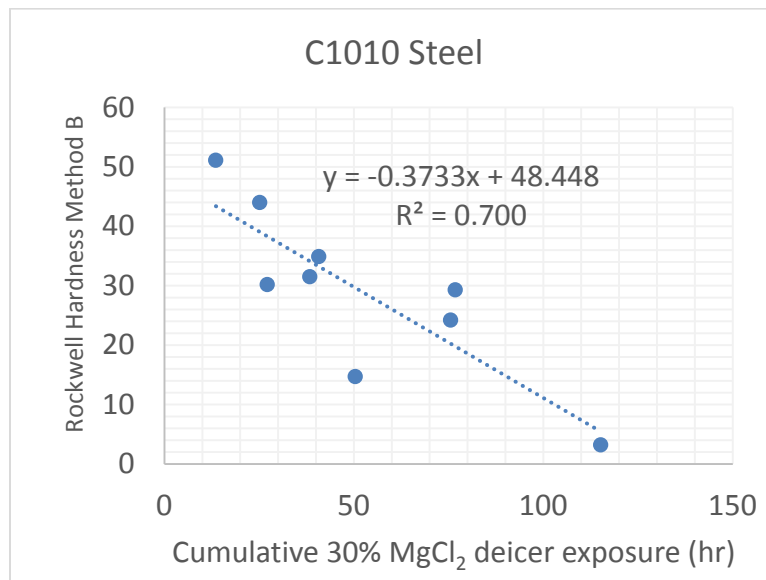


Figure 4.7: Rockwell hardness of carbon steel coupons as possible indicator of MgCl₂ deicer exposure

Figure 4.8 illustrates that the mass change of metallic coupons cannot serve as a reliable indicator of cumulative MgCl₂ deicer exposure. There was neither a clear trend nor a strong correlation between these two parameters. Note that under the investigated conditions, the mass change values for all the aluminum alloy specimens was 0%.

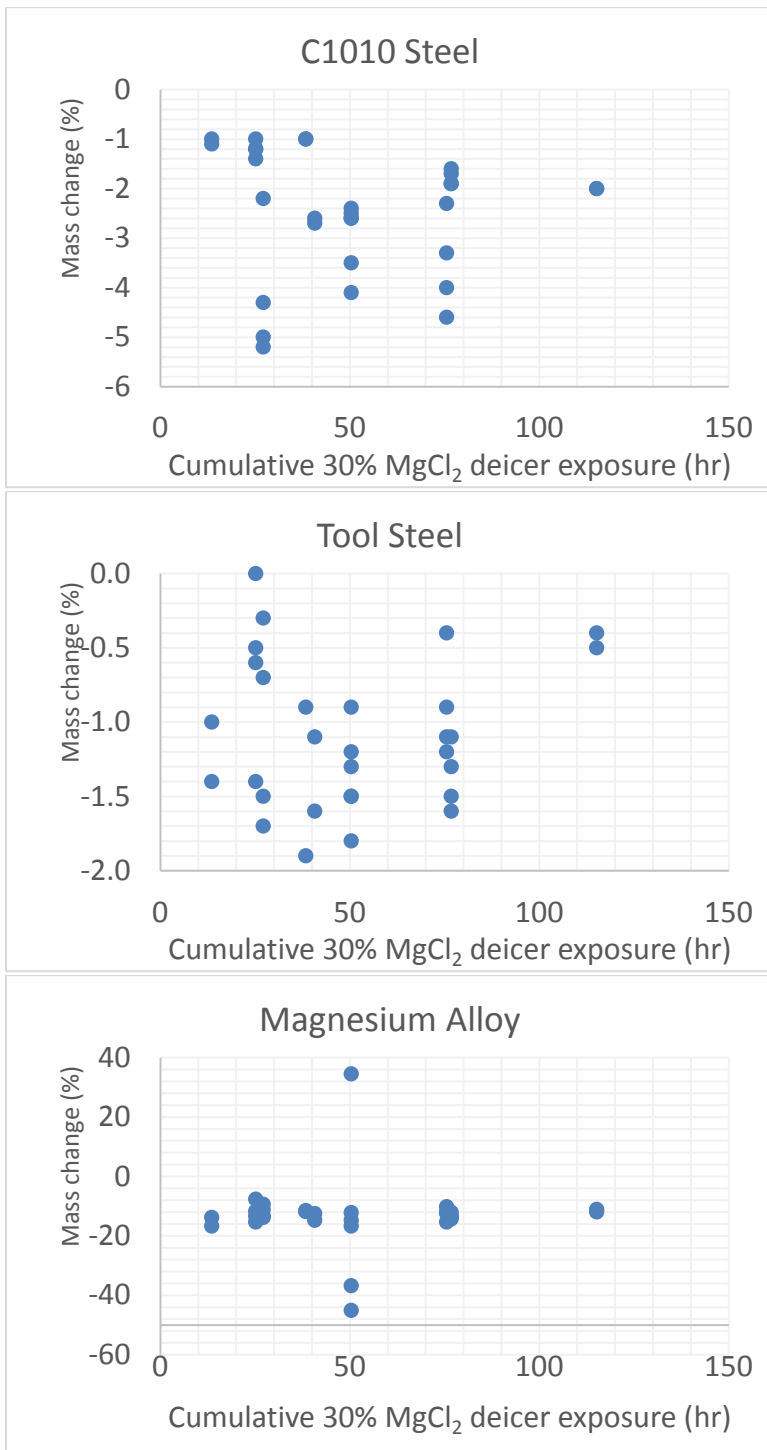


Figure 4.8: Mass loss of metallic coupons as a function of MgCl₂ deicer exposure

Figure 4.9 illustrates that the surface resistivity of magnesium alloy coupons cannot serve as a reliable indicator of cumulative MgCl₂ deicer exposure. There was neither a clear trend nor a

strong correlation between these two parameters. Furthermore, the surface resistivity readings on the corroded coupons featured high variability, which was the same issue that plagued the other types of metallic coupons.

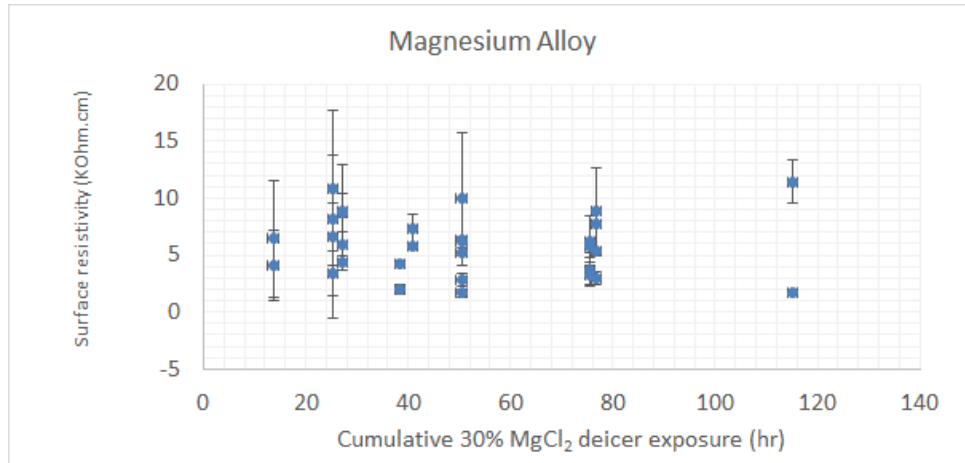


Figure 4.9: Surface resistivity of magnesium alloy coupons as a function of MgCl₂ deicer exposure

Figure 4.10 illustrates that the digital photos of metallic coupons cannot serve as a reliable indicator of cumulative MgCl₂ deicer exposure. After significant exposure to MgCl₂ deicer solutions, the entire surface of steel coupons could be entirely covered with corrosion products, and the percent of corroded area no longer changes sensitively to the change in the amount of MgCl₂ the coupon has been exposed to. In the case of magnesium alloy, significant exposure to MgCl₂ deicer eventually disintegrated parts of the coupons, making them unreliable for sensor applications. In the case of aluminum alloy, no apparent surface distress could be observed even after significant MgCl₂ deicer exposure (even though such exposure is known to compromise the internal microstructure of the aluminum alloy).

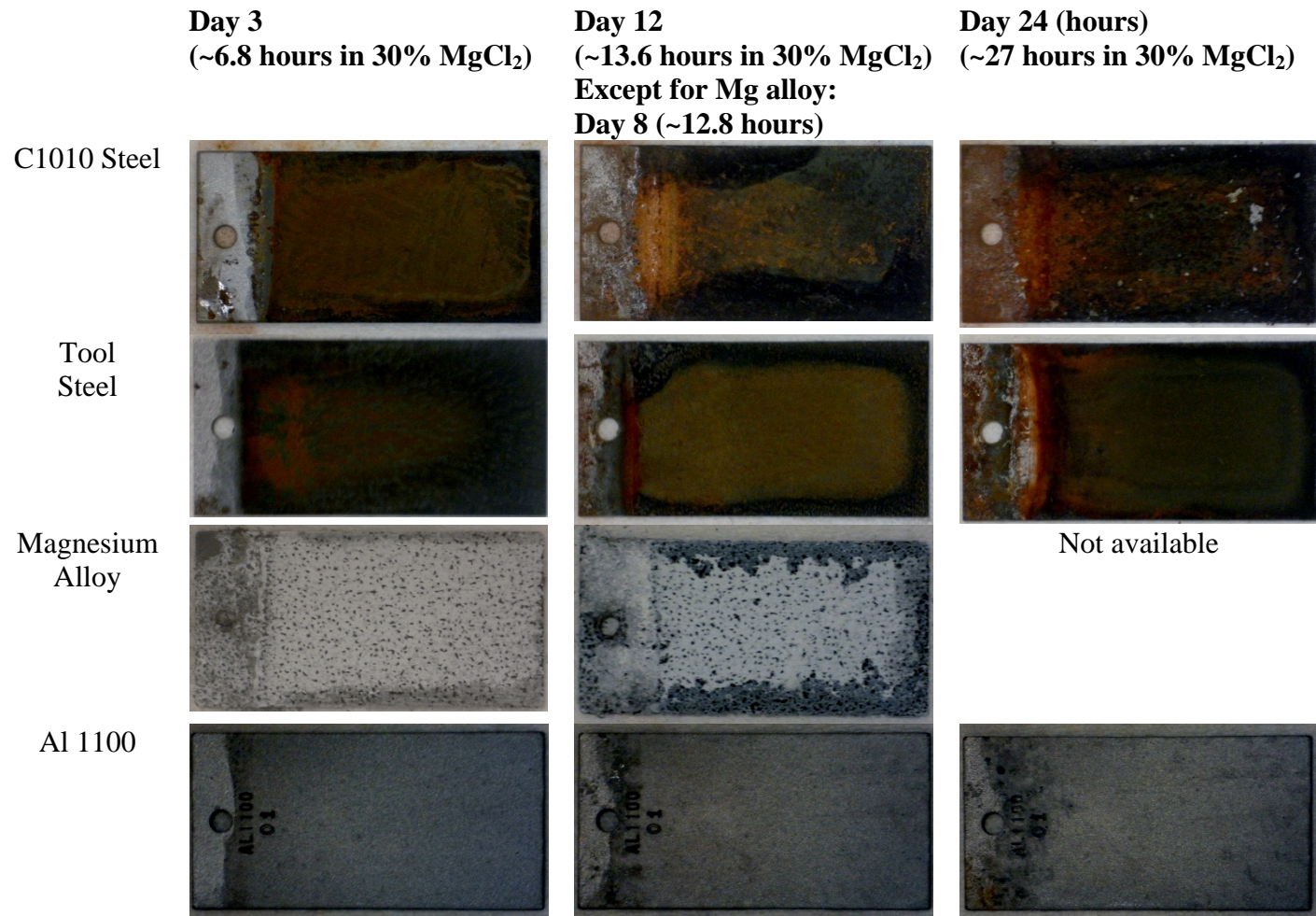


Figure 4.10: Representative digital photos of metallic coupons as a function of metal type and MgCl₂ deicer exposure

4.3 POLYMERIC SPECIMENS

Laboratory tests were designed and conducted to assess the feasibility of using polymeric specimens to assess the cumulative exposure to $MgCl_2$ deicer. A total of eight polymers were identified to be superabsorbent candidates and tested for chloride binding capacity. These included: Amberlite, polyethene, polyvinylalcohol, polytetrafluoroethylene, dextrose, polyethylene glycol, chitosan, and polyacrylic acid (PAC). Most of them (except chitosan and PAC) failed to exhibit ability to bind free chlorides. Chitosan and PAC only exhibited significant chloride binding capacity when the free chloride anion concentration exceeded 0.21 M. Furthermore, chitosan is water soluble and biodegradable, which makes it difficult to serve as a reliable field-deployable sensor. Similarly, PAC can quickly age and degrade in the field environment with UV light and microorganisms. As such, polymers were deemed unsuitable for the intended application.

4.4 CONCLUDING REMARKS

The work in this study suggest that it is possible to deploy standard mortar specimens (with careful considerations given to their placement and orientation etc.), randomly sample them periodically (e.g., after each winter season), and test their surface resistivity (non-destructively) or mechanical properties (destructively) to indicate the deicer exposure at the given specific site. For field validation of this method, the history of deicing operations (e.g., frequency and application rates) and traffic/climatic conditions of the select bridge deck would need to be recorded for subsequent analysis. Prior to the deployment, surface-sensitive properties (e.g. surface resistivity, and absorption capacity) of the mortar slabs would need to be measured, in order to establish a baseline.

This method is inexpensive to deploy, and the output from the method would be an exposure rank that correlates with the cumulative $MgCl_2$ exposure at the surface of the concrete in the target area (e.g., a specific bridge deck). As such, this would allow ODOT to select the most problematic sites if damage mitigation measures are required.

5.0 DAMAGE ANALYSIS TOOL

5.1 INTRODUCTION

This chapter is devoted to the development of a tool for estimating current deicer damage of concrete decks and for predicting the time to future states of damage on the basis of the field investigation data in Chapter 3. The damage state tool may also allow users to estimate the benefit of employing a damage mitigation procedure.

One way to determine the life-cycle performance of bridge decks is to use risk rating factors (Stewart 2001). Risk rating factors tend to increase with time, as the bridge deck ages and deteriorate. The major causes of bridge deck deterioration include material characteristics, construction quality, freeze-and-thaw cycles, deicer exposure, overload trucks, etc. For this study, the damage state tool mainly focuses on the severity of concrete damage caused by deicer exposure.

Unlike the laboratory testing, in which all tested samples were subjected to similar environmental conditions, the concrete samples cored from the field decks experienced much more complicated conditions. As such, it is challenging to evaluate the overall properties of field concrete pavements or structures by analyzing their core samples. The following two factors further complicate the analysis. First, it is not realistic to obtain sufficient number of core samples to enable a comprehensive testing program. Second, the core samples may not statistically represent the overall field concrete which is spatially variable in nature.

Figure 5.1 presents schematic illustration of the concrete pavement or structure in a small area but with high variability in external environmental conditions. Surface scaling and/or depression may lead to the formation of some small reservoirs on the concrete. Concrete at these small reservoirs (e.g., area A) can accumulate more deicers than the adjacent areas. Therefore, area A and area B would experience different number of F/T cycles and exposure to different deicer concentrations. Note that higher deicer concentration may increase or decrease the number of F/T cycles inside the concrete and thus affect the degree of physical attack, depending on the specific deicer concentration and concrete temperature. Higher deicer concentration generally accelerates the rate of chemical attack by the residual deicer inside the concrete, especially during summer.

How to accurately evaluate the condition of concrete bridge deck using a limited number of core samples is useful for bridge owners to implement preservation or repair/rehabilitation strategies in a timely fashion. The following sections describe a simple model based on the percolation theory. By combining the historical maintenance information and permeability and strength testing results from core samples, the current service condition of bridge decks can be reasonably evaluated.

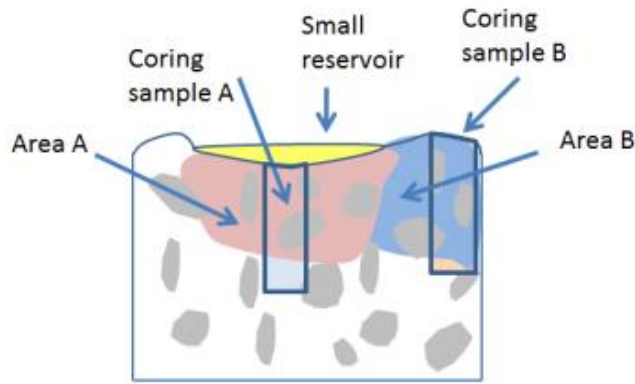


Figure 5.1: Schematic illustration of field concrete in a small area but with different external environmental conditions

5.2 PREDICTION OF THE SERVICE CONDITION OF THE CURRENT BRIDGES

5.2.1 Gas Permeability

According to the percolation theory, the gas permeability of field concrete can be predicted by the following equation:

$$G_c = G_{eff} \left(\frac{p-p_c}{p} \right)^\tau \quad (5.1)$$

where G_{eff} is the effective gas permeability of field concrete, G_c is a constant representing the gas permeability of the new concrete, p and p_c are the relative density of the field concrete and the porosity threshold that leads to the percolation corresponding to the gas permeability. The most important parameter here is the critical exponent τ . In the percolation theory, the critical exponent τ and the θ_c are considered as universal with values of 1.3 and 0.58 in two dimensions, and 2.0 and 0.16 in three dimensions.

5.2.2 Mechanical Properties

The mechanical strength of field concrete (a porous material) as a function of the porosity can also be predicted by a power law, which can be written as:

$$\sigma_{eff} = \sigma_c \left(\frac{\theta - \theta_c}{\theta} \right)^{-\mu} \quad (5.2)$$

where σ_{eff} is the real strength of field concrete, σ_c is a constant representing the strength of the new concrete, θ and θ_c are the relative density of the field concrete and the percolation threshold

corresponding to mechanical properties. Previous study showed that, for the mechanical properties in a percolation system, the value of μ is (Margolina 1988):

$$\mu = 0.45 \pm 0.06 \quad (5.3)$$

5.2.3 Coupling the Influential Factors

Previous studies generally consider the critical exponents in porous media as universal values. However, this universality will be broken if the microstructure of the material does not vary regularly. As a result, it is important to establish the relationship between the critical exponents and the porosity of concrete with exposure to coupling effects. Accordingly, the porosity of the concrete plays the most important role for the service life prediction. The performance of the concrete can be written as a function of several parameters, including the F/T cycles, mechanical loading history, and deicer attack. Therefore, it can be written as:

$$\mathbf{P} = \mathbf{f}(\mathbf{F/T}, \boldsymbol{\sigma}, \mathbf{C}) \quad (5.4)$$

where C represents chemical degradation of the concrete as a result of deicer attack and σ represents physical degradation of the concrete as a result of external mechanical stresses. Assuming the three factors to be independent of each other, Equation (4) can be written as:

$$\mathbf{P} = \mathbf{f}(\mathbf{F/T}, \mathbf{C})\mathbf{g}(\boldsymbol{\sigma}) = \mathbf{T}(\mathbf{Service\ life}) \quad (5.5)$$

We assume that all factors follow the power law relationships as follows:

$$f(F/T) = Q_1 \left(\frac{\xi - \xi_c}{\xi} \right)^{-f} \quad (5.6)$$

$$g(\sigma) = Q_2 \left(\frac{\xi - \xi_c}{\xi} \right)^{-s} \quad (5.7)$$

$$h(C) = Q_3 \left(\frac{\xi - \xi_c}{\xi} \right)^{-c} \quad (5.8)$$

Therefore, the service life can be predicted as:

$$P = f(F/T)g(\sigma)h(C) = T(\mathbf{Service\ life}) = P_0 \left(\frac{\xi - \xi_c}{\xi} \right)^{(f+s+c)} \quad (5.9)$$

where f , s , and t represent the critical exponents corresponding to the F/T cycling, external mechanical stress, and chemical attack, respectively. ξ and ξ_c are the relative density of the field concrete and the threshold value corresponding to the service life. For chemical attack, the degradation could be considered as a function of deicing chemical quantity and this function could be considered as linear. For physical attack, the degradation could be considered as a function of F/T cycles and overload truck loadings, which are known to induce cracking of the concrete and increase its porosity.

Equation (9) could be written as:

$$\mathbf{P} = \mathbf{P}_0 \boldsymbol{\varphi}^{(f+s+c)} \quad (5.10)$$

where $\varphi = \frac{\xi - \xi_c}{\xi}$.

In Equation (5.10), the values of f , s , and c can be defined as:

$$f = \alpha \frac{F/T_{real}}{F/T_{design}} \quad (5.11)$$

$$s = \beta(\text{percentage of the overload trucks}) \quad (5.12)$$

$$c = \gamma \frac{\text{Real quantity}}{\text{Designed maximum quantity}} \quad (5.13)$$

where α , β , γ represent the relative weights of F/T cycles, fatigue stresses, and chemical attack, which are assumed to be 0.5-0.6, 0.1-0.2, and 0.3-0.4, respectively. As a result, the rank of the bridge decks can be evaluated by the ratio of P/P_0 according to equation (10). In this equation, φ is the average value calculated based on equation (1) and (2). The scores of 0.8-1.0, 0.65-0.8, 0.5-0.65, and below 0.5 correspond to good, satisfactory, fair, and poor, respectively.

Calculation example:

Table 5.1 presents a summary table of the 12 ODOT concrete bridge decks, with the current ratings by the ODOT method and the new ratings by the CSIL method. The CSIL method is explained as follows. Take bridge 09268S as an example, the tested gas permeability was $61.6 \times 10^{-17} \text{ m}^2/\text{s}$. Put this value as G_{eff} in Equation (5.1), and set the G_c value as $6.0 \times 10^{-17} \text{ m}^2/\text{s}$ as a uncompromised dense concrete would feature this level of impermeability. Based on the percolation theory, the value of the critical exponent τ is 2.0. As a result, the value of $\frac{p-p_c}{p}$ can be determined according to Equation (5.1) as 0.32. Put the new splitting tensile strength (1,000 psi), tested splitting tensile strength (848 psi), and critical exponent $\mu = 0.4$ in equation (5.2), the value of $\frac{\theta - \theta_c}{\theta}$ will be 0.66. Then the average value of $\frac{p-p_c}{p}$ and $\frac{\theta - \theta_c}{\theta}$, 0.46, will be defined as the relative density parameter, $\varphi = \frac{\xi - \xi_c}{\xi}$. The real MgCl_2 deicer usage on this bridge was 105 gal/ln-mi per year and the real F/T cycles was 25 per year. We set the α , β and γ values in Equations (5.11) to (5.13) to be 0.5, 0.2, and 0.4, respectively. If the bridges experienced coupling effects, the critical exponents should be calculated according to Equation (5.10). For example, if the design service life of the bridge is 100 years, and the average design number of F/T cycles is 60 times each year, the total design F/T cycles should be $100 \times 60 = 6000$ cycles. Using the estimate from the recent years' data, the real total experienced F/T cycles for this bridge was 1000 cycles over the past 40 years, then the value of f in Equation (5.11) is $0.5 \times 1000/6000 = 0.08$. As the percentage of the real overload trucks was 10%, the value of s is $0.1 \times 0.1 = 0.01$. For the deicer exposure, the ratio of the real quantity of the deicer usage over the designed maximum value is defined as the value of c . If the designed maximum deicer quantity is 2000 gal/ln-mi/FY (this value is determined by the designation of local standard), the value of c could be determined by $0.4 \times 105/2000 = 0.02$. Therefore, the general critical exponent is $0.08 + 0.01 + 0.02 = 0.11$. According to Equation (10), the average rank of the bridge is $0.46^{0.11} = 0.92$.

Table 5.1: Summary of the 12 ODOT concrete bridge decks, with the new ratings by CSIL

Bridge No.	Splitting tensile strength (psi)	Rating by ODOT	Rating by Corrosion & Sustainable Infrastructure Lab (CSIL)	Relative Density Parameter, ρ	Gas Permeability, (in 10^{-17} m ² /s)	Traffic (ADT)	Truck %	Year Built	Average annual no. of F/T cycles	Annual deicer usage (gal/ln-mi/FY)
09268S	848±202	5-FAIR	90% - 92% (GOOD)	0.46	61.6	56700	10	1972	25	105
00576	648±9	4-POOR	35% - 41% (POOR)	0.33	61.6	6450	8	1927	102	130
08958F	739±146	6-SATISFACTORY	87% - 88% (GOOD)	0.47	28.4	7790	11	1973	26	367
08682	606±47	4-POOR	36% - 37% (POOR)	0.37	27.3	14200	15	1962	119	2662
18940	422±31	7-GOOD	48% - 56% (FAIR)	0.20	52.6	20600	10	2002	41	2091
16440	570±55	7-GOOD	36% - 37% (POOR)	0.31	39.1	8332	33	1985	174	2058
19681	664±255	7-GOOD	53% - 57% (FAIR)	0.47	16.8	5454	42	2003	248	3006
18525	523±138	6-SATISFACTORY	78% - 81% (SATISFACTORY)	0.28	35.9	13500	3	2002	93	551
19268	876±11	7-GOOD	* used a w/c of 0.28 & different materials	0.76	9.5	3100	11	2005	133	2525
16358	589±106	7-GOOD	69% - 74% (SATISFACTORY)	0.28	73.5	12801	10	1986	26	1024
16534	465	6-SATISFACTORY	26% - 34% (POOR)	0.20	86.5	9793	16	1985	26	3784
16844	809	6-SATISFACTORY	83% - 85% (GOOD)	0.48	39.4	29440	7	1990	90	166

5.3 CONCLUDING REMARKS

A simplistic empirical-mechanistic model was developed to evaluate the conditions of the current bridge decks. This was made possible by combining percolation theory and the power law behavior of strength and permeability to accommodate input parameters of F/T cycle times, ADT, deicer usage, and engineering properties measured from core samples (e.g., splitting tensile strength and gas permeability coefficient).

This work revealed that the current inspection methods used by ODOT for ranking the conditions of the concrete bridge decks may not be suitable for some decks exposed to the combined effect of F/T cycles and MgCl₂ deicer. Specifically, we identified some decks that had ODOT ranking of GOOD (7) or SATISFACTORY (6), yet would feature low rankings using the developed damage analysis tool (e.g., below 50%). The mechanical testing and microscopic characterization (e.g., reported in Chapter 3) confirmed the validity of the new tool, as it better captures the concrete's internal damage that shows little signs of surface distress.

For future improvements of this model, it is desirable to adopt a probabilistic approach to predicting the chloride contamination of concrete, concrete deterioration due to deicer, and chloride-induced rebar corrosion (*Stewart and Val 2003*). Such a reliability-based approach takes into account the uncertainties associated with various fundamental stochastic processes and interactions, and ensures that the probability of concrete failure is kept at an acceptable level. According to Attwood et al. (*Attwood et al. 1991*), “reliability, defined as the probability of survival in a given period of time, forms the basis of most design codes”. Furthermore, fatigue damage models based on the continuum damage mechanics (*Li et al. 2001*) and/or transport-based concrete durability models may be modified and adopted for predicting deicer-induced damage to the concrete matrix.

6.0 ACCELERATED LABORATORY EVALUATION OF SURFACE TREATMENTS FOR PROTECTING CONCRETE BRIDGE DECKS FROM “SALT SCALING”

6.1 INTRODUCTION

The durability of concrete structures has substantial economic, social, and environmental implications. The issue is exacerbated in cold regions where the concrete is at the risk of freeze-thaw cycling and physical and chemical attack by chemical deicers (*Pigeon and Pleau 1995*). Physical mechanisms of attack by deicers can lead to damage of Portland cement concrete (PCC) in the common forms of scaling, map cracking, or paste disintegration (*Sutter 2008*). Deicers may also pose detrimental effects on concrete infrastructure through their reactions with cement paste and/or aggregates and thus reduce the integrity and strength of the concrete (*Sutter 2008; Shi 2009a, 2010a and 2011*). Finally, roadway deicers often use chlorides as their freezing point depressant, and the ingress of chloride anions into concrete can induce the corrosion of rebar or dowel bar in concrete and lead to premature deterioration of reinforced concrete (*Shi 2012; Liu, 2012; Yu, 2010; Shi, 2010b*).

Sodium chloride (NaCl) remains the principal roadway deicer in use despite its well-known corrosive effects on metals. The scaling of concrete in the presence of NaCl-based deicers, referred to as “salt scaling”, has been recognized as the main cause of frost-related concrete deterioration. It is one of the main culprits contributing to concrete failures of outdoor construction in cold climates, such as concrete roadways, airfield pavements, bridge decks, sidewalks, and driveways. Scaling refers to the local peeling and gradual damage of the concrete surface, often due to cyclic freezing and thawing (*ACI Committee, 1996*). This damage is characterized by the removal of small chips or flakes of binder or mortar (*Arnfelt 1943; Valenza 2006*), often leading to the exposure of coarse aggregate. While this surface distress may not cause significant degradation of mechanical properties of the overall concrete, it can expose the concrete to ready ingress of moisture and aggressive salts and accelerate the deterioration of concrete durability (*Valenza 2007a*). Scaling can occur on concrete surfaces independent of deicer application, as the aqueous solution in the concrete pores near the surface freezes and thaws due to temperature fluctuations and exert expansive forces inside the concrete microstructure. Chloride deicers can aggravate the scaling problem as moisture tends to move toward zones with higher salt concentrations via osmosis and adds to the normal hydraulic pressure. The presence of deicers can increase the rate of cooling and thus may increase the number of freeze/thaw cycles in concrete; yet it can also reduce the freezing point of the pore solution and thus may decrease the number of freeze/thaw cycles in concrete. These opposing effects define the physical distress in concrete caused by deicers, and a pioneering laboratory study revealed the worst conditions at a low concentration (5% NaCl) and optimum conditions at a moderately high concentration (13% NaCl) (*Litvan 1975*). Another study suggested that concrete containing relatively high concentrations of dissolved salts can provide better resistance to scaling than concrete with plain water in its pores (*Korhonen 2002*).

Early research argued that the best protection against "salt scaling" would be a reduction of porosity (Litvan 1975). It is now generally believed that the use of properly cured, air-entrained concrete would prevent physical damage by the freeze/thaw cycling (Williams 2003). For an air-entrained concrete, the spacing factor seems to be its key air void characteristic to allow sufficient resistance to salt scaling (Öttl 2006). It should be noted that air entrainment only slows the freeze-thaw process instead of preventing it (Korhonen 2002).

Valenza and Scherer (Valenza 2007a and 2007b) and Jana (Jana 2007) have reviewed the mechanisms, factors and characteristics influencing concrete scaling. It is believed that proper air entrainment, finishing, and curing can provide far better protection for concrete than other solutions (Jana 2007). While this minimizes physical damage induced by salt precipitation and crystallization, the optimization of concrete properties cannot effectively address the chemical attack to concrete by salt solution. For instance, it has been reported that sodium chloride solution can cause softening of the concrete paste and increase its porosity, through the leaching of calcium cations from cement hydrates or the dissolution of the Portlandite, i.e., $\text{Ca}(\text{OH})_2$ (Shi 2009; Marchand 1994).

In this context, many efforts have been made to protect concrete from chloride-based deicers, among which surface treatments are widely implemented by transportation agencies to preserve their bridge decks and other structures. The application of a surface treatment is recommended for additional protection, especially when the concrete lacks proper air entrainment or has other deficiencies related to curing or finishing. By design, the surface treatment slows down the ingress of water and salt solutions and can reduce the risks associated with freeze/thaw damage, salt scaling, and rebar or dowel bar corrosion for concrete in cold regions (Jana 2007). Commercially available products for concrete surface treatments can be classified into three groups: sealer or coating (that forms a continuous film on the skin of concrete), pore blocker (that reacts with Portlandite and forms insoluble products), and pore liner (that repels water) (Medeiros and Helene 2009; UNI EN 2004).

A number of studies have evaluated the performance of different types of surface treatments as a means of protection for concrete. Mamaghani et al. reported an evaluation of five sealer treatments for protecting concrete bridge decks. An ultra-low-viscosity epoxy sealer was found to be the most efficient at enhancing the concrete's resistance to scaling and chloride penetration (Mamaghani 2009). Zhao et al. evaluated the use of six surface treatments for concrete durability and demonstrated that a three-layer epoxy system and a silane-based surface treatment could significantly enhance the concrete's resistance to chloride, air and water (Zhao 2010). Medeiros and Helene and Almusallan et al. also examined the performance of several surface treatments on the durability of concrete and found epoxy and polyurethane products to be highly effective in enhancing the concrete's resistance to chloride diffusion, water absorption and chemical corrosion (Medeiros 2009; Almusallam 2003). Numerous studies have investigated and confirmed the benefit of silane-based pore liners on the durability of concrete (Basheer 2006; Sandrolini et al. 2012; Pigino et al. 2012; Franzonia 2013; Mamaghani 2007; Ibrahim 1999). Ghoddousi et al. reported that the most effective treatment for the corrosion resistance of reinforced concrete was the combination of a "silane + siloxane" primer with an acrylic top coat (Ghoddousi 2007). They concluded that no single coating could improve the resistance of concrete to all types of deterioration (Ghoddousi 2007). Medeiros and Helene and Moon et al. concluded that the double or triple coating systems were more effective for concrete durability than those with a single coating (Medeiros 2009; Moon et al. 2007).

Only limited studies have been conducted to evaluate various surface treatments for better resistance of concrete to freeze/thaw damage or salt scaling (Basheer 2006; Mamaghani 2007). There is still a need to focus on the surface treatments suitable for preserving concrete in the presence of NaCl-based deicers and to reveal the main characteristics of surface treatments that protect the concrete from salt scaling. The objective of this study is to evaluate the performance of select products for surface treatment of Portland cement concrete structures, particularly their effectiveness in protecting the concrete from potential damage caused by deicer and freeze/thaw cycling (a.k.a., salt scaling).

In this accelerated laboratory study, several commercial products of surface treatment were included in the test program, including three concrete sealers, two crack sealants, and two water repellents. To characterize the product longevity under traffic, the abrasion resistance of concrete treated by each product was tested. To characterize the product effectiveness, the surface treated concrete cylinders were subjected to the joint action of 15 freeze/thaw (F/T) and wet/dry (W/D) cycles and exposure to a diluted deicer simulated by 3 wt.% NaCl solution (and various $MgCl_2$ solutions as well). The mass loss of these concrete cylinders during the freeze/thaw cycles was periodically measured. To help interpret the difference in product performance, the surface-treated concrete specimens were tested for their water absorption rates, gas permeability, and water contact angle. For all the laboratory tests, the untreated concrete was used as control.

6.2 EXPERIMENTAL PROCEDURE

6.2.1 Concrete Constituents, Mixing, and Curing

An ASTM specification C150-07 Type I/II GU Portland cement from Diamond Mountain, MT was used. Coarse aggregates (with maximum size of 9.5 mm) and fine aggregates (clean, natural silica sand, maximum size of 4.75mm) were purchased from the JTLGroup (Belgrade, MT). A chemical agent, triethylamine (TEA) was used for accelerating the early-age strength of concrete. The mix proportion of concrete is summarized in Table 6.1. Note that a half dosage of air entraining agent was used in this study to fabricate the concrete cylinders, and this half air entrainment was designed to accelerate the physical scaling damage induced by the freeze/thaw cycles.

Table 6.1: Mix proportion and properties of concrete

Mix proportion of concrete, kg/m ³						Properties of fresh and hardened concrete				
Cement	Water	TEA	Fine aggregate	Coarse aggregate	Air entrainment	Slump, mm	Air content of fresh concrete, %	Pore volume, %	Compressive strength at 28d, psi	Splitting tensile strength at 28d, psi
407	223.9	0.2035	655	1022	0.02442	210	2.9	10.14	4450	926









The sand and coarse aggregates were added to the mixing container and mixed until a homogeneous mixture was obtained. Then the cement was added and mixed again until a homogeneous mixture was obtained. At the same time, TEA was added into the water and stirred until full dissolution. Then, the water was added from a graduated cylinder and mixed until the concrete was homogeneous and reached the desired consistency. The batch was remixed periodically during the casting of the test specimens, and the mix container was covered to prevent water evaporation. The concrete specimens were made in 2" diameter and 4" height (50.8 mm×101.6 mm) polyvinyl chloride molds. In the first 24 h after molding, the concrete specimens were placed on a rigid surface and at a relative humidity (RH) of about 50% and covered to minimize possible water evaporation. Subsequently, the specimens were de-molded and cured in a moisture room with an ambient temperature of 23°C and RH of about 100% for 27 days. The properties of fresh and hardened concrete are summarized in Table 6.1.

6.2.2 Surface Treatments

After wet curing, the specimens were moved from the moist room to dry conditions at an ambient temperature of 23°C and RH of 30% for 24 h. Then a brush was used to coat all the exposed surfaces of the concrete cylinders with each type of select surface coating. In this study, seven products for concrete surface treatment were utilized.

Table 6.2 lists the technical information about these surface coatings and the appearance of the concrete cylinders after treatment. Non-coated concrete cylinders were also prepared as control. After surface treatment, all cylinders were cured in a dry condition at a temperature of 23°C and RH of 30% for 24 h.

Table 6.2: Technical data about the surface treatments

Type of the treatment	Product code name	Manufacturer	Type and main constituent	Viscosity	Strength of the surface coating	Concrete after treatment
Control	Control	n/a	n/a	n/a	n/a	
Sealer	KB-PP	KwikBond Polymers	Polymer (Resin, Cumene hydro peroxide, and accelerator)	<25cps	Bond strength>500 psi; Compressive strength>3000 psi; Tensile strength>2000 psi	
	KB-PS	KwikBond Polymers	Polymer (Resin, Promoter and cumene hydro peroxide)	<25cps	Bond strength>500psi; Compressive strength>3000 psi; Tensile strength>2000 psi	
	T48-CS	Castek Inc.	Epoxy (Resin, and Hardener)	1200-1600cps	Bond strength: 100% substrate failure; Compressive strength=5000 psi; Tensile strength=1800 psi	
Crack sealant	T70 MX30	Castek Inc.	High Molecular Weight Methacrylate (Resin, promoter and initiator)	10-25cps	Bond strength>615 psi; Compressive strength>3500 psi; Tensile strength>500 psi	
	T78	Castek Inc.	MMA Polymer (Resin, and powder hardener)	<5-10cps	Compressive strength=12800 psi; Tensile strength=8100 psi	
Water repellent	ATS-42	Advanced Chemical Technologies, Inc.	Alkyltrialkoxo silane	penetration depth into concrete=0.4in	n/a	
	ATS-100	Advanced Chemical Technologies, Inc.	VOC Compliant Alkyltrialkoxo silane	Penetration depth into concrete=0.4-0.6in	n/a	

6.2.3 Abrasion Resistance Test

The abrasion resistance testing of concrete specimens was conducted in accordance with ASTM C944/C944M- 12 Standard Test Method for Abrasion Resistance of Concrete or Mortar Surfaces by the Rotating-Cutter Method. To determine the abrasion resistance, three 2"×4" cylindrical specimens were used. Before the tests, specimens were kept in the open-air environment for 24 h to keep all test specimens in equivalent moisture condition and the initial weight and height of specimens were recorded. The abrasion resistance was tested by using a drill press device with a chuck capable of holding and rotating the abrading cutter at a speed of 200 r/min and exerting a normal load of 44 lbf on the specimen surface. Specimens were abraded for three cycles of two minutes for each cycle (a total of six minutes). After each abrading cycle, a high pressure air blower was used for cleaning up the loose dust or particles on the concrete surface, and then the mass loss and height change were measured and calculated.

6.2.4 Salt Scaling Test

The concrete cylinders with or without surface treatment were immersed into a plastic container containing 3% NaCl solution for 24 h. Then the concrete cylinders were surface-dried with paper towel and weighed. Next, all the cylinders were placed back into a closed container and transferred with solution into the freezer at $-20 \pm 1^\circ\text{C}$ for 24 h. After this freezing stage, the specimens (along with the plastic box) were placed in the laboratory environment at $23 \pm 2^\circ\text{C}$ and with a RH ranging from 45 to 55% for 12 h. Once the ice in the plastic container was completely thawed, the cylinders were transferred onto a wood plate and dried for 12 hours, at which time each of the specimens was weighed and their mass recorded. This freeze/thaw and wet/dry cycle was repeated 15 times. After drying at 3, 7, 10, 13, and 15 cycles, the mass change of each concrete cylinder was tested.

Note that a sufficiently low temperature (-20°C) and sufficient amount of time (24h) were both crucial to ensure the complete freezing of the concrete pore solution. By design, this test protocol simulated the salt scaling of the field concrete in an accelerated manner. For concrete structures in the field environment, often the number of their freeze/thaw cycles is estimated from the number of times the ambient air temperature crosses the 0°C threshold (divided by two). This method tends to substantially overestimate the actual number of freeze/thaw cycles that occurred inside the concrete, especially when the presence of deicer solution significantly reduces the freezing point of the pore solution.

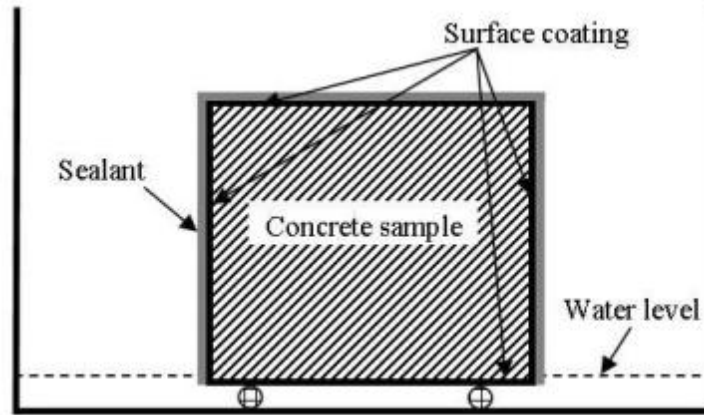
6.2.5 Water Absorption Test

In order to evaluate the water resistance of various surface-treated concrete, the water absorption test was conducted in accordance with ASTM C1585-13 Standard Test Method for Measurement of Rate of Absorption of Water by Hydraulic-Cement Concretes. A concrete sample with 2" diameter and 2" height was used for this test, as shown in Figure 6.1a.

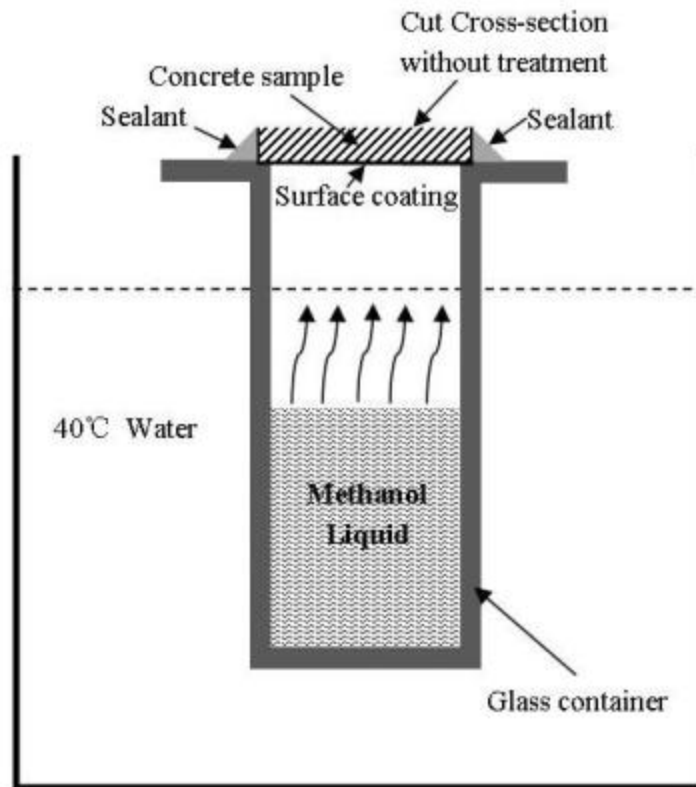
6.2.6 Gas Permeability Test

Gas permeability tests of concrete were conducted in order to evaluate the impermeability of various surface-treated concrete specimens in accordance with the apparatus and procedures proposed by Alshamsi and Imran (2002). The tests were performed using liquid methanol as the gas source for determining the gas transport properties. A $\frac{1}{2}$ " thick specimen was cut from a 2"×4" concrete cylinder

sample and then oven-dried at 60°C for 72 h to remove the moisture within the specimen. Subsequently, the specimen was sealed on each side of the cell with an epoxy sealant in order to avoid any leakage of methanol vapor, as shown in Figure 6.1b. The gas permeability coefficient was then calculated using the equations detailed elsewhere (*Han 2013*)



(a)



(b)

Figure 6.1: Schematic illustration of: (a) water absorption test setup; (b) gas permeability test setup

6.2.7 Water Contact Angle Measurements

Water contact angle is a measure of the hydrophobicity of the surface-treated concrete. A Video Contact Angle Analysis System, VCA 2500XE manufactured by Advanced Surface Tech, was used for water contact angle measurements. A 1/2" thick specimen was cut from each select 2" by 4" concrete cylinder and then subjected to water contact angle testing. To minimize potential inaccuracy due to the water absorption by the concrete, all the specimens were maintained at a saturated- surface-dry (SSD) condition. Before the test, a filter paper was used to wipe the residual water from the surface of the specimens. Distilled water was used for the water contact angle testing, and at least 20 measurements were recorded for each specimen.

6.3 RESULTS AND DISCUSSION

6.3.1 Abrasion Resistance of concrete with Various Surface Treatments

The abrasion resistance of surface-treated concrete is a good indicator of the longevity of the surface treatment under repetitive traffic loadings. In this study, the same concrete was used for evaluating the select surface treatments, allowing for the abrasion resistance data to differentiate the properties of surface treatments. The results of abrasion resistance of the concrete with or without surface treatment are shown in Figure 6.2.

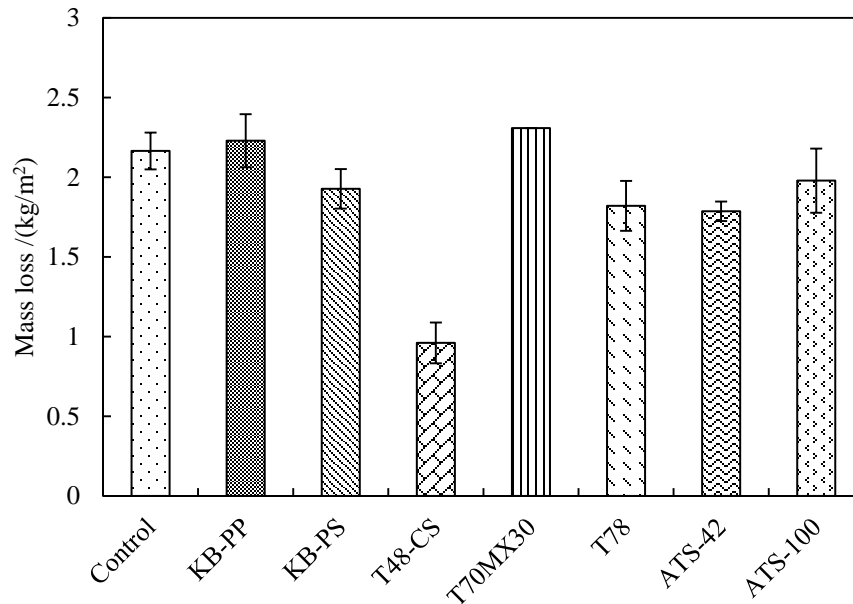


Figure 6.2: Abrasion mass loss of concrete samples with various surface treatments. The error bars show the standard deviations.

As shown in Figure 6.2, the treatment by the epoxy-based sealer T48-CS provided the best performance in enhancing the abrasion resistance of the concrete. Two other products, T78 and ATS-42, also slightly increased the abrasion resistance of concrete. Technical data of surface treatments recorded in Table 6.2

indicated that T48-CS and T78 have a higher strength than the other products and base concrete, which at least partially contributed to their effectiveness in protecting the concrete from abrasion. Other film-forming sealers or sealants were reported to feature compressive strength that was similar to or lower than the concrete substrate, and their presence had no significant impact on the abrasion resistance of concrete. For the silane-based water repellent, ATS-42, a slight enhancement on the abrasion resistance of the concrete was observed, which may be attributable to the formation of a stronger surface layer of concrete caused by the reaction between silica gel and Portlandite (*Sandrolini et al. 2012*). Another possible mechanism is that some surface treatments reduced the friction coefficient of the concrete surface, which contributed to the lower mass loss of the concrete to abrasion.

6.3.2 Scaling Resistance of concrete with Various Surface Treatments

The mass loss of concrete cylinders after the salt scaling test is a direct indicator of salt scaling resistance of the surface-treated concrete vs. the untreated concrete. It is cautioned that the adsorption of salt solution and its reaction with cement hydration products may lead to some mass gain. In the dilute NaCl solution, however, such mass gain is dwarfed by the mass loss due to freeze/thaw damage and spalling of the concrete (Shi, 2010a). Figure 6.3 presents the exterior images of the scaled concrete cylinders after the deicer exposure and 15 F/T and W/D cycles, while Figure 6.4 presents their mass loss data after a given number of F/T and W/D cycles. These results show that all types of surface treatment produced a significant improvement on the salt scaling resistance of the concrete. After the 15 F/T and W/D cycles, the mass losses of all surface-treated concrete were less than 3%, but a 30% mass loss was observed for the concrete without any surface treatment. In other words, 90% or more of salt scaling of the concrete was avoided by the presence of surface coatings, as shown in Figure 6.4a.

Though only minor mass loss was observed for the surface-treated concrete cylinders, Figure 6.4b indicates that the performance of various surface treatments can still be differentiated once the salt scaling data of the untreated concrete were removed from the comparisons. Among them, the epoxy-based sealer T48-CS and the silane-based water repellent ATS-42 exhibited the best performance in providing the concrete substrate with outstanding resistance to salt scaling. Similar results have also been reported elsewhere (*Mamaghani 2009; Zhao 2010*). Under the investigated conditions, the polymer based sealers KB-PP and KB-PS showed a relatively inferior performance with moderate amount of mass loss and noticeable scaling.

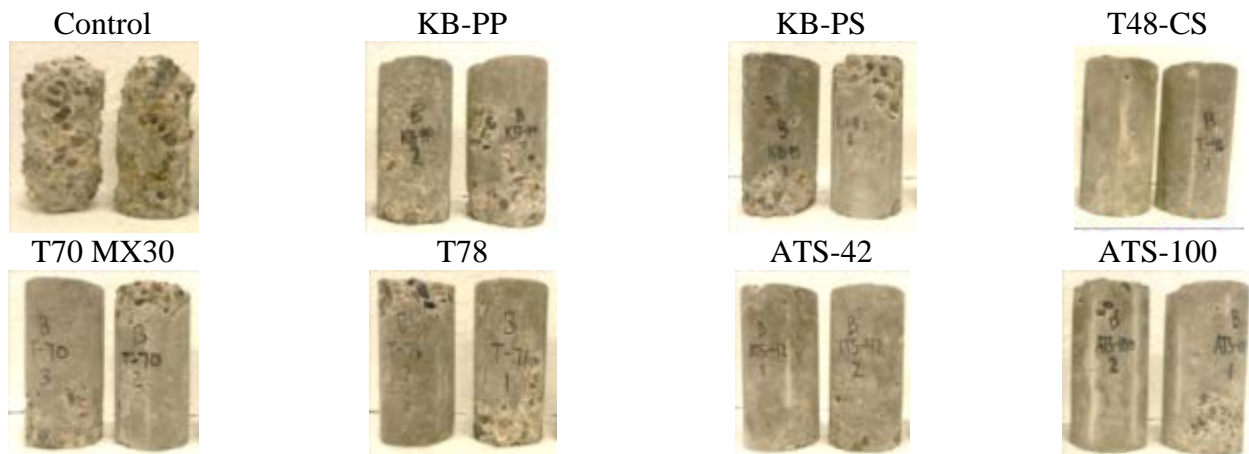
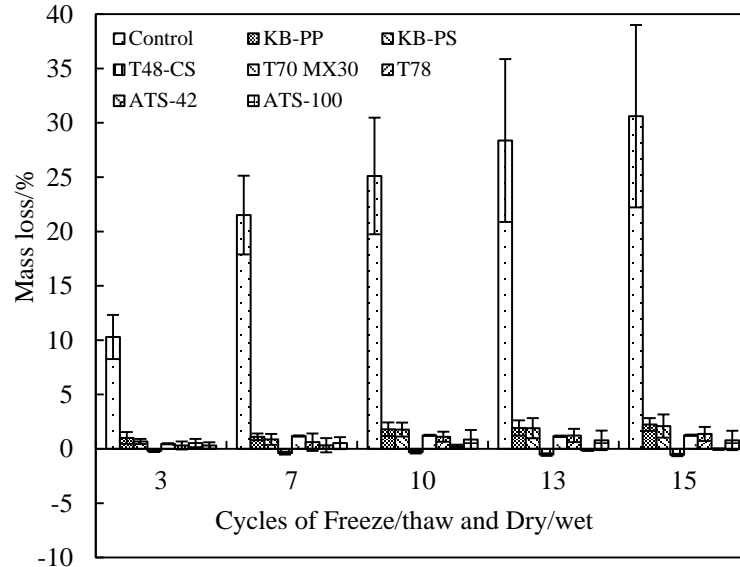
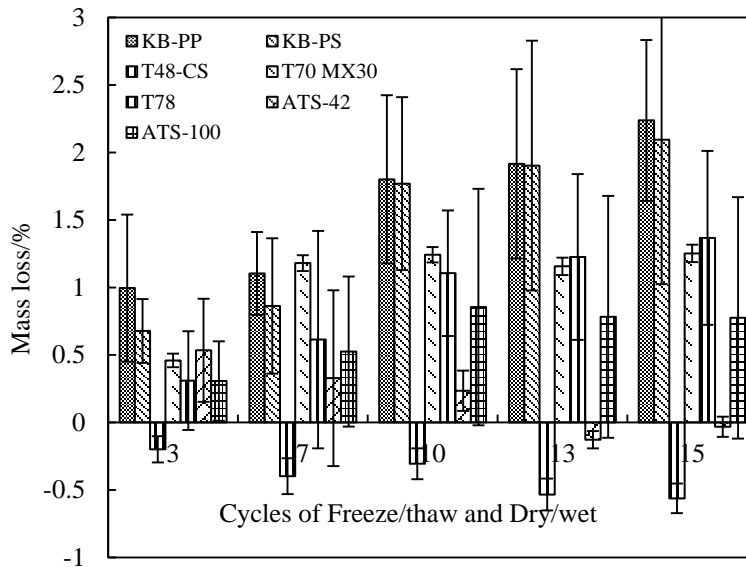


Figure 6.3: Exterior images of concrete cylinders after the deicer exposure and 15 F/T and W/D cycles



(a)



(b)

Figure 6.4: Mass loss of concrete cylinders after the deicer exposure and a given number of F/T and W/D cycles. The error bars show the standard deviations.

6.3.3 Water Absorption of Concrete with Various Surface Treatments

The water absorption behavior of concrete has a strong relationship with durability related properties (Han et al. 2013; De Schutter, 2004). The higher the water absorption rate of the concrete, the more rapidly it is likely to deteriorate. In this study, the water absorption behavior of surface-treated concrete

provides good indication of how impermeable the surface layer is, which can be affected by the hydrophobicity of the surface coating itself and by the microstructure of the surface concrete altered by the surface coating. The rate of water absorption of the concrete with or without surface treatments is shown in Figure 6.5.

As shown in Figure 6.5, no matter which kind of surface treatment was applied to the concrete, the initial rate of water absorption of surface treated concretes were reduced by up to 70% compared with that of the untreated concrete. Several products, T48-CS, T70 MX30, T78, ATS-42 and ATS-100, were especially resistant to water and demonstrated a much lower initial absorption rate than the control. Since the concrete substrate was the same, the secondary rate of water absorption of the concrete treated by some products was comparable to that of the untreated concrete. This suggests that the benefits of those surface treatments can diminish if sufficient time is allowed for the water to penetrate into the concrete. Relative to KB-PP and KB-PS, the lower initial rates of water absorption of T48-CS, T70 MX30 and T78 confirm their higher impermeability to water, due to either higher hydrophobicity of the surface layer or its denser microstructure. For the water repellents (ATS-42 and ATS-100) treated concrete, lower initial rates of water absorption were also observed. These results were consistent with those reported previously (Medeiros 2009). This initial water resistance can be explained by the penetration of alkyltrialkoxysilane into the concrete pores and the formation of hydrophobic lines on the pore walls to dramatically decrease the capillary suction of water by the concrete surface layer (Sandrolini et al. 2012). ATS-100 featured deeper penetration depth than AT-42 (see Table 6.2), which is likely why the ATS-100 treated concrete featured lower secondary rate of water absorption than the AT-42 treated concrete (as shown in Figure 6.5). The concrete treated by T48-CS, T78, and ATS-100 featured a desirably low secondary water absorption rate, implying the longevity of water impermeability of these treated concrete surfaces.

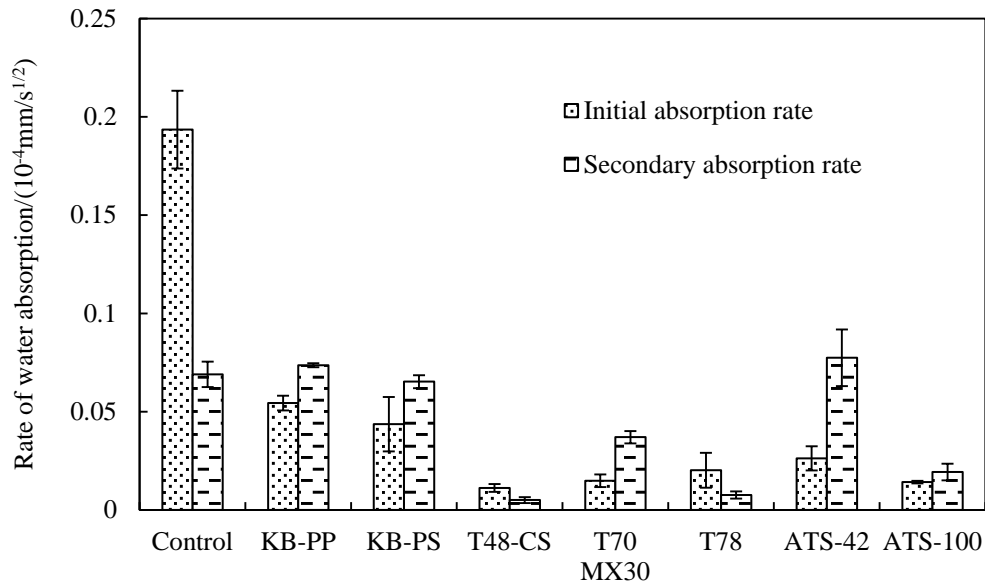


Figure 6.5: Rates of water absorption of concrete specimens with various surface treatments. The error bars show the standard deviations.

6.3.4 Gas Permeability of Concrete with Various Surface Treatments

The results for the gas permeability tests of concrete with various surface treatments are shown in Figure 6.6. In this study, the gas permeability data can also reflect the ability of the surface layer to prevent gas penetration. Once again the same concrete was used.

As shown in Figure 6.6, the epoxy-based sealer T48-CS provided the best protection from gas penetration into concrete, which indicated a highly impermeable, dense microstructure of the epoxy-modified concrete surface. As shown in Table 6.2, the viscosity of T48-CS was far greater than that of other surface coatings. While this provides the benefit of gas impermeability, the penetration of this specific sealer into the concrete substrate is also much less than that of the other low-viscosity, sealers or sealants. Considering its outstanding resistance to abrasion and salt scaling, it may serve as an excellent top coat for concrete surface. Yet, to ensure longevity of surface protection of concrete under traffic (e.g., bridge decks), it may be best to combine this sealer with the use of a water repellent (e.g., ATS-100 and ATS-42). The compatibility of such combined surface treatment strategies merit further investigation and optimization.

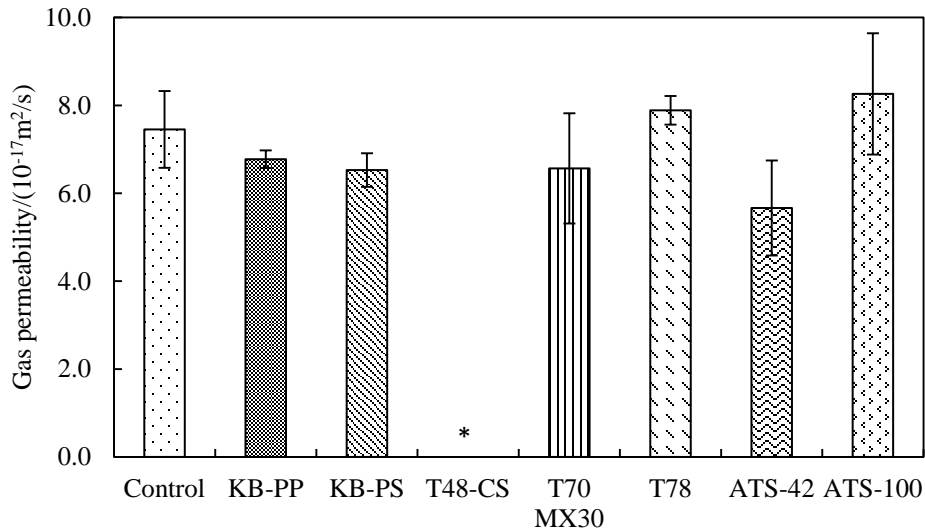


Figure 6.6: Gas permeability coefficient of samples with various surface treatments. Average value and standard deviation are shown.

Note: * indicates the gas permeability of T48-CS treated concrete is too small to test

The concrete treated with the water repellent ATS-42 also demonstrated lower gas permeability than the untreated concrete, which indicated that ATS-42 can lead to the formation of denser microstructure on the surface layer of the concrete. This result was consistent with other studies that report the depth of carbonation of concrete can be reduced by the usage of water repellent (*Basheer 2006*).

6.3.5 Water Contact Angle of Concrete with Various Surface Treatments

Most of the organic sealers and water repellents claimed to be “water repellent”. However, few studies had examined the hydrophobicity of the treated surface of concrete. In this study, the water contact angles of the concrete with or without surface treatments were tested. The results are illustrated in Figure 6.7.

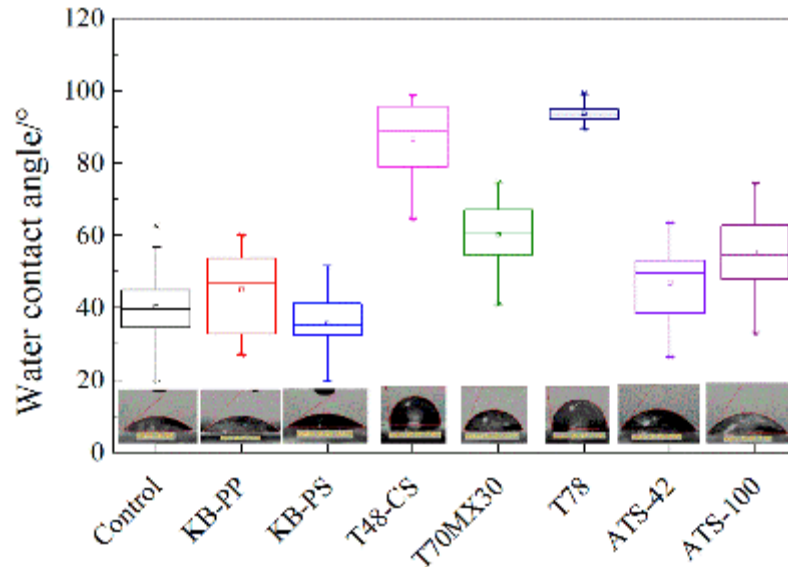


Figure 6.7: Water contact angle of samples with various surface treatments

The water contact angle of the treated concrete surface provides a strong indicator of the surface free energy and the surface hydrophobicity. As shown in Figure 6.7, the treatments with T48-CS and T78 provided remarkable increases in the water contact angle of the concrete surface relative to the control. In other words, the untreated concrete surface was inherently hydrophilic, whereas these two surface coatings turned the concrete surface somewhat hydrophobic. This was a desirable alternation of the surface as it helps slow down the ingress of water into the concrete. T70 MX30 and ATS-100 also demonstrated significant increases in the water contact angle, while KB-PP, KB-PS, and ATS-42 exhibited water contact angles similar to those of the control.

Combining the results of water contact angle in Figure 6.7 and water absorption rate in Figure 6.5, it can be seen that the water absorption rates generally showed a strong inverse correlation with the water contact angle of the treated concrete surface. However, the salt scaling resistance was affected by factors more than the water contact angle. The concrete treated by T78 and ATS-100 with significantly enhanced water contact angles did not exhibit outstanding salt scaling resistance, but the concrete treated by ATS-42 with minor enhanced water contact angle exhibited relatively high scaling resistance. This was likely due to the high gas permeability of T78 and ATS-100 and the low gas permeability of ATS-42, which indicated high and low levels of porosity in the concrete bulk, respectively. The difference in the bulk material porosity was likely affected by the penetration depth of the surface treatment material into the concrete, the bond integrity of the bond between these two, etc.

6.3.6 Splitting Tensile Strengths of the Samples Protected by Various Surface Treatments

Figure 6.8 and Figure 6.9 show the splitting tensile strengths of concrete samples protected by various surface treatments and then exposed to F/T and W/D cycles in 3% NaCl and 3% MgCl₂ solution, respectively. The splitting tensile strengths of all samples decreased after 3 F/T and W/D cycles in 3% NaCl. The control sample and the samples surface treated with KB-PP, KB-PS, T48-CS, and T70 MX30 showed increased splitting tensile strengths after 8 F/T + W/D cycles, while the T-78, ATS-42, and ATS-100 showed decrease after 8 F/T + W/D cycles. Most of the samples showed decreased splitting tensile strengths after 15 F/T + W/D cycles, except T 48CS and ATS-100, which showed increase of splitting tensile strength.

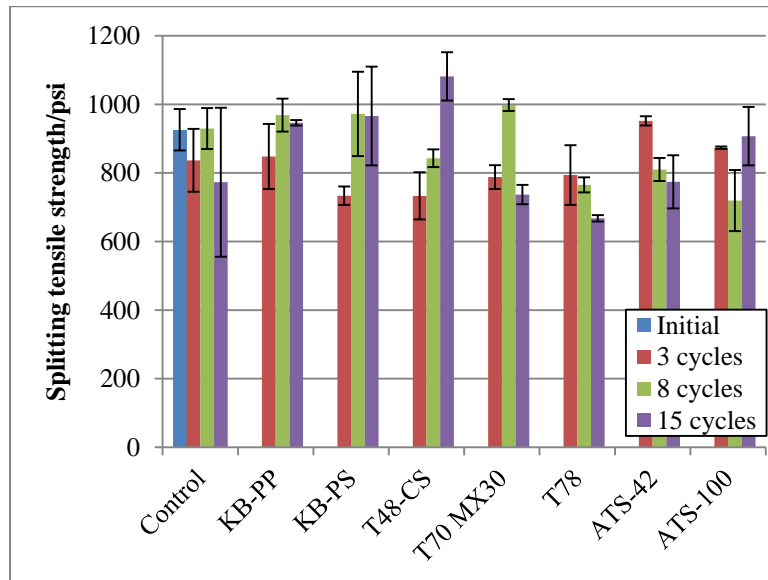


Figure 6.8: Splitting tensile strength of concrete samples surface treated with different sealers after F/T and W/D cycles in 3% NaCl solution

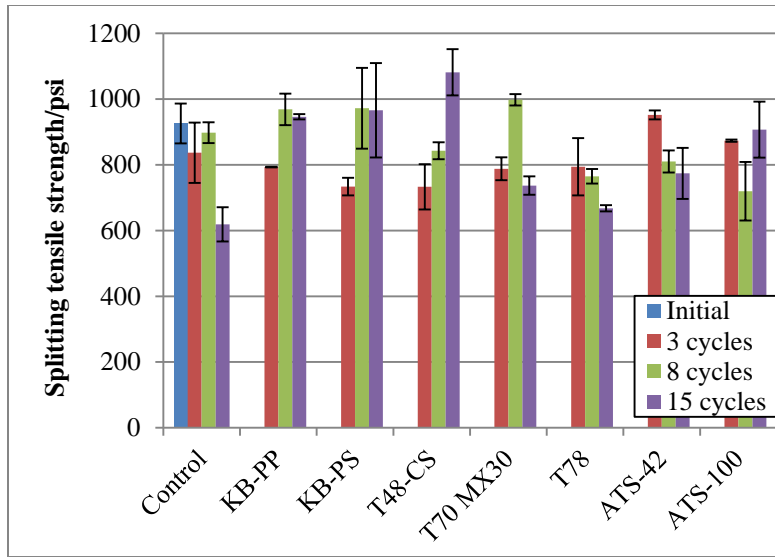


Figure 6.9: Splitting tensile strength of concrete samples surface treated with different sealers after F/T and W/D cycles in 3% MgCl₂ solution

As shown in Figure 6-9, the splitting tensile strengths of all samples decreased after 3 F/T and W/D cycles in 3% MgCl₂. Unlike the NaCl tests, the splitting tensile strength of all the MgCl₂ samples increased after 8 F/T + W/D cycles. However, they sharply decreased after 15 F/T and W/D cycles. The splitting tensile strengths generally ranged between 400 psi (2.8 MPa) and 500 psi (3.4 MPa), except those treated by T78. They were much lower than splitting tensile strengths of the concrete samples after 15 times of F/T and W/D cycles in NaCl solution, which were about 600 psi (4.1 MPa) to 800 psi (5.5 MPa).

6.4 CONCLUSIONS AND FUTURE WORK

In this accelerated laboratory study, several commercial products of surface treatment were used to evaluate their effectiveness on protection of concrete from salt scaling under the joint action of 15 freeze/thaw and wet/dry cycles and exposure to a diluted deicer simulated by 3 wt.% NaCl solution. The results indicated that all of the surface treatments exhibited outstanding performance. After 15 freeze/thaw and wet/dry cycles, the mass loss of surface treated concrete was substantially reduced by 90% or more compared to untreated specimens. The epoxy-based sealer T48CS exhibited the best performance in protecting the concrete from salt scaling and featured the highest abrasion resistance as well as the lowest water absorption rates and gas permeability coefficient. Coincidentally, the concrete surface treated by this product showed the highest water contact angle. The water repellent ATS-42 exhibited the 2nd best performance in protecting the concrete from salt scaling and featured the 2nd highest abrasion resistance as well as the 2nd lowest gas permeability coefficient. However, it did not exhibit outstanding benefits in reducing the water absorption rates or in increasing the water contact angle. The results suggest that high resistance to both gas and water penetration is a crucial property for a good surface treatment applied to concrete.

If based solely on the splitting tensile strengths after 15 F/T and W/D cycles, T48CS and ATS-100 were the best performing surface treatments in 3% NaCl and T78 was the best performing surface treatment in 3% MgCl₂.

Future work should explore the penetrating ability and concrete-bond strength and bond longevity of the select surface treatments. Mechanistic studies may be conducted to link their protective performance to their penetrating and bonding properties, hydrophobicity, etc. Furthermore, efforts will be devoted to further enhancing the durability of surface treatments under abrasion, F/T and W/D cycling, etc. and the application of self-healing technology and nanotechnology to enhance such polymers (*He et al. 2009; Shi, 2009*) is an important line of research. The other line of research would be to optimize the combined use of sealer/sealant and water repellent as a cost-effective solution to achieving long-term protection of concrete against abrasion and salt scaling.

7.0 ACCELERATED LABORATORY EVALUATION OF OVERLAYS FOR PROTECTING CONCRETE BRIDGE DECKS FROM “SALT SCALING”

7.1 INTRODUCTION

This chapter will focus on the accelerated laboratory evaluation of overlays. Depending on the level of concrete deterioration and chloride contamination, the most appropriate mitigation methods may vary. For instance, for concrete with significant chloride contamination, simply sealing the concrete surface may not stop chloride-induced corrosion from occurring. Removal of the top concrete layer or electrochemical chloride extraction may be necessary before the bridge deck is protected by a topical treatment of coating or sealer. For concrete showing significant signs of cracking, the use of a crack sealant such as high molecular weight methacrylates (HMWM), epoxies or urethanes may be required before a topical treatment of the bridge deck.

Surface treatments provide either a non-penetrating film (coating) or penetration into concrete pores such as pore blocker or hydrophobic pore liner (sealer) to protect concrete from the ingress of water, chlorides, and other deleterious substances (e.g., gasoline, diesel, and sulfates) and UV light, or at least slow their rate of intrusion. In addition to sealing the hardened concrete with coatings or penetrating sealers, other methods to be explored may involve but are not limited to polymer-modified cementitious overlay, fiber-reinforced cementitious overlay, and highly flowable, reactive powder concrete as a repair material.

In this chapter, the overall performances of different types of overlays were evaluated. The bond strength, splitting tensile strength, abrasion resistance, and gas permeability of the concrete slabs treated with different types of overlays after F/T and W/D cycles in NaCl and MgCl₂ solutions were tested.

7.2 MATERIALS AND METHODS

7.2.1 Materials and Proportion of Concrete Substrate Slabs

For this study, an ASTM specification C150-07 Type I/II GU Portland cement from Diamond Mountain, MT was used. Coarse aggregates (with maximum size of 9.5 mm) and fine aggregates (clean, natural silica sand, maximum size of 4.75mm) were purchased from the JTLGroup (Belgrade, MT). A chemical agent, triethylamine (TEA), was used as early strength accelerator for accelerating the early age strength of concrete. The mix proportion and properties of concrete is listed in Table 7.1. Table 7.2 and Table 7.3 list the information of the cement based overlay and the organic overlays, respectively. Figure 7.1 and 7.2 give the preparation process of the cement based overlay and the organic overlays.

Table 7.1: Mix Proportion and Properties of Concrete

Mix proportion of concrete, kg/m ³						Properties of fresh and hardened concrete				
Cement	Water	TEA	Fine aggregate	Coarse aggregate	Air entrainment	Slump, mm	Air content of fresh concrete, %	Pore volume, %	Compressive strength at 28d, psi	Splitting tensile strength at 28d, psi
407	223.9	0.203 5	655	1022	0.02442	210	2.9	10.14	4450	926

7.2.2 Information of Overlays

Table 7.2: Information of cement based overlays

Code name	Mixing proportion	Applying procedure
Control	Cement: Water: Water reducer: Sand: Air entrainment agent=1:0.38:0.0093:3:0.001	Mixing the water reducer and air entrainment with water firstly; then the cement and sand were mixed with water solution for 5 minutes.
Latex modified mortar overlay	(Cement + Latex (Solid)): Water: Sand: Air entrainment agent= (0.8+0.2):0.38:0.20: 3:0.001	Mixing the Latex and air entrainment with water firstly; then mix the water with cement and sand together for 5 minutes.
Silica Fume modified mortar overlay	(Cement+ Silica fume): Water: Water reducer: Sand: Air entrainment agent= (0.9+0.1): 0.38:0.012: 3:0.001	Mixing the water reducer and air entrainment agent, then mix the cement, silica fume with sand and water solution together for 5 minutes.
Fiber reinforced mortar overlay	(Cement+ Silica fume): Water: Water reducer: Nanofiber: Nanoclay: Sand: Air entrainment agent= (0.9+0.1):0.38:0.0127:0.0025: 0.005:3:0.001	Firstly, half of water was mixed with nanofiber and nanoclay for 24h with an ultrasonicator. Then, mix the water reducer and air entrainment agent with the other half of water; Finally, the cement, silica fume, sand and water solution were all mixed together for 5 minutes.

Table 7.3: Information of organic overlays

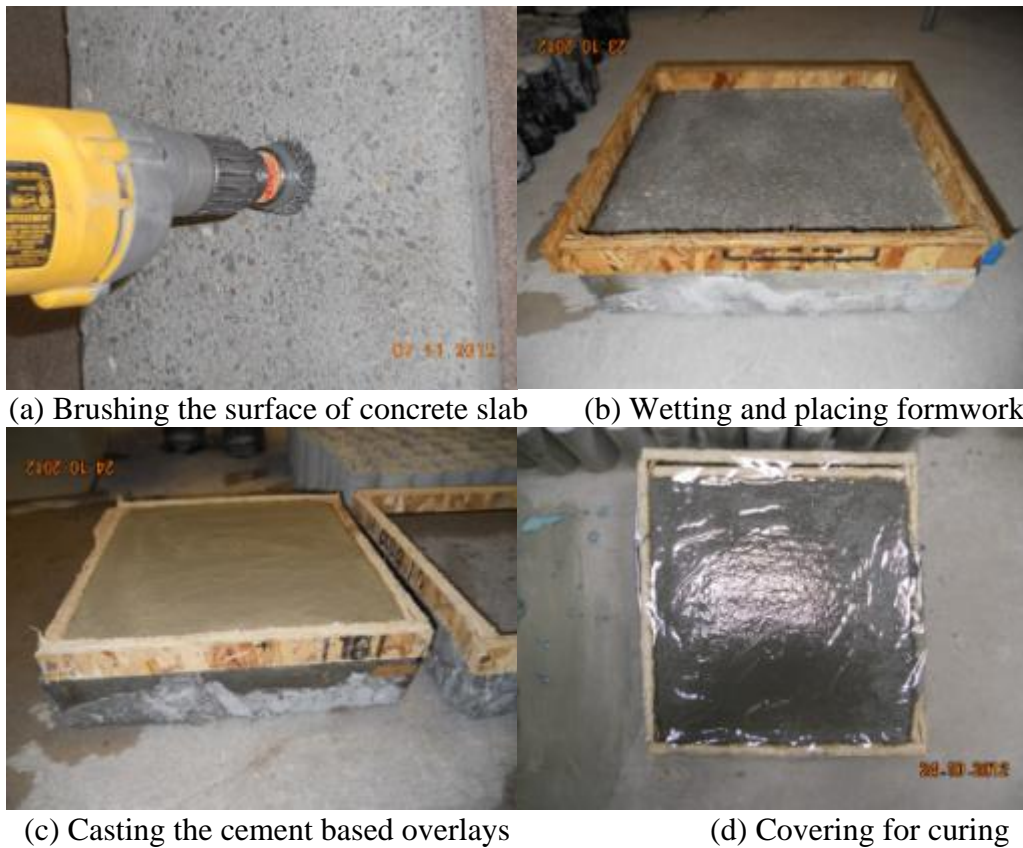
Code name	Manufacturer	Type and main constituent	Mixing proportion	Applying procedure
T-48 Low Modulus Polysulfide Epoxy Overlay	Castek Inc., A Transpo Industries Company	Polymer (Resin)	Primer: Resin	Two coats of the Resin was applied to the surface of the concrete using a paintbrush prior to the application of the Overlay
		Polymer (Resin, Hardener, and powder)	Overlay: Resin 1/2 Hardener by the volume of Resin 11.55lbs Powder by 1L of resin.	Resin and Hardener were thoroughly mixed together in a large bowl. The mixture was then added to Powder and mixed together. The entire mix was poured onto the concrete slab and evened out across the surface with a flat spoon. The overlay was left to cure for 20 minutes and then a layer of aggregate was applied to the base coat after 20 minutes of curing until complete coverage was achieved. The overlay was left to cure for 24 hours, after which the excess aggregate was brushed off.
PPC-1121	KwikBond Polymers	Polymer (Resin, promoter and initiator)	Primer: Resin 32.3g Promoter by 1L of resin 32.3g Initiator by 1L of resin	Resin and promoter were thoroughly mixed together before adding initiator. After mixing in the initiator, two coats of the mixture was applied to the surface of the concrete slab with a paintbrush and allowed to cure for 24 hours (before application of the Overlay layer).
		Polymer (Resin, catalyst, accelerator and aggregate)	Overlay: Resin 1.6% Catalyst by the volume of resin 4% Accelerator by the volume of resin 14 lbs Sand and Rock Mix by 1L of resin	Resin and catalyst were thoroughly mixed together before adding accelerator. After mixing in accelerator, the entire mixture was added to the Sand and Rock mix and stirred together until even. The entire mixture was then scooped onto the concrete slab and spread until even. The overlay was left to cure for 24 hours. No aggregate broadcast was required.

7.2.3 Images of the Application of Overlays

For cement based overlays, after moisture cured at $23 \pm 1^\circ\text{C}$ and RH 100% for 28 days, the concrete slabs were dried at $23 \pm 1^\circ\text{C}$ and RH 50% for 24 hours. A wire brush was used to polish the slabs until the paste on the surface of the slabs was removed (see Figure 7.1a). The slabs were wetted, and a wood mold with thickness of 1 inch was placed around the slabs (see Figure 7.1b). Then the overlay mixtures were cast into the form and sealed with a plastic sheet (see Figure 7.1c and Figure 7-.d). The slabs were transferred to a moisture room at $23 \pm 1^\circ\text{C}$ and RH 100% for another 28 days.

For organic overlays, the concrete slabs were moisture cured for 56 days, then the slabs were dried and polished as similar to the cement based. Since a dry surface was required for organic overlays, the surface of the slabs was kept dry before applying the organic overlays.

After placing the organic overlays, the slabs were placed in a room at $23 \pm 1^\circ\text{C}$ and RH 50% for 24 hours.



(a) Brushing the surface of concrete slab (b) Wetting and placing formwork
(c) Casting the cement based overlays (d) Covering for curing

Figure 7.1: Preparation of the cement based overlays



(a) Overlay T48

(b) Overlay PPC-1121

Figure 7.2: Preparation of the organic overlays

7.3 EXPERIMENTAL METHODS FOR EVALUATING THE OVERLAYS

7.3.1 Procedures of Freeze/Thaw and Wet/Dry Cycles

Laboratory measurements of changes to Portland Cement Concrete (PCC) through freeze/thaw cycling in the presence of deicers were conducted following the SHRP H205.8 test method entitled “Test Method for Rapid Evaluation of Effects of Deicing Chemicals on Concrete” with minor modifications. The SHRP H205.8 test evaluates the effects of chemical deicing formulations and freeze/thaw cycling on the structural integrity of small test specimens of non-air-entrained concrete. The method quantitatively evaluates degradation of the specimen through weight loss measurements. This test method is not intended to be used in determining the durability of aggregates or other ingredients of the concrete.

After the sealers/coatings/overlays cured, the cylinder or slabs were dried for 24 h. After drying, the cylinder or slabs were immersed into a plastic box containing 3% NaCl solution for another 24 h, at which time they were weighed. The specimens were returned to the NaCl solution, and the plastic box was placed into the freezer for 12 h at $-17.8 \pm 2.7^{\circ}\text{C}$ (-0.04°F). However, for concrete cylinders treated with sealer/coating or water repellent, the average temperature in the middle of solution was about $-5.0 \pm 1.0^{\circ}\text{C}$ after every freezing step. For concrete slabs with overlays, the average temperature in the middle of solution was about $5.0 \pm 1.0^{\circ}\text{C}$. Such discrepancies in the actual temperature and the target temperature were attributable to the latent heat in the concrete specimens. An analogy can be made to the difference between the air temperature and the temperature inside a concrete deck in the service environment. Subsequently, the specimens (along with the plastic box) were placed in the laboratory environment at $23 \pm 1.7^{\circ}\text{C}$ (73.4°F) and with a relative humidity ranging from 45 to 55% for 8 h. After the ice in plastic box was completely thawed, the specimens were transferred to a wood plate at ambient laboratory conditions for 4 hours. This freeze/thaw and wet/dry cycle was repeated 10 or 15 times as required. After drying, the target properties were.

7.3.2 Splitting Tensile Strength

Splitting tensile strength testing was performed in accordance with ASTM C496/ C496M-11 Standard Test Method for Splitting Tensile Strength of Cylindrical Concrete Specimens, using 2" x 4" cylindrical specimens.

7.3.3 Bond Strength

Bond strength testing of overlays was performed in accordance with ASTM C1583 / C1583M - 04 Standard Test Method for Tensile Strength of Concrete Surfaces and the Bond Strength or Tensile Strength of Concrete Repair and Overlay Materials by Direct Tension (Pull-off Method), shown as in Figure 7.3. Before the testing, a steel brush was used to clean the surface of the overlays.



Figure 7.3: Bond strength tests

7.3.4 Gas Permeability

Gas permeability tests were performed using liquid methanol as the gas source to determine the gas transport properties. A 1/2'' thick specimen was cut from a 2x4'' concrete cylinder sample and then oven-dried at 105°C for 24 h to remove the moisture within the specimen. Subsequently, the specimen was placed and sealed on the top of a cell with epoxy sealant to avoid any leakage of methanol vapor as shown in Figure 7.4.

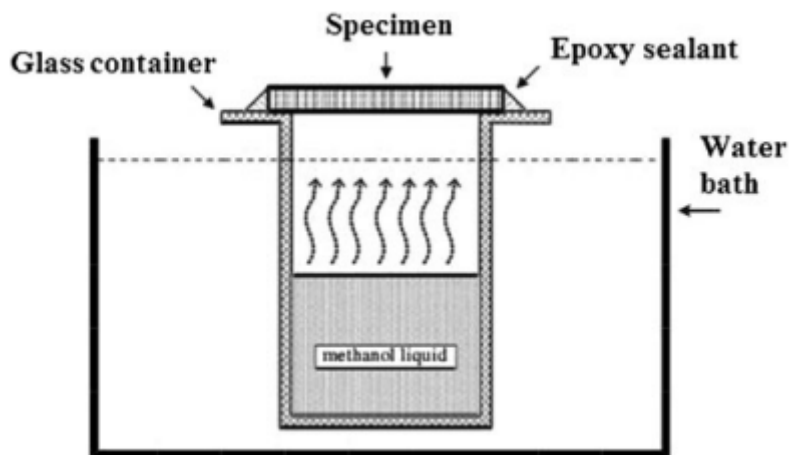


Figure 7.4: Schematic drawing for the gas permeability test setup

The initial weight of the whole specimen setup including the cell, methanol liquid, specimen, and epoxy sealant was measured at the beginning of the test. The values of mass variation versus time due to the vaporization of methanol liquid at a constant 40 °C water bath temperature during the test were continuously recorded at each time interval until a steady-state mass loss was reached. The gas permeability coefficient k (m²/s) was then calculated using the following equations.

$$pv = 10^{\left(\frac{8.0809 - 1582.2}{239.76 + T}\right)} \quad (7.1)$$

$$\eta = 10^{-7} (4.7169T^{0.618} - 99e^{-8.7593 \times 10^{-4}T} + 94e^{-7.916 \times 10^{-3}T} + 5) \quad (7.2)$$

$$Q = \frac{266 \times 10^{-3} m'}{10^{\left(\frac{8.0809 - 1582.2}{239.76 + T}\right)}} T \quad (7.3)$$

$$k = \frac{2L\eta P_2 Q}{A(P_1^2 - P_2^2)} \quad (7.4)$$

where pv is the absolute pressure of vapor (N/m²), T is the absolute temperature (K), g is the dynamic viscosity (N/m²), Q is the volumetric flow rate (m³/s), m' is the rate of mass loss (g/s), P_1 is the inlet pressure (N/m²), P_2 is the outlet pressure (N/m²), L is the length of the sample (m), and A is the cross sectional area perpendicular to the flow direction (m²).

For concrete slabs covered by cement-based overlays, a core with 2'' diameter was drilled from slabs, and the core was cut into three pieces that included only overlay (0.5''), overlay (0.5'') + concrete (0.5''), and only concrete (0.5''). For organic overlays, 2 pieces were cut from the drilled cores: overlay (1/3'') + concrete (2/3'') and only concrete (0.5''). Figures 7.5 and 7-6 show the sectioned samples.



Figure 7.5: Samples of cement based overlays including overlay (0.5'') and concrete (0.5'') used for gas permeability test



Figure 7.6: Samples of organic overlays including overlay (1/3") and concrete (2/3") used for gas permeability test

7.3.5 Abrasion Resistance

All the abrasion resistance testing of concrete samples was conducted in accordance with ASTM C944/C944M-2009 Standard Test Method for Abrasion Resistance of Concrete or Mortar Surfaces by the Rotating-Cutter Method. The apparatus is shown in Figure 7.7. To determine the abrasion resistance, 2" × 4" cylindrical specimens or drilled samples with diameters of 2" were used. Before performing tests, specimens were kept in the open-air environment for at least 24 hours to keep all test specimens in equivalent moisture condition at the start time of abrasion testing. Specimens were abraded for three cycles of two minutes each (total of six minutes) at 44 lbf load.

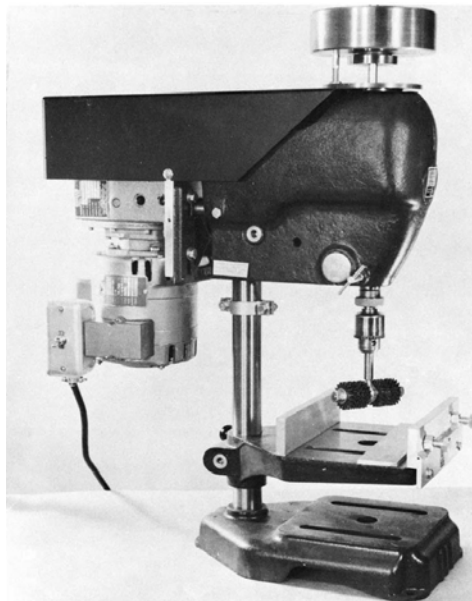


Figure 7.7: Rotating-Cutter Drill Press

7.4 RESULTS AND DISCUSSION

7.4.1 Bond Strength

Figure 7.8 illustrates the change in bond strength of different overlays after 10 cycles of F/T and W/D in 15% NaCl and MgCl₂ solutions. In general, the bond strength of the cementitious overlays (SFMO and FMO) increased after F/T and W/D cycles in both NaCl and MgCl₂ solutions. The bond strength increases were statistically significant for SFMO and FMO exposed to 15% MgCl₂ solutions. The organic overlays (T48 and PPC-1121) showed decreased bond strength after F/T and W/D cycles in 15% NaCl solution. The bond strength reductions were statistically significant for PPC-1121 exposed to 15% NaCl or MgCl₂ solutions. The bond strength of T48 increased significantly after cyclic exposure to the 15% MgCl₂ solutions. The organic modified overlay (LMO) showed significantly decreased bond strength after F/T and W/D cycles in 15% MgCl₂ solution.

For cement based overlays, before starting the exposure cycles, the age of overlays and substrate concrete were 28 d and 56 d, respectively. The organic overlays only needed 24-hour curing after casting; as such, before starting the exposure cycles, the age of organic overlay and substrate concrete were 1 d and 56 d, respectively.

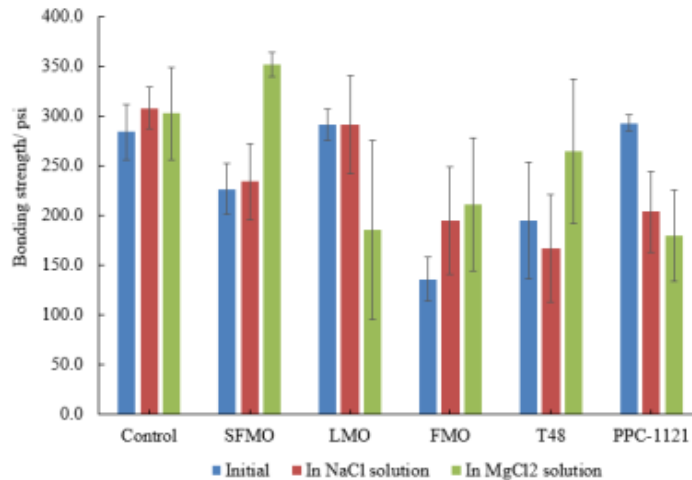


Figure 7.8: Bond strengths of various overlays

Figure 7.9 gives the images of bond strength tests after F/T and W/D cycles in 15% NaCl and MgCl₂ solutions. The fracture of all cementitious overlays, including the control (without overlay), SFMO, and FMO, of the initial bonding tests occurred at the interfaces between the overlays and the substrates. However, after F/T and W/D cycles, most of the fractures occurred in the substrates rather than at the interfaces. This phenomenon proved the assumption that the bond strength of the interfaces between the cementitious overlay and the concrete substrates will be strengthened during the F/T and W/D cycles because of the further hydration process.

For the organic overlays (T48 and PPC-1121) and organic modified overlay (LMO), the fracture of the initial bonding tests occurred at the interfaces between the overlays and the substrates. After the F/T and

W/D cycles, the fracture still occurred at the interfaces between the overlays and the substrates, except the T48 in $MgCl_2$, which showed increased bond strength after the F/T and W/D cycles (Figure 7.8).



PPC-1121 organic overlay



Figure 7.9: Digital photos of concrete samples after bond strength tests

7.4.2 Splitting Tensile Strength

Figure 7.10 gives the splitting tensile strength of different overlays after 10 F/T and W/D cycles in 15% NaCl and MgCl₂ solutions. As demonstrated in Figure 7.10, unlike the bond strength, the splitting tensile strengths of all samples decreased after F/T and W/D cycles compared to the initial condition, except the initial and SFMO overlays. The T48 overlay showed the highest decreasing rate while the SFMO showed the lowest decreasing rate. Splitting tensile strength mainly depends on the concrete substrate rather than the overlay; therefore, the effects of the F/T and W/D damage were the main reason for the decrease of the splitting tensile strengths. In addition, the difference between the initial splitting tensile strengths resulted from the various mechanical properties of the overlays.

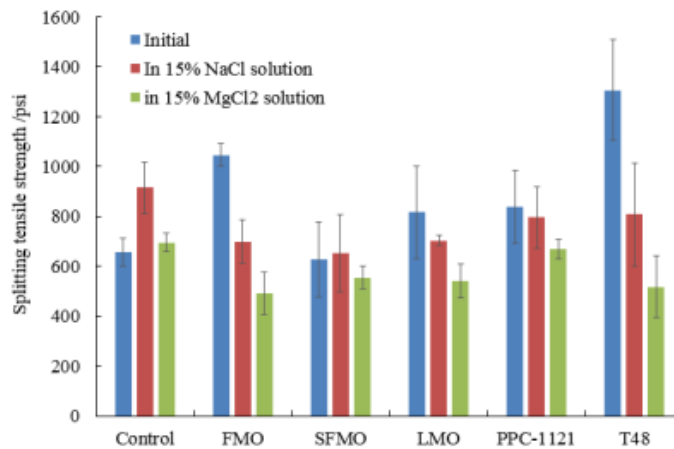


Figure 7.10: Splitting tensile strengths of various overlays

7.4.3 Abrasion Resistance

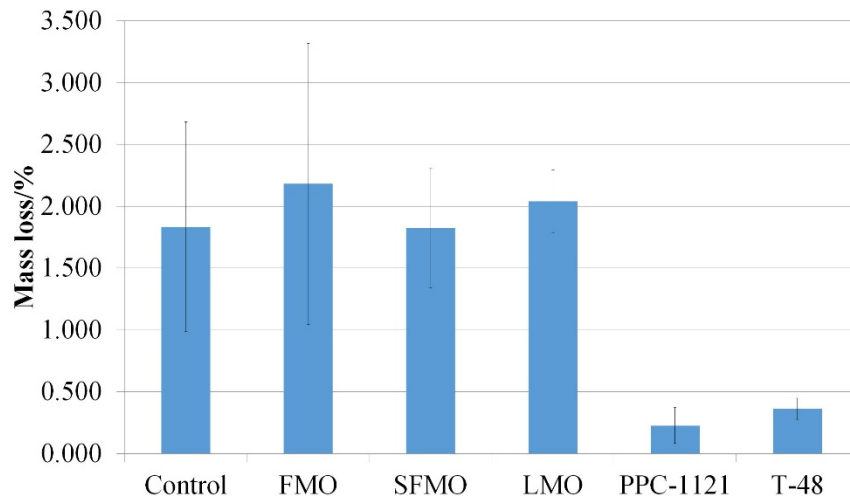
Figure 7.11 gives the results of the abrasion resistance tests of the samples after F/T and W/D cycles in 15% NaCl solution. The figures labelled a, b, and c represent the mass loss, height change, and mass change vs. height change, respectively. As shown in Figure 7.11a, the organic overlays (T48 and PPC-1121) showed lower mass loss than the cementitious overlays (control, FMO, SFMO, and LMO). These results agreed with the height change shown in Figure 7.11b, in which the organic overlays showed much lower values than the cementitious overlays.

Figure 7.12 gives the results of the abrasion resistance tests of the samples after F/T and W/D cycles in 15% $MgCl_2$ solution. Figure 7.12a, Figure 7.12b and Figure 7.12c represent the mass loss, height change, and mass change vs. height change, respectively. As in Figure 7.11, the organic overlays (T48 and PPC-1121) showed lower mass loss and less height change than the cementitious overlays (control, FMO, SFMO, and LMO).

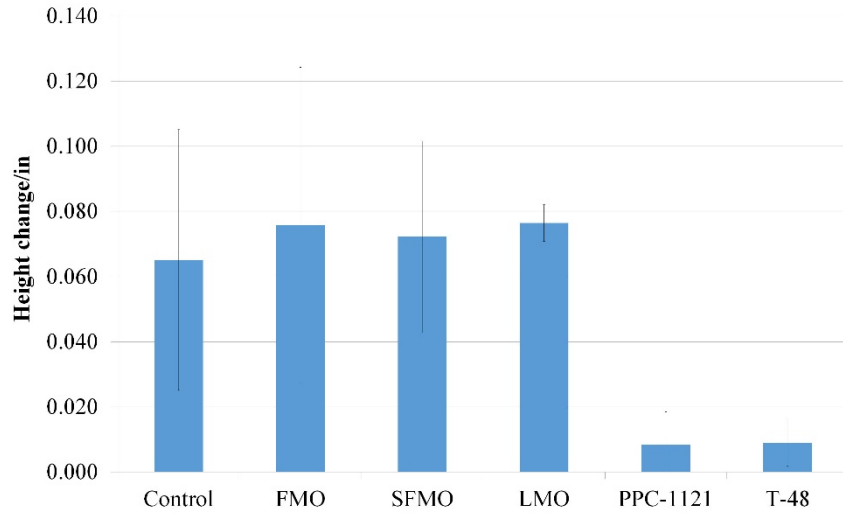
Figure 7.11 and Figure 7.12 showed the abrasion resistance of concrete (control samples) exposed to F/T and W/D cycles in 15% $MgCl_2$ solution was greater than concrete exposed to F/T and W/D cycles in 15% NaCl solution. However, the splitting tensile strength results showed that concrete exposed to F/T and W/D cycles in $MgCl_2$ solution had lower tensile strength than concrete exposed to similar cycles in NaCl. This result agreed with the results shown in Chapter 6.

The two cementitious modified overlays (FMO and SFMO) showed similarly high mass losses of approximately 2% in NaCl and $MgCl_2$ solutions. This demonstrated that the fibers and silica fume were not beneficial in providing resistance against “salt scaling” by NaCl or $MgCl_2$ deicers.

The latex modified overlay (LMO) showed much lower mass loss after F/T and W/D cycles in $MgCl_2$ solution than in NaCl solution.

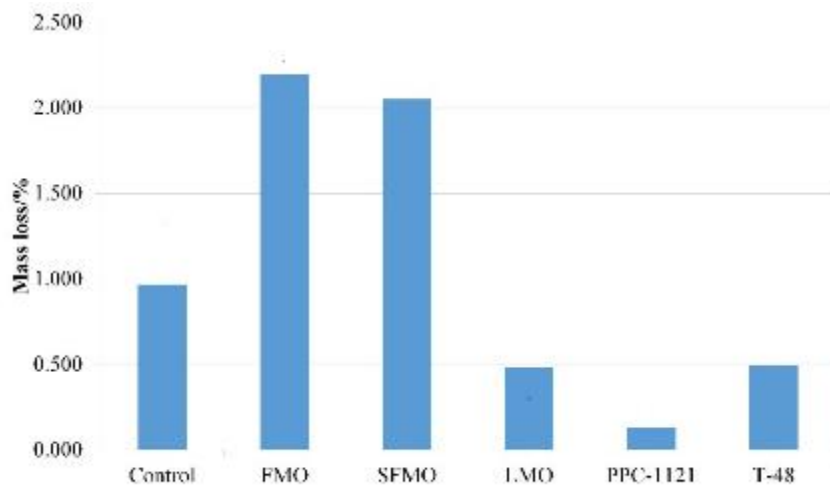


(a) Mass loss

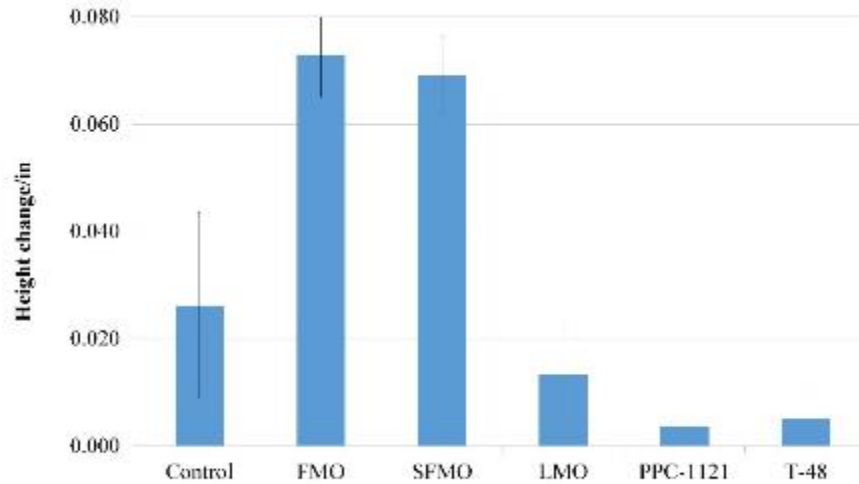


b) Height change

Figure 7.11: Abrasion resistance of various overlays after F/T W/D cycles in 15% NaCl solutions



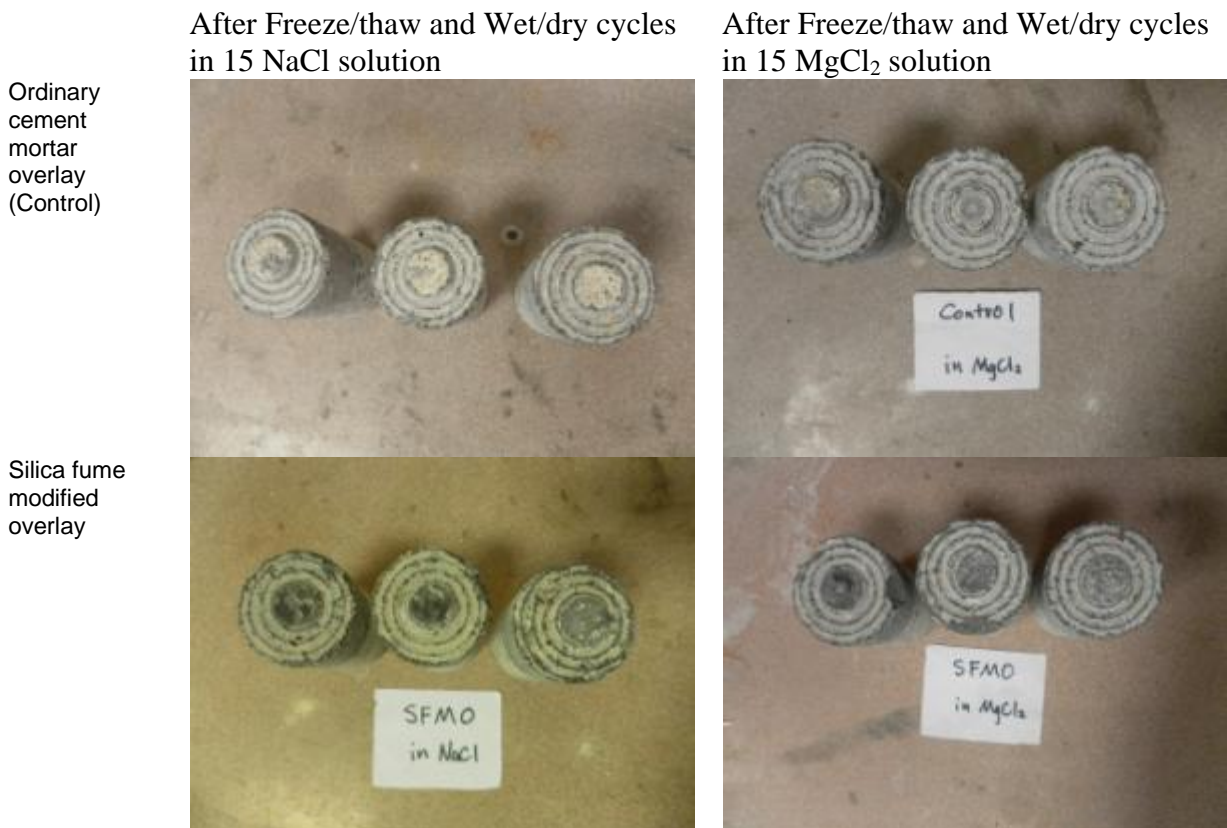
(a) Mass loss



(b) Height change

Figure 7.12: Abrasion resistance of various overlays after F/T W/D cycles in 15% MgCl₂ solutions

Figure 7.13 gives the images of abrasion tests after F/T and W/D cycles in 15% NaCl and MgCl₂ solutions. The polymer overlays (T48 and PPC-1121) had intact edges after abrasion test, while the cementitious overlays showed scaling at the edges.



Latex modified overlay



Micro-fiber modified overlay



T-48 organic overlay



PPC-1121 organic overlay



Figure 7.13: Abrasion test surfaces of cored overlay cylinders after freeze/thaw and wet/dry cycles in 15% NaCl solutions

7.4.4 Gas Permeability

Figure 7.14 and Figure 7.15 give the result of the gas permeability tests of the samples after F/T and W/D cycles in 15% NaCl and MgCl₂ solutions, respectively. The polymer overlays (T48 and PPC-1121) showed lower gas permeability than the cementitious overlays (control, FMO, SFMO, and LMO) in both NaCl and MgCl₂ solutions. In addition, as mentioned before, the MgCl₂ led to more severe chemical damage to the concrete than NaCl due to the chemical reaction between the MgCl₂ and the C-S-H in the concrete. This reaction results in the decalcification of the C-S-H phase leaving behind a more porous phase. The gas permeability of the control samples after F/T and W/D cycles in MgCl₂ show higher value than those in NaCl, confirming this assumption.

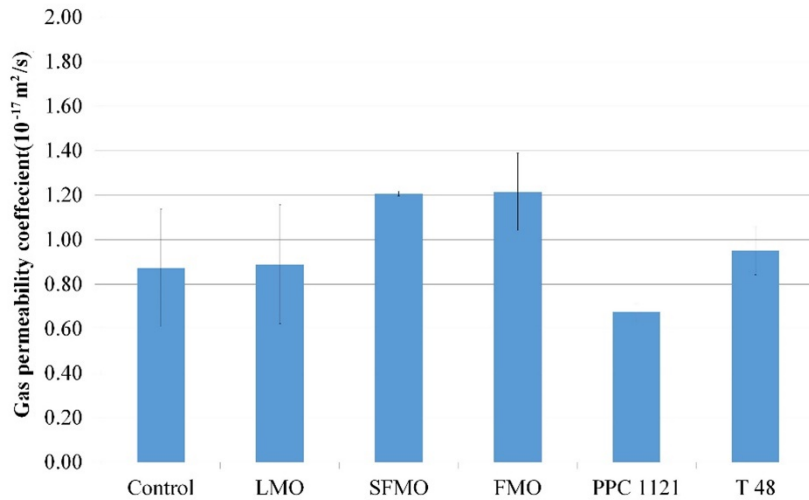


Figure 7.14: Gas permeability of various overlays after F/T and W/D cycles in 15% NaCl solutions

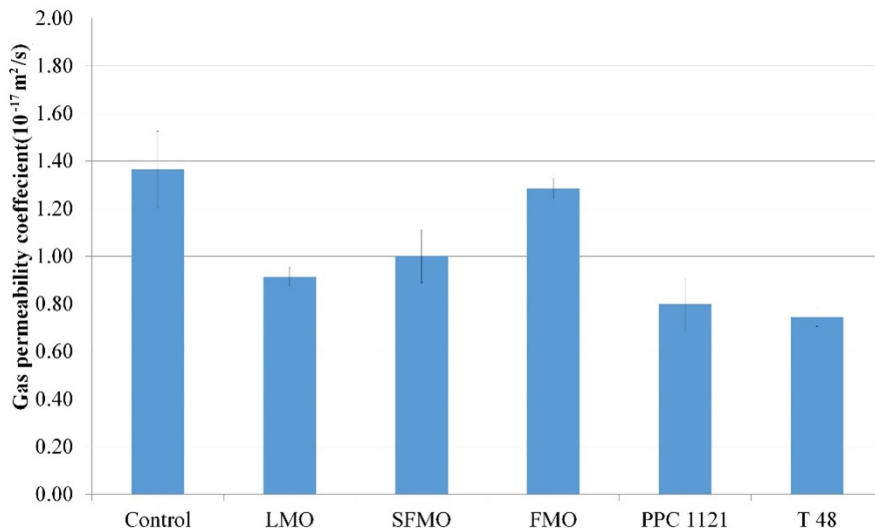


Figure 7.15: Gas permeability of various overlays after F/T and W/D cycles in 15% MgCl₂ solutions

7.5 CONCLUSIONS

The bond strength, splitting tensile strength, abrasion resistance, and gas permeability of the concrete slabs treated with different types of overlays were tested after F/T and W/D cycles in NaCl and MgCl₂ solutions. Different types of overlays exhibited different performance behaviors.

The two cementitious overlays (silica fume modified overlay - SFMO and fiber modified overlay - FMO) and the T-48 polymer overlay all showed an increase in their bond strength after F/T and W/D cycles in 15% MgCl₂ solutions. In contrast, the SFMO and FMO cementitious overlays showed an increase in their bond strength after F/T and W/D cycles in 15% NaCl solution, but the T-48 polymer overlay showed a decrease in its bond strength. The latex modified overlay (LMO) and the other polymer overlay (PPC-1121) showed a decrease in their bond strength after F/T and W/D cycles in 15% MgCl₂ solution, whereas the LMO showed little change and the PPC-1121 showed a decrease in bond strength after F/T and W/D cycles in 15% NaCl solution. In summary, only the cementitious overlays (SFMO and FMO) exhibited increased bond strength after F/T and W/D cycles in both NaCl and MgCl₂ solutions.

For all the overlay-protected concrete slabs, their splitting tensile strength decreased after F/T and W/D cycles in MgCl₂ and NaCl solutions. Among them, the SFMO exhibited the lowest reduction, whereas the T-48 overlay exhibited the highest reduction. The splitting tensile strength was mainly dependent on the concrete substrate rather than the overlay. As such, the physicochemical damage of the concrete substrate by the combined effect of F/T cycles and chloride deicer was the main reason underlying the observed reductions. The difference in the initial splitting tensile strength, however, was directly related to the mechanical properties of the overlays. Among the overlays tested, the FMO and T-48 featured relatively high initial splitting tensile strengths, whereas the SFMO featured relatively low initial ones.

The overlays were tested for their abrasion resistance after “salt scaling”. The polymer overlays (T-48 and PPC-1121) showed lower mass loss than the cementitious overlays (control, FMO, SFMO, and LMO), and this also agreed well with the height changes induced by abrasion. The two cementitious modified overlays (FMO and SFMO) showed similarly high mass losses of approximately 2% in NaCl and MgCl₂ solutions. This demonstrated that the fibers and silica fume were not beneficial in providing resistance against “salt scaling” by NaCl or MgCl₂ deicer. In contrast to the cementitious overlays, the LMO exhibited much lower mass loss after F/T and W/D cycles in MgCl₂ solution than in NaCl solution. This was mainly from the pore blocking effect by the latex addition.

The gas permeability testing results indicated that the concrete slabs treated with polymer overlays (T-48 and PPC-1121) had lower gas permeability than those treated with cementitious overlays (control, FMO, SFMO and LMO) after exposure to F/T and W/D cycles in both NaCl and MgCl₂ solutions. Relative to NaCl, the samples exposed to MgCl₂ featured higher gas permeability coefficients, indicating more severe damage of its microstructure.

8.0 CONCLUSIONS AND RECOMMENDATIONS

8.1 CONCLUSIONS

Anti-icing strategy with $MgCl_2$ liquids has been widely used by ODOT districts and is believed to be very successful by participating winter maintenance survey respondents. Usage of ice control chemicals has generally been increasing during the past ten years due to colder weather, higher traffic volumes and higher level of service. This trend seems to be continuing and has raised some concerns regarding its negative effects on existing highway infrastructure. Nonetheless, the vast majority of the participating ODOT winter maintenance managers did not think that there has been any significant deteriorating effect of $MgCl_2$ on the ODOT concrete bridge decks. In contrast, a majority of bridge managers believed that freeze-thaw damage and chloride deicers both contribute to the premature deterioration of bridge decks, even though they disagreed on the level of influence.

This study, while focusing on examining the relevant data from Oregon, has demonstrated the general approach that other agencies could implement or adopt in developing environmental exposure maps for their infrastructure. In order to investigate the root cause of premature deterioration of concrete bridge decks in cold climates, it is useful to develop these exposure maps over time. Nonetheless, this study has revealed that currently agencies may not have complete and well-defined records of the relevant data.

This work highlights challenges in data collection. Significant amount of historical air or deck temperature data are required to calculate the number of freeze/thaw cycles. Ideally, more detailed records on precipitation and traffic volumes would also facilitate the understanding of how weather, deicer, traffic, etc. might contribute to the premature deterioration of concrete bridge decks. Future study should examine how such exposure maps would facilitate decision-making once sufficient data become available for data mining and statistical analyses.

This work also reports the collection, examination and testing of field concrete cored from 12 selected ODOT bridge decks (predominantly exposed to $MgCl_2$ deicer, at random locations without severe cracking), as well as those of field concrete cored from two Utah DOT bridge decks (predominantly exposed to NaCl deicer at locations without apparent surface distress) and two Nebraska Department of Roads bridge decks (mainly exposed to KAc deicer, at locations with apparent surface distress). The field cores were tested for their mechanical properties and transport properties. They were also subjected to staining tests to detect possible chloride penetration, carbonation, and ASR, and subjected to petrographic analysis to characterize their paste and air contents. For the ODOT bridge decks, additional microscopic investigation was conducted to better understand the concrete deterioration in the presence of $MgCl_2$ deicer.

The following are the key findings from the field investigation:

8. For the vast majority of the deck cores, no significant deterioration was apparently visible other than surface scaling. In other words, there were generally no signs of significant longitudinal, transverse or diagonal cracking and no evidence of visible precipitates. The only exception was for the Nebraska deck cores, which showed signs of microcracking due to ASR.

9. The concrete bridge decks exposed to KAc or $MgCl_2$ deicer showed significant reductions in their splitting tensile strength and microhardness, whereas those surface-distress-free decks exposed to NaCl deicer did not.
10. The observed considerable strength reduction in the ODOT and Nebraska bridge decks was more likely due to the exposure to $MgCl_2$ and KAc deicers (possibly in combination with F/T cycles and traffic loadings).
11. Visual inspection would be misleading for assessing the condition of concrete bridge decks exposed to $MgCl_2$ deicer, as the chemical attack by $MgCl_2$ generally does not exhibit apparent signs of distress (until severe disintegration of the concrete occurs).
12. Even if the detectable chloride penetration per the $AgNO_3$ spray method is as little as 0.1 inches (2.5 mm), this does not guarantee the integrity of the concrete exposed to $MgCl_2$ deicer. At least half of cored ODOT bridge decks exhibited a spacing factor higher than 200 microns (0.008 inches) per the ASTM C457 test method, indicating that they no longer have a proper air-void system for freeze-thaw resistance.
13. The role of $MgCl_2$ in the carbonation and ASR of field concrete, if any, is not significant, but KAc may play a significant role in contributing to ASR in concrete containing reactive aggregate.
14. The microscopic evidence further suggested that the concrete in the field environment had been affected by both physical and chemical damage by $MgCl_2$.

In addition, the accelerated cold lab testing results demonstrated that the influence of the $MgCl_2$ deicer on the concrete samples was different from the NaCl deicer. NaCl can lead to observable physical damage (e.g., F/T damage in the form of surface scaling), whereas $MgCl_2$ can lead to chemical damages (mainly Ca-leaching) from the inside of the concrete.

The work in this study suggests it is possible to deploy a significant number of standard mortar specimens, randomly sample them periodically, and test their surface resistivity and mechanical properties to indicate the cumulative $MgCl_2$ deicer exposure at the given specific site. This method (detailed in Table 4.4 and Table 4.5) is inexpensive to deploy, and the output from the method would be an exposure rank that correlates with the cumulative $MgCl_2$ exposure at the surface of the concrete in the target area (e.g., a specific bridge deck).

A simplistic empirical-mechanistic model was developed to evaluate the conditions of the bridge decks. This was made possible by combining percolation theory and a power law relationship using F/T cycle times, ADT, and deicer usage as parameters. This work revealed that the current inspection methods used by ODOT for ranking the conditions of the concrete bridge decks may not be suitable for some decks exposed to the combined effect of F/T cycles and $MgCl_2$ deicer. The mechanical testing and microscopic characterization confirmed the validity of the new tool, as it better captured the concrete's internal damage that showed little signs of surface distress.

In a laboratory study, several commercial surface treatment products were evaluated for their effectiveness on protecting concrete from salt scaling under the joint action of 15 freeze/thaw and wet/dry cycles and exposure to a diluted deicer simulated by 3 wt.% NaCl solution. The results indicated that all

of the surface treatments exhibited outstanding performance. After 15 freeze/thaw and wet/dry cycles, the mass loss of surface treated concrete was substantially prevented by 90% or more compared to the untreated condition. The epoxy-based sealer T48-CS exhibited the best performance in protecting the concrete from salt scaling and featured the highest abrasion resistance as well as the lowest water absorption rates and gas permeability coefficient. Coincidentally, the concrete surface treated by this product showed the highest water contact angle. The results suggest that high resistance to both gas and water penetration is a crucial property for a good surface treatment applied to concrete. If based solely on the splitting tensile strengths after 15 times F/T and W/D cycles, T48-CS and ATS-100 were the best performing surface treatments in 3% NaCl and T78 was the best performing surface treatment in 3% MgCl₂.

The bond strength, splitting tensile strength, abrasion resistance, and gas permeability of the concrete slabs treated with different types of overlays were tested after F/T and W/D cycles in NaCl and MgCl₂ solutions. Only the cementitious overlays (SFMO and FMO) exhibited increased bond strength after F/T and W/D cycles in both NaCl and MgCl₂ solutions. The T48 polymer overlay showed increased bond strength after F/T and W/D cycles in 15% MgCl₂ solutions. For all the overlay-protected concrete slabs, their splitting tensile strengths exhibited significant reductions after F/T and W/D cycles in MgCl₂ and NaCl solutions. Among them, the SMFO exhibited the least reduction. The overlays were also tested for their abrasion resistance after “salt scaling”. The polymer overlays (T48 and PPC-1121) showed lower mass loss than the cementitious overlays (control, FMO, SFMO, and LMO), and this agreed with the height changes induced by abrasion. The LMO exhibited much lower mass loss after F/T and W/D cycles in MgCl₂ solution than in NaCl solution. The gas permeability testing results indicated that the concrete slabs treated with organic overlays (T48 and PPC-1121) featured lower gas permeability than those treated with cementitious overlays (control, FMO, SFMO and LMO) after exposure to F/T and W/D cycles in both NaCl and MgCl₂ solutions.

8.2 IMPLEMENTATION RECOMMENDATIONS

It is highly recommended that deicer type and application rate, traffic volume and truck traffic volume, road weather conditions (deck temperature, air temperature, precipitation, etc.), concrete mix design, and deck maintenance records be archived into an integrated bridge preservation program. Alternatively, such data should be added to the existing bridge management system. The inventory of such data would then enable agencies to investigate the role of such variables in the durability of their concrete bridge decks and potentially alter their approach to winter maintenance operations and/or other practices accordingly.

To address the potential risk of MgCl₂, NaCl and KAc deicers, agencies such as ODOT should continue to implement changes in the concrete mix design and in the construction, maintenance, or rehabilitation practices for concrete decks. The current inspection protocol should be updated to address the challenges posed by MgCl₂ deicer, and the damage analysis tool developed in this study should be implemented and continually improved.

Surface treatments, especially penetrating sealers and water repellents should be used to protect new concrete and existing concrete without too much chloride contamination. Under the investigated conditions, one good product identified was the epoxy-based sealer T48-CS. For any surface treatment to be used, it is important to select products with high resistance to both gas and water penetration to maximize the concrete’s resistance to “salt scaling” by NaCl or MgCl₂.

When the concrete surface has deteriorated to a more severe degree, overlays (instead of sealers) should be used. For concrete decks exposed to F/T and W/D cycles and both NaCl and MgCl₂ deicers, the cementitious overlays (SFMO and FMO) should be used. For those mainly exposed to MgCl₂ deicer, the T48 polymer overlay is a good candidate. For areas that are also subjected to studded tires and high risk of abrasion, the polymer overlays (e.g., T48 and PPC-1121) should be used instead of cementitious overlays.

Future work should be conducted to explore the penetrating ability and concrete-bond strength and bond longevity of surface treatments. Mechanistic studies may be conducted to link their protective performance to their penetrating and bonding properties, hydrophobicity, etc. Furthermore, efforts should be devoted to further enhance the durability of surface treatments under abrasion, F/T and W/D cycling, etc. and the application of self-healing technology and nanotechnology to enhance such polymers. The other line of research would be to optimize the combined use of sealers/sealants and water repellants as a cost-effective solution to achieving long-term protection of concrete against abrasion and salt scaling.

9.0 REFERENCES

ACI Committee 302. *Guide for Concrete Floor and Slab Construction*, ACI 302.1R-96, American Concrete Institute, Farmington Hills, MI, 1996.

Almusallam, A.A., F.M. Khan, S.U. Dulaijan, and O.S.B. Al-Amoudi. Effectiveness of Surface Coatings in Improving Concrete Durability. *Cement and Concrete Composites*, Vol.25, No. 4–5, 2003, pp. 473-481.

Alshamsi, A.M., and H.D.A. Imran. Development of a Permeability Apparatus for Concrete and Mortar. *Cement Concrete Research*, Vol. 32, No. 6, 2002, pp. 923-929.

Arnfelt, H. *Damage on Concrete Pavements by Wintertime Salt Treatment*. Volume 66 of Meddelande. Statens Väginstytut, Stockholm. 1943.

Attwood, D., M.A. Nessim, A. Ghoneim, A. Cormeau, and M.S. Cheung. Application of Reliability Theory to In-Service Monitoring and Maintenance of Parking Garages. *Canadian Journal of Civil Engineering*, Vol. 18, No. 5, 1991, pp. 781-788.

Balachandran, C., J. Olek, P.R. Rangaraju, and S. Diamond. Role of Potassium Acetate Deicer in Accelerating Alkali-Silica Reaction in Concrete Pavements. *Transportation Research Record: Journal of the Transportation Research Board*, No. 2240, Transportation Research Board of the National Academies, Washington, D.C., 2011, pp.70-79.

Baroghel-Bouny, V., P. Belin, M. Maultzsch, and D. Henry. AgNO₃ Spray Tests: Advantages, Weaknesses, and Various Applications to Quantify Chloride Ingress into Concrete. Part 1: Non-Steady-State Diffusion Tests and Exposure to Natural Conditions. *Materials and Structures*, Vol. 40, 2007, pp. 759-781.

Basheer, L., and D.J. Cleland. Freeze-Thaw Resistance of Concrete Treated with Pore Liners. *Construction and Building Materials*, Vol.20, No. 10, 2006, pp. 990–998

Cody, R.D., P.G. Spry, A.M. Cody, and G.-L. Gan. The Role of Magnesium in Concrete Deterioration. Final Report-Iowa DOT HR-355. The Iowa Highway Research Board, Iowa State University, Ames, IA, 1994.

Cody, R.D., A. M. Cody, P. G. Spry, and G.-L. Gan. Experimental Deterioration of Highway Concrete by Chloride Deicing Salts. *Environmental & Engineering Geoscience*, Vol. 2, No. 4, 1996, pp. 575-588.

De Schutter, G., and K. Audenaert. Evaluation of Water Absorption of Concrete as a Measure for Resistance Against Carbonation and Chloride Migration. *Materials and Structures*, Vol. 37, No. 9, 2004, pp. 591-596.

Deja, J. and G. Loj. Effects of Cations Occurring in the Chloride Solutions on the Corrosion Resistance of Slag Cementitious Materials. Presented at Infrastructure Regeneration and Rehabilitation Improving the Quality of Life through Better Construction - A Vision for the Next Millennium, Sheffield, U.K. 1999.

Fay, L., and X. Shi. Laboratory Investigation of Performance and Impacts of Snow and Ice Control Chemicals for Winter Road Service. *ASCE Journal of Cold Regions Engineering*, Vol. 25, No. 3, 2011, pp. 89-114.

Fay, L., and X. Shi. Environmental Impacts of Chemicals for Snow and Ice Control: State of the Knowledge. *Water, Air & Soil Pollution*, Vol. 223. 2012, pp. 2751–2770.

FHWA. How Do Weather Events Impact Roads? Federal Highway Administration. Washington, D.C., 2005.

Fischel, M. *Evaluation of Selected Deicers Based on a Review of the Literature*. Colorado Department of Transportation. Denver, CO. 2001.

Franzonia, E., B. Piginoa, and C. Pistolesib. Ethyl Silicate for Surface Protection of Concrete: Performance in Comparison with Other Inorganic Surface Treatments. *Cement and Concrete Composites*, Vol. 44, 2013, pp. 69-76.

Ghoddousi, P., A.M. Raiss Ghasemi, and T. Parhizkar. The Effect of Concrete Quality on Performance of Surface Treatment Materials. In: Rudolph N. Kraus, Tarun.R. Naik, Peter Claisse, Sadeghi -Pouya, ed. *Proceedings International Conference: Sustainable Construction Materials and Technologies, 2007* Coventry, Special papers proceedings, Pub. UW Milwaukee CBU, 2007, pp 78-84.

Glass, G.K., and N.R. Buenfeld. The Presentation of the Chloride Threshold Level for Corrosion of Steel in Concrete. *Corrosion Science*, Vol. 29, No. 5, 1997, pp. 1001-1013.

Han, B., Z. Yang, X. Shi, and X. Yu. Transport Properties of Carbon-Nanotube/Cement Composites. *Journal of Materials Engineering and Performance*, Vol. 22, No. 1, 2013, pp. 184-189.

He, X., and X. Shi. Self-Repairing Coating for Corrosion Protection of Aluminum Alloys. *Progress in Organic Coatings*, Vol. 65, 2009, pp. 37-43.

Helmy, M., A.A. Amer, and H. El-Didamony. Chemical Attack on Hardened Pastes of Blended Cements - Part 1: Attack of Chloride Solutions. *Zement-Kalk-Gips*. Vol. 44, No. 1, 1991, pp. 46-50.

Hong, K., and R.D. Hooton. Effects of Cyclic Chloride Exposure on Penetration of Concrete Cover. *Cement and Concrete Research*, Vol. 29, No. 9, 1999, pp. 1379-1386.

Hover, K.C. Air Content and Density of Hardened Concrete. In ASTM STP169D-EB: Significance of Tests and Properties of Concrete and Concrete-Making Materials, ed. Lamond, P.F. & Pielert, J.H., ASTM, West Conshohocken, PA, 2006, Chapter 26.

Ibrahim, M., A. Al-Gahtani, M. Maslehuddin, and F. Dakhil. (1999). Use of Surface Treatment Materials to Improve Concrete Durability, *Journal of Materials in Civil Engineering*, Vol. 11, No. 1, 1999, pp. 36-40.

Jana, D. Concrete Scaling-A Critical Review. Presented in the Proceeding to the 29th Conference on Cement Microscopy, Quebec City, Canada, 2007.

Jang, J. W., I. Iwasaki, H.J. Gillis, and P.W. Weiblen. Effect of Corrosion-Inhibitor-Added Deicing Salts and Salt Substitutes on Reinforcing Steels: I. Influence of Concentration. *Advanced Cement Based Materials*, Vol. 2, No. 4, 1995, pp.145-151.

Julio-Betancourt, G.A. *Effect of De-icer and Anti-icer Chemicals on the Durability, Microstructure, and Properties of Cement-Based Materials*. Doctoral Thesis, University of Toronto, Canada. 2009.

Korhonen, C. *Effect of High Doses of Chemical Admixtures on the Freeze-Thaw Durability of Portland Cement Concrete*. U.S. Army Corps of Engineers, Engineering Research and Development Center. ERDC/CRREL TR-02-5, 2002.

Lee, H., R.D. Cody, A.M. Cody, and P.G. Spry. Effects of Various Deicing Chemicals on Pavement Concrete Deterioration. Presented in Proceedings Mid-Continent Transportation Symposium. 2000.

Li, Y., Y. Fang, N. Seeley, S. Jungwirth, E. Jackson, M. Mills, G. Hansen, and X. Shi. Corrosion of Chloride Deicers to Highway Maintenance Equipment: A Renewed Perspective and Laboratory Investigation. *Transportation Research Record: Journal of the Transportation Research Board*, No. 2361, Transportation Research Board of the National Academies, Washington, D.C., 2013, pp. 106-113.

Li, Z., and L. Su. Freeze-Deicer Salt Scaling Resistance of Concrete. Presented in the Proceedings of the 12th International Conference on Engineering, Science, Construction, and Operations in Challenging Environments. Earth and Space 2010. 2010.

Li, Z.X., T.H. Chan, and J.M. Ko. Fatigue Analysis and Life Prediction of Bridges with Structural Health Monitoring Data—Part I: Methodology and Strategy. *International Journal of Fatigue*, Vol. 23, No. 1, 2001, pp. 45-53.

Litvan, G.G. (1975). Phase Transitions of Adsorbates: VI, Effect of Deicing Agents on the Freezing of Cement Paste. *Journal American Ceramic Society*, Vol. 58, No. 1-2, 1975, pp. 26-30.

Liu, Y. and X. Shi. Stochastic Modeling of Service Life of Concrete Structures in Chloride-Laden Environments. *Journal of Materials in Civil Engineering*, Vol. 24, No. 4, 2012, pp. 381-390.

Mamaghani, Iraj.H.P., C. Moretti, and B.A. Dockter. Application of Sealing Agents in Concrete Durability of Infrastructure Systems. Research Report No. UND 2006-01. North Dakota Department of Transportation (NDOT), Bismarck, 2007. www.dot.nd.gov/divisions/materials/research_project/UND0601final.pdf. Accessed May 19, 2009.

- Mamaghani, Iraj H. P., C. Moretti, B.A. Dockter, L. Falken, and J. Tonnenson. (2009). Evaluation of Penetrating Sealers for Reinforced Concrete Bridge Decks. *Transportation Research Record: Journal of the Transportation Research Board*, No. 2018, Transportation Research Board of the National Academies, Washington, D.C., 2009, pp. 86-96.
- Marchand, J., E.J. Sellevold, and M. Pigeon. The Deicer Salt Scaling Deterioration of Concrete – An Overview. *American Concrete Institute*, SP 145-1, 1994, pp. 1-46.
- Margolina, A., and W. Souheng. Percolation Model for Brittle – Tough Transition in Nylon/Rubber Blends. *Polymer*, Vol. 29, 1988, pp. 2170-2173.
- Martinez, F., and R. Poecker. *Evaluation of Deicer Applications on Open Graded Pavements*. Oregon Department of Transportation. Salem, OR. 2006.
- Medeiros, M.H.F., and P. Helene. Surface Treatment of Reinforced Concrete in Marine Environment: Influence on Chloride Diffusion Coefficient and Capillary Water Absorption. *Construction and Building Materials*, Vol. 23, No. 3, 2009, pp. 1476-1484.
- Moon, H.Y., D.J. Shin, and D.S. Choi. Evaluation of the Durability of Mortar and Concrete Applied with Inorganic Coating Material and Surface Treatment System. *Construction and Building Materials*, Vol. 21, No. 2, 2007, pp. 362-369.
- Moukwa, M. Characteristics of the Attack of Cement Paste by MgSO₄ and MgCl₂ from Pore Structure Measurements. *Cement Concrete Research*, Vol. 20, No. 1, 1990, pp. 148-158.
- Neville, A. Chloride Attack of Reinforced Concrete: An Overview. *Materials and Structures*, Vol. 28, No. 2, 1995, pp. 63-70.
- Otsuki, N., S. Nagataki, and K. Nakashita. Evaluation of AgNO₃ Solution Spray Method for Measurement of Chloride Penetration into Hardened Cementitious Matrix Materials. *ACI Materials Journal*, Vol. 89, No. 6, 1992, pp. 587-592.
- Öttl C. Frost/Deicing Salt Resistance of Concrete Pavements with Unsuitable Air Void Characteristics, Otto Graf J., Vol. 17, pp. 45-55. [Online]. 2006. Available: http://www.mpa.uni-stuttgart.de/publikationen/otto_graf_journal/ogj_2006/beitrag_oetl.pdf . Accessed November 17, 2008.
- Özgan, E., S. Serin, H. Gerengi, and İ. Arslan. Multi-Faceted Investigation of the Effect of De-icer Chemicals on the Engineering Properties of Asphalt Concrete. *Cold Regions Science and Technology*, Vol. 87, 2013, pp. 59–67.
- Pan, T., X. He, and X. Shi. Laboratory Investigation of Acetate-Based Deicing/Anti-Icing Agents Deteriorating Airfield Asphalt Concrete. *Journal of the Association of Asphalt Paving Technologists (AAPT)*, Vol. 77, 2008, pp. 773-793.

- Pigeon, M. and R. Pleau. *Durability of Concrete in Cold Climates*. New York, NY: E and FN Spon. 1995.
- Pigino, B., A. Leemann, E. Franzoni, and P. Lura. Ethyl Silicate for Surface Treatment of Concrete Part II: Characteristics and Performance. *Cement and Concrete Composite*, Vol. 34, No. 3, 2012, pp. 313–321
- Polder, R.B., and W.H. Peelen. Characterisation of Chloride Transport and Reinforcement Corrosion in Concrete under Cyclic Wetting and Drying by Electrical Resistivity. *Cement and Concrete Composites*, Vol. 24, No. 5, 2002, pp. 427-435.
- Qiu, L., and W.A. Nixon. Effects of Adverse Weather on Traffic Crashes: Systematic Review and Meta-Analysis. *Transportation Research Record: Journal of the Transportation Research Board*, No. 2055, Transportation Research Board of the National Academies, Washington, D.C., 2008, pp. 139-146.
- Ramakrishna, D.M., and T. Viraraghavan. Environmental Impact of Chemical Deicers—A Review. *Water, Air, and Soil Pollution*, Vol. 166, No. 1-4, 2005, pp. 49-63.
- Rangaraju, P.R., K.R. Sompura, J. Olek, S. Diamond and J. Lovell. Potential for Development of Alkali-Silica Reaction in Presence of Airfield Deicing Chemicals. Presented in the Proceedings of the 8th International Conference on Concrete Pavements, Colorado Springs, 2005.
- Rangaraju, P.R., K.R. Sompura and J. Olek. Investigation into Potential of Alkali-Acetate Based Deicers in Causing Alkali-Silica Re-action. In Compendium of Papers CD for the Transportation Research Board 85th Annual Meeting, Washington, D.C., 2006.
- Rangaraju, P.R., and J. Desai. Effectiveness of Selected SCMs in Mitigating ASR in Presence of Potassium Acetate Deicer Solution. In Compendium of Papers CD for the Transportation Research Board 85th Annual Meeting, Washington, D.C., 2006.
- Rangaraju, P.R., and J. Olek. *Potential for Acceleration of ASR in the Presence of Pavement Deicing Chemicals*. Final Report IPFR-01-G-002-03- 9, Innovative Pavement Research Foundation, Airport Concrete Pavement Technology Program, Skokie, IL; 2007.
- Rangaraju, P.R. Influence of Airfield Pavement Deicing and Anti-Icing Chemicals on Durability of Concrete. Presented in the Proceedings 2007 FAA Worldwide Airport Technology Transfer Conference, Atlantic City, New Jersey, USA. 2007.
- Rechenberg, V.W., and H.-M. Sylla. The Effect of Magnesium on Concrete. *ZKG International*, Vol. 49, No. 1, 1996, pp. 44-56.
- Rønning, T.F. *Freeze-Thaw Resistance of Concrete. Effect of: Curing Conditions, Moisture Exchange and Materials*. Doctoral Thesis. The Norwegian Institute of Technology. 2001.
- Roosevelt, D. Bridge Deck Anti-icing System in Virginia: Lessons Learned from a Pilot Study. Virginia Transportation Research Council. Richmond, VA. 2004.
http://www.virginiadot.org/vtrc/main/online_reports/pdf/04-r26.pdf. Accessed May 19, 2009.

- Rösli, A., and A.B. Harnik. *Improving the Durability of Concrete to Freezing and Deicing Salts*. Durability Building Materials and Components. ASTM Special Technical Publication STP-691, ASTM, Philadelphia, 1980, pp. 464-473.
- Sandrolini, F, E. Franzoni, and B. Pigino. Ethyl Silicate for Surface Treatment of Concrete Part 1: Pozzolanic Effect of Ethyl Silicate. *Cement and Concrete Composite*, Vol. 34, No. 3, 2012, pp. 306-312.
- Shahdah, U., and L. Fu. Quantifying the Mobility Benefits of Winter Road Maintenance – A Simulation Based Analysis. Presented at TRB 89th Annual Meeting Compendium of Papers DVD. Transportation Research Board. Washington, D.C., 2010.
- Shi, X. *Impact of Airport Pavement Deicing Products on Aircraft and Airfield Infrastructure*. Washington, D.C.: National Academies Press. 2008.
- Shi, X. Winter Road Maintenance: Best Practices, Emerging Challenges and Research Needs. *Journal of Public Works & Infrastructure*, Vol. 2, No. 4, 2010, pp. 318-326.
- Shi, X., K. Fortune, R. Smithlin, M. Akin, and L. Fay. Exploring the Performance and Corrosivity of Chloride Deicer Solutions: Laboratory Investigation and Quantitative Modeling. *Cold Regions Science and Technology*, Vol. 86, 2013, pp. 36-44.
- Shi, X., L. Fay, M.M. Peterson, M. Berry, and M. Mooney. A FESEM/EDX Investigation into How Continuous Deicer Exposure Affects the Chemistry of Portland Cement Concrete. *Construction and Building Materials*, Vol. 25, No. 2, 2011, pp. 957-966.
- Shi, X., L. Fay, M.M. Peterson, and Z. Yang. Freeze-Thaw Damage and Chemical Change of a Portland Cement Concrete in the Presence of Diluted Deicers. *Materials and Structures*, Vol. 43, No. 7, 2010a, pp. 933-946.
- Shi, X., L. Fay, Z. Yang, T.A. Nguyen, and Y. Liu. Corrosion of Deicers to Metals in Transportation Infrastructure: Introduction and Recent Developments. *Corrosion Reviews*, Vol. 27, No. 1-2, 2009a, pp. 23-52.
- Shi, X., M. Akin, T. Pan, L. Fay, Y. Liu, and Z. Yang. Deicer Impacts on Pavement Materials: Introduction and Recent Developments. *The Open Civil Engineering Journal*, Vol. 3, 2009a, pp. 16-27.
- Shi, X., M. Akin, T. Pan, L. Fay, Y. Liu, and Z. Yang. Deicer Impacts on Pavement Materials: Introduction and Recent Developments. *The Open Civil Engineering Journal*, Vol. 3, 2009b, pp. 16-27.
- Shi, X., N. Xie, K. Fortune, and J. Gong. Durability of Steel Reinforced Concrete in Chloride Environments: An Overview. *Construction and Building Materials*, Vol. 30, 2012, pp. 125-138.
- Shi, X., N. Xie, K. Fortune, and J. Gong. Durability of Steel Reinforced Concrete in Chloride Environments: An Overview. *Construction and Building Materials*, Vol.30, 2012b, pp. 125-138.

- Shi, X., S.W. Goh, M. Akin, S. Stevens, and Z. You. Exploring the Interactions of Chloride Deicer Solutions with Nano/Micro-Modified Asphalt Mixtures using Artificial Neural Networks. *ASCE Journal of Materials in Civil Engineering*, Vol. 24, No. 7, 2012a, pp. 805–815.
- Shi, X., T.A. Nguyen, Z. Suo, Y. Liu, and R. Avci. Effect of Nanoparticles on the Anticorrosion and Mechanical Properties of Epoxy Coating. *Surface and Coatings Technology*, Vol. 204, No. 3, 2009, pp. 237-245.
- Shi, X., Y. Liu, M. Mooney, M. Berry, B. Hubbard, and T.A. Nguyen. Laboratory Investigation and Neural Networks Modeling of Deicer Ingress into Portland Cement Concrete and Its Corrosion Implications. *Corrosion Reviews*, Vol. 28, No. 3-4, 2010b, pp. 105-153.
- Shi, X., Y. Liu, M. Mooney, M. Berry, B. Hubbard, and T.A. Nguyen. Laboratory Investigation and Neural Networks Modeling of Deicer Ingress into Portland Cement Concrete and Its Corrosion Implications. *Corrosion Reviews*, Vol. 28, No. 3-4, 2010, pp. 105-153.
- Spragg, R.P., J. Castro, W. Li, M. Pour-Ghaz, P.T. Huang, and J. Weiss. Wetting and Drying of Concrete using Aqueous Solutions Containing Deicing Salts. *Cement and Concrete Composites*, Vol. 33, No. 5, 2011, pp. 535-542.
- Spragg, R.P., J. Castro, W. Li, M. Pour-Ghaz, P.T. Huang, and J. Weiss. Wetting and Drying of Concrete in the Presence of Deicing Salt Solutions. In TRB 90th Annual Meeting Compendium of Papers DVD. Washington, D.C., 2011.
- Stanish K.D., R.D. Hooton, and M.D.A. Thomas. *Testing the Chloride Penetration Resistance of Concrete: A Literature Review*. Toronto, ON: Canada, University of Toronto, Toronto, ON, Canada. 1997.
- Stewart, M.G. Reliability-Based Assessment of Ageing Bridges using Risk Ranking and Life Cycle Cost Decision Analyses. *Reliability Engineering & System Safety*, Vol. 74, No. 3, 2001. pp. 263-273.
- Strong, C.K., Z. Ye, and X. Shi. Safety Effects of Winter Weather: The State of Knowledge and Remaining Challenges. *Transport Reviews*, Vol. 30, No. 6, 2010, pp. 677-699.
- Sujay, M., D. Wingard, and P.R. Rangaraju. Assessing Potential Reactivity of Aggregates in Presence of Potassium Acetate Deicer. *Transportation Research Record: Journal of the Transportation Research Board*, No. 2232, Transportation Research Board of the National Academies, Washington, D.C., 2011, pp. 10-24.
- Sutter, L., K. Peterson, S. Touton, T. Van Dam, and D. Johnston. Petrographic Evidence of Calcium Oxychloride Formation in Mor-Tars Exposed to Magnesium Chloride Solution. *Cement Concrete Research*, Vol. 36, No. 8, 2006, pp. 1533-1541.

Sutter, L., K. Peterson, G. Julio-Betancourt, D. Hooton, T. Van Dam, and K. Smith. *The Deleterious Chemical Effects of Concentrated Deicing Solutions on Portland Cement Concrete*. Final Report No. SD2002-01-F. South Dakota Department of Transportation. 2008.

Truschke, C., Peterson, K., Van Dam, T., Peshkin, D., DeDene, C., & DeDios, R. Investigation of Portland Cement Concrete Exposed to Automated Deicing Solutions on Colorado's Bridge Decks. *Transportation Research Record: Journal of the Transportation Research Board*, No. 2220, Transportation Research Board of the National Academies, Washington, D.C., 2011, pp. 1-11.

UNI EN 1504-2. *Products and Systems for the Protection and Repair of Concrete Structures. Definitions, Requirements, Quality Control and Evaluation of Conformity – Part 2: Surface Protection Systems for Concrete*. 2004.

Usman, T., L. Fu, and L.F. Miranda-Moreno. Quantifying Safety Benefit of Winter Road Maintenance: Accident Frequency Modeling. *Accident Analysis & Prevention*, Vol. 42, No. 6, 2010, pp. 1878-1887.

Val, D.V., and M.G. Stewart. Life-Cycle Cost Analysis of Reinforced Concrete Structures in Marine Environments. *Structural Safety*, Vol. 25, No. 4, 2003, pp. 343-362.

Valenza II, J.J. and G.W. Scherer. Mechanism for Salt Scaling. *Journal American Ceramic Society*, Vol. 84, No. 4, 2006, pp. 1161-1179

Valenza II, J.J., and G.W. Scherer. A Review of Salt Scaling: I. Phenomenology. *Cement and Concrete Research*, Vol. 37, No. 7, 2007a, pp. 1007-1021.

Valenza II, J.J., and G.W. Scherer. A Review of Salt Scaling: II . Mechanisms. *Cement and Concrete Research*, Vol. 37, No. 7, 2007b, pp. 1022-1034.

Van Dam, T.J., K.R. Peterson, L.L. Sutter, and K.D. Smith. Durability of Concrete Pavements used in Aircraft Deicing Facilities. Presented in: TRB 87th Annual Meeting Compendium of Papers DVD, Washington, D.C. Paper No. 08-2231. 2008.

Wakeley, L.D., T.S. Poole, C.A. Weiss, and J.P. Burkes. Geochemical Stability of Cement-Based Composites in Magnesium Brines. Presented in: Proceedings of the 14th International Conference on Cement Microscopy, Costa Mesa, CA. 1992.

Williams, D. *Past and Current Practices of Winter Maintenance at the Montana Department of Transportation*. White Paper, Dec. [Online]. 2003.

http://www.mdt.mt.gov/publications/docs/brochures/winter_maint/wintmaint_whitepaper.pdf Accessed November 17, 2008.

Yamasaki, R.S. *Journal of Paint Technology*. Vol. 39, No. 509, 1967, pp. 394-397.

Ye, Z., D. Veneziano, and X. Shi. Estimating Statewide Benefits of Winter Maintenance Operations. *Transportation Research Record: Journal of the Transportation Research Board*, No. 2329, Transportation Research Board of the National Academies, Washington, D.C., 2013, pp. 17-23.

Yu, H., X. Shi, W.H. Hartt, and B. Lu. Laboratory Investigation of Reinforcement Corrosion Initiation and Chloride Threshold Content for Self-Compacting Concrete. *Cement and Concrete Research*, Vol. 40, No. 10, 2010, pp. 1507-1516.

Zapata, C.E., D. Andrei, M.W. Witzak, and W.N. Houston. Incorporation of Environmental Effects in Pavement Design. *Road Materials and Pavement Design*, Vol. 8, No. 4, 2007, pp. 667-693.

Zhao, Y., P. Du, and W. Jin. Evaluation of the Performance of Surface Treatments on Concrete Durability. *Journal of Zhejiang University- Science A*, Vol. 11, No. 5, 2010, pp. 349-355.

APPENDIX A

**DEICER USAGE PER YEAR FOR EACH ODOT BRIDGE SELECTED IN
THIS STUDY**

DEICER USAGE PER YEAR FOR EACH ODOT BRIDGE SELECTED IN THIS STUDY

Bridge	Category	District	deicer_05	deicer_06	deicer_07	deicer_08	deicer_09	deicer_10	deicer_11	deicer_12	Total Deicer Usage (gln)	Average Annual Deicer Usage (gln)	Lane Miles
19268	1	2B	250	490	365	650	450	210	220	770	3405	426	0.169
19681	2	13				735	1545	1605	1740	1520	7145	1429	0.475
18940	3	2B							945	655	1600	800	0.383
18525	4	8				15	280	100	390	360	1145	229	0.513
16534	5	2B							520	515	1035	518	0.137
16440	6	12				270	485	460	740	360	2315	463	0.225
16358	7	2B							520	475	995	498	0.486
16844	8	8		55	90	340	140	15	45	325	1010	144	1.145
08958F	9	2B							400	470	870	435	1.186
00576	10	8					65	35	45	120	265	66	0.511
09268S	11	2B							400	470	870	435	4.128
08682	12	8				375	1545	1130	1050	620	4720	944	0.355